NACA TN 3738

NATIONAL ADVISORY COMMITTEE FOR AERONAUTICS

TECHNICAL NOTE 3738

THEORETICAL AND EXPERIMENTAL INVESTIGATION OF THE SUBSONIC-FLOW FIELDS BENEATH SWEPT AND UNSWEPT WINGS WITH TABLES OF VORTEX-INDUCED VELOCITIES

By William J. Alford, Jr.

Langley Aeronautical Laboratory
Langley Field, Va.

NACA

Washington

August 1956

H

NATIONAL ADVISORY COMMITTEE FOR AERONAUTICS

TECHNICAL NOTE 3738

THEORETICAL AND EXPERIMENTAL INVESTIGATION OF THE SUBSONIC-FLOW FIELDS BENEATH SWEPT AND UNSWEPT WINGS WITH TABLES OF VORTEX-INDUCED VELOCITIES

By William J. Alford, Jr.

SUMMARY

The flow-field characteristics beneath swept and unswept wings as determined by potential-flow theory are compared with the experimentally determined flow fields beneath swept and unswept wing-fuselage combinations. The potential-flow theory utilized considered both spanwise and chordwise distributions of vorticity as well as the wing-thickness effects. The perturbation velocities induced by a unit horseshoe vortex are included in tabular form.

The results indicated that significant chordwise flow gradients existed beneath both swept and unswept wings at zero lift and throughout the lift range. The theoretical predictions of the flow-field characteristics were qualitatively correct in all cases considered, although there were indications that the magnitudes of the downwash angles tended to be overpredicted as the tip of the swept wing was approached and that the sidewash angles ahead of the unswept wing were underpredicted. The calculated effects of compressibility indicated that significant increases in the chordwise variation of flow angles and dynamic-pressure ratios should be expected in going from low to high subsonic speeds.

INTRODUCTION

The almost universal present-day employment of external stores, such as missiles, bombs, or fuel tanks on fighter airplanes, and nacelles on bomber airplanes, has indicated the need for more detailed information regarding the flow characteristics in the vicinity of the wing in order to estimate the aerodynamic loads on these objects when fixed in the wing flow field and to evaluate the launching and jettison characteristics of missiles, bombs, or fuel tanks. In addition, numerous present-day airplanes are incorporating wing sweep, lower aspect ratios, and shorter tail length, all of which may tend to bring the various airplane components in closer proximity to the wing.

For airplane designs of the past, in which the component parts (for example, the wing and the tail) were separated by reasonable distances, the wing-interference effects could be calculated with sufficient accuracy by a number of horseshoe vortices distributed along a single lifting line (refs. 1 to 4). However, because of the mathematically singular nature of the single vortex, this theory is valid only for regions that are at a distance of at least one wing chord from the vortex location. (See ref. 1.)

The purpose of the present paper is to show that the flow characteristics beneath the wing can be calculated if the lifting wing is assumed to be represented by a multiple arrangement (both chordwise and spanwise) of horseshoe vortices and if the effects of thickness are accounted for. The velocities induced by the airfoil-section thickness distribution, which are often neglected, are considered by using the appropriate singularity (source sink) distribution (ref. 5) in conjunction with simple sweep theory (ref. 6). Detailed experimental flow fields were obtained around swept and unswept wing-fuselage combinations and are compared with the wing-alone theoretical flow fields.

The details of the calculative procedure are developed in appendixes. The velocities induced by a unit horseshoe vortex in the chordwise, vertical, and lateral directions for a large range of distances are included in tabular form. The calculated first-order effects of compressibility on the flow characteristics for a subcritical Mach number of 0.80 are also presented.

SYMBOLS

A aspect ratio

b wing span, ft

c local wing chord, ft

$\bar{c}$ mean aerodynamic chord, ft

c_{av} average wing chord, ft

c_l wing-section lift coefficient

c_{l_α} section lift-curve slope

C_L total lift coefficient

C_{L_α} incompressible lift-curve slope

$C_{L_{\alpha,M}}$	compressible lift-curve slope
C_D	drag coefficient
C_m	pitching-moment coefficient measured about quarter chord of mean aerodynamic chord
l	fuselage length, 7.61 ft
S	wing area, sq ft
s	semiwidth of horseshoe vortex, ft
d_{max}	maximum fuselage diameter, 0.70 ft
t	airfoil thickness, ft
λ	taper ratio
Λ	local sweep angle, deg
V	free-stream velocity, ft/sec
V_R	resultant velocity, ft/sec
u	backwash perturbation velocity in direction of x-axis, positive rearward (fig. 3), ft/sec
u_s	backwash perturbation velocity induced by two-dimensional airfoil-section thickness distribution (see appendix A), ft/sec
v	sidewash perturbation velocity in direction of y-axis, positive to the right (fig. 3), ft/sec
w	downwash perturbation velocity in direction of z-axis, positive downward (fig. 3), ft/sec
q_l	local dynamic pressure, lb/sq ft
q_o	free-stream dynamic pressure, lb/sq ft
ϵ	downwash angle between free-stream-velocity vector and resultant-velocity vector in xz-plane, positive downward (fig. 3), deg
σ	sidewash angle between free-stream-velocity vector and resultant-velocity vector in xy-plane, positive toward left wing tip (fig. 3), deg

x,y,z right-hand Cartesian coordinate system in which x is positive downstream, y is positive to the right, and z is positive upward (fig. 3), ft

$\Delta x, \Delta y, \Delta z$ distances in the x-, y-, and z-directions, respectively, from space point of interest to centroidal location of mth, nth vortex

n spanwise vortex index (see appendix A)

m chordwise vortex index (see appendix A)

α inclination of wing from zero-lift attitude, deg

Γ three-dimensional vortex circulation strength, ft^2/sec

Γ_s two-dimensional vortex circulation strength, ft^2/sec

ϕ perturbation velocity potential, ft^2/sec

ϕ_s two-dimensional perturbation velocity potential (also referred to as chordwise accumulation of vorticity when increased by a factor of 2.0), ft^2/sec

F_u backwash factor (see appendix B)

F_v sidewash factor (see appendix B)

F_w downwash factor (see appendix B)

M Mach number

$\beta = \sqrt{1 - M^2}$

Subscripts:

a additional or lift-induced characteristics

n characteristics of airfoil section normal to local lines of constant percent thickness

s characteristics of streamwise airfoil section in two-dimensional flow

c/2 characteristics referred to half-chord line

c/4 characteristics referred to quarter-chord line

te characteristics referred to trailing edge

Primes indicate equivalent incompressible characteristics.
Bars indicate centroidal locations of the vortices.

MODELS AND TESTS

The models about which the flow surveys were made consisted of both swept- and unswept-wing—fuselage combinations. Drawings of the wing-fuselage combination are presented in figure 1. The wing of the swept-wing—fuselage combination had 45° sweep of the quarter-chord line, an aspect ratio of 4.0, a taper ratio of 0.3, and NACA 65A006 airfoil sections parallel to the plane of symmetry. The wing of the unswept-wing—fuselage combination had 0° sweep of the one-half-chord line, an aspect ratio of 3.0, a taper ratio of 0.5, and NACA 65A004 airfoil sections parallel to the plane of symmetry. The fuselage consisted of an ogival nose section, a cylindrical center section, and a truncated tail cone. The fuselage ordinates are presented in table I.

The tests were made in the Langley 300 MPH 7- by 10-foot tunnel at a velocity of 100 miles per hour. Experimental results are presented for angles of attack from -8° to 24° for the swept-wing—fuselage model and from -8° to 16° for the unswept-wing—fuselage model.

The flow characteristics were obtained with a rake of hemispherically headed probes utilizing both downwash- and sidewash-angle orifices in conjunction with pitot-static orifices to measure dynamic pressure. The instrument employed in this investigation is similar to that employed in reference 1 and is shown installed on one of the test models in figure 2. The flow surveys were made over the right wing with the model inverted to minimize support-strut interference and, therefore, represent conditions (due to model symmetry) under the left wing of the model.

Consideration of the angularity rake calibration, data-reduction process, method of rake support, possible errors in misalinement, and inherent wind-tunnel misalinement angles indicates that the downwash data are accurate within approximately $\pm 1.0^\circ$, the sidewash data are accurate within approximately $\pm 1.5^\circ$, and the dynamic-pressure-ratio data are accurate within approximately ± 0.025.

THEORETICAL METHODS

The characteristics of a field of flow can be completely defined by the magnitude and direction of the local velocity vectors. It is generally convenient to express the direction in terms of the angles ϵ in the vertical plane and σ in the lateral plane and to express the magnitude in terms of local dynamic pressure q_l. In order to determine the foregoing flow characteristics by use of theory, a knowledge is required of the induced velocities contributed by the various surfaces responsible for disturbing the free-stream flow. The discussion of the calculative procedure will be restricted in the present section to a brief general description with the specific details and equations enlarged upon in appendix A. The principal factors necessary to describe the flow characteristics are defined schematically in figure 3.

In the calculation procedures employed, it was assumed that the flow was potential and planar, and, hence, the effects of boundary-layer separation and the rolling up and displacement of the trailing-vortex wake have been neglected. The effects of the presence of the fuselage have also been neglected since the variation of upwash angle induced by the circular-cross-section fuselage decays rapidly with lateral distance. This variation in upwash angle is presented in figure 4 as a function of lateral distance, nondimensionalized with respect to the swept-wing semispan. For the swept-wing configuration, the ratio of fuselage diameter to wing span is 0.13. For the lateral locations for which the swept-wing calculations have been made, $y\Big/\frac{b}{2} = 0.50$ and $y\Big/\frac{b}{2} = 0.75$, the fuselage-induced upwash angles are seen from figure 4 to be approximately 8 percent of wing angle of attack for the inboard location and approximately 3 percent for the outboard location. For the midsemispan location of the unswept wing, which has a ratio of fuselage diameter to wing span of 0.16, the fuselage-induced upwash angle is approximately 10 percent of the wing angle of attack.

The foregoing discussion has considered only the effects of the fuselage alone. Examination of reference 4 indicates that the mutual-interference effects caused by the addition of a wing to the fuselage produce only slight changes in the exposed wing-span load distribution. Since the calculations of present interest are critically affected by lift coefficient and since the comparison of theory with experiment is most readily made for comparable lift coefficients, the small changes in load distribution indicated by reference 4 are assumed negligible. For regions closer to the fuselage, however, or for larger ratios of fuselage diameter to wing span, it is evident from figure 4 that the presence of the fuselage should be considered. In this respect, the analyses of references 4 and 7 may be useful.

In order to determine the flow characteristics in close proximity to the wing, it is necessary to account for both the lift-induced velocities and the nonlifting or thickness-induced velocities. The former velocities are primarily a function of wing angle of attack and plan-form geometric characteristics, whereas the latter velocities are independent of angle of attack and are primarily a function of the local airfoil-section thickness distribution, modified by plan-form characteristics. Extensive theoretical investigations of the zero-lift velocity distributions on the surface of unswept and sweptback wings have been reported in references 8 to 11 and indicate that the isobars, that is, lines of constant pressure, tend to be parallel to the local lines of constant percent thickness for regions not too close to the wing root or tip. Reference 9 also shows that the effect of aspect ratio on the backwash velocities is negligible for aspect ratios that are of present interest (aspect ratios of 4 and 3 for the swept and unswept wings, respectively). In view of this, and with consideration of the simple sweep theory of reference 6, the present paper considers the airfoil sections normal to the local lines of constant percent thickness to be two dimensional in nature.

The perturbation velocities of the two-dimensional-airfoil thickness distribution may be determined by either conformal transformations as reported in references 12 to 14 or by use of the appropriate singularity distribution as determined by the methods of reference 5 or 15. The present paper utilized the method of reference 5 in combination with the simple sweep theory of reference 6, as described in appendix A, in order to account approximately for the effects of either sweep or taper or both.

In the calculation of the lift-induced velocities, the present procedure utilizes, primarily, four horseshoe vortices distributed in the chordwise direction at each of 10 spanwise locations, thus making a total of 40 horseshoe vortices. The chordwise vortices are assumed to have equal circulation strengths but unequal chordwise spacing. The stratagem is then to sum the induction effects at points that lie midway between any two adjacent chordwise vortices (where possible) for regions near the wing chord, and thereby minimize the objectionable singularity effects mentioned previously in the "Introduction". This procedure is hereinafter referred to as the finite-step method. An illustrative calculation of the lift-induced velocities beneath the swept wing is presented in table II.

In calculating the sidewash velocities, the finite-step method becomes increasingly inaccurate as the vertical distance from the wing chord plane is decreased. Further study of the assumed horseshoe vortex system (see appendix A) indicated that the sidewash velocity would approach zero as the wing chord plane was approached. This characteristic is not consistent with reality in that the lateral gradient in load or vorticity implies the existence of sidewash velocities on the wing surface.

By use of unpublished theoretical studies made by Percy J. Bobbitt of the Langley Aeronautical Laboratory (see appendix A), the sidewash velocity at the wing chord plane may be estimated and a more realistic variation of sidewash velocity with vertical distance effected.

The velocities induced by a unit horseshoe vortex in the vertical, lateral, and longitudinal directions, which are necessary in the present methods, were computed by the equations given in reference 16 and are presented in tables III, IV, and V for a large range of distances.

The spanwise load or vorticity distributions were determined by the method of reference 17. In order to eliminate errors involved in estimating the lift-curve slopes of the wings under consideration, the comparisons of theory with experiment were made at the same lift coefficient.

The calculated first-order effects of compressibility were obtained by use of the three-dimensional Prandtl-Glauert transformation as given by Göthert in reference 18. The procedure utilized in the present investigation is described in appendix A.

COMPARISON OF THEORY AND EXPERIMENT

In analyzing the flow-field characteristics and in correlating experimental and theoretical characteristics, it is often desirable to have as a reference level the experimental force and moment characteristics of the models. These data for the models of the present investigation are presented in figures 5 and 6.

Flow angularities are presented in terms of the angles ϵ and σ. In the sign convention adopted (fig. 3), positive values of ϵ indicate a downflow, positive values of σ represent an outflow (toward left wing tip), and values of q_l/q_o greater than unity indicate regions of superpressure relative to free-stream conditions. It should be noted that the induced angles ϵ and σ must be combined with the geometric angles of attack and sideslip, respectively, to be applicable for use in load-estimation procedures.

The effects of vertical location on the flow characteristics below the swept wing are shown in figure 7. The effects of wing lift coefficient on the flow characteristics 15 percent of the local wing chord below the one-half and three-quarter semispan locations of the swept wing are presented in figures 8 and 9, respectively, and for the midsemispan location of the unswept wing in figure 10. The calculated effects of compressibility for a subcritical Mach number of 0.80 and for a vertical location 25 percent of the local wing chord below the midsemispan location of the swept wing are presented in figure 11.

Swept-Wing Model

Examination of the flow characteristics beneath the midsemispan of the swept-wing model at zero lift (fig. 7(a)) indicates the existence of significant chordwise gradients for all the flow parameters. The severity of these gradients diminishes as the distance from the wing is increased.

Comparison of the values predicted by theory with the experimental values indicates that the representation of the airfoil-section thickness distribution by a two-dimensional singularity distribution (ref. 5) modified by simple sweep theory (appendix A) gives excellent qualitative agreement for all vertical locations considered. The magnitudes of the flow parameters due to thickness are, in general, also well predicted, although the downwash angles are underpredicted for the regions immediately ahead of the wing chord.

The flow characteristics at a wing lift coefficient of 0.49 are shown in figure 7(b). The chordwise gradients mentioned previously are seen to be more severe than for the zero-lift condition (fig. 7(a)). For this lift coefficient (0.49) the lift-induced effects, in general, completely overshadow the thickness effects and cause large changes in the downwash and sidewash angles in addition to reductions in the dynamic-pressure ratios.

Good agreement is in evidence for the downwash angles except for the nearest vertical location where the theory overestimates conditions immediately ahead of the wing leading edge. This overestimation is presumed to be due to the assumption in the theory of the two-dimensional type of chordwise load distribution that implies full leading-edge suction and, hence, unrealistically large induced effects in this vicinity.

In the case of the sidewash angles (fig. 7(b)), the assumed finite-step theory is seen to become increasingly inaccurate as the vertical distance from the wing chord plane is decreased. The modified theory (see appendix A), which effects a more realistic variation of sidewash velocity with vertical distance (particularly near the chord plane), is seen generally to agree more closely with the experimental results than does the finite-step method. The modified theory was used in the rest of the incompressible sidewash calculations presented in this paper.

The prediction of the dynamic pressures (fig. 7(b)) by use of the finite-step method is seen to be good for all chordwise and vertical locations presented.

Since it has been shown that the decay in the flow distortions can be calculated, it would be desirable to consider in more detail the predictability of the flow throughout a more complete lift range. A comparison of the theoretical and experimental flow fields existing 15 percent of the local wing chord beneath the midsemispan location of the swept wing is presented in figure 8.

With a change in sign of the flow angles at the most negative lift coefficient ($C_L = -0.53$), the conditions existing on the upper or suction side of the wing when at positive lift may, because of model symmetry, be examined. The flow parameters indicate the existence of extremely high values of downwash and sidewash angularity as well as large dynamic pressures. Examination of the pitching-moment curve presented in figure 5 indicates an unstable break at approximately this lift coefficient in the positive lift range ($C_L = 0.49$), which signifies a loss of lift at the wing tip and indicates the existence of nonpotential flow. The potential-flow theory utilized cannot then be expected to predict the magnitude of the flow parameters for these conditions.

As the lift coefficient is reduced to $C_L = -0.26$, a rather good description of the downwash angles is given by use of theory (fig. 8(a)). Good agreement is also obtained throughout the positive lift range to $C_L = 0.89$, which is rather surprising since at this lift coefficient the flow on the suction side of the wing is nonpotential. At $C_L = 1.09$, the theory is seen to overpredict the downwash ahead of the leading edge and to underpredict it over the chord proper. This is presumed to be due to the rearward movement of the experimental local center of pressure that is associated with leading-edge stalling.

Examination of figures 8(b) and 8(c) indicates that the calculated sidewash angles and dynamic pressures are in reasonable agreement over the entire lift range with the exception of the extreme cases, $C_L = -0.53$ and 1.09 where nonpotential conditions exist.

In order to determine the ability of calculations to predict the effect of spanwise position on the flow characteristics, a comparison with the conditions existing 15 percent of the local wing chord below the three-quarter semispan location of the swept wing is presented in figure 9. The zero-lift flow angles (fig. 9(a)) and dynamic pressures (fig. 9(b)) are well predicted, which indicates that the zero-lift flow characteristics are still essentially two dimensional in nature at $y/\frac{b}{2} = -0.75$. As the lift coefficient is increased, however, the agreement between theory and experiment is seen to deteriorate for the downwash angles (fig. 9(a)) in that the theory gives values too high over the chord region. This overestimation is presumed to be due to assuming a two-dimensional type of chordwise load distribution to exist at this spanwise station for $C_L = 0.23$ and to a combination of the aforementioned in conjunction with the proximity of the rolled-up tip vortex for $C_L = 0.49$. In spite of the defects in predicting the downwash angles, the sidewash angles and dynamic pressures are seen to be reasonably well predicted. It should be noted that the experimental downwash angles are slightly lower at the outboard location $\left(y/\frac{b}{2} = -0.75 \text{ in fig. } 9(a)\right)$ than at the inboard location $\left(y/\frac{b}{2} = -0.50 \text{ in fig. } 8(a)\right)$, whereas the sidewash angles are slightly higher. The dynamic pressures appear to be relatively unaffected by spanwise station for the two stations presented (figs. 8(c) and 9(b)).

Unswept-Wing Model

A comparison of the flow characteristics at a distance 15 percent of the local wing chord beneath the unswept wing is presented in figure 10. The predicted downwash characteristics (fig. 10(a)) are, in general, subject to the same discussion and limitations as those for the swept wing; the only notable differences were the underprediction of the downwash ahead of the leading edge, whereas there was an overprediction for the swept wing (fig. 8(a)). The cause of the nonpotential nature of the flow above the wing chord plane, as evidenced by the break in the pitching-moment curve (fig. 6), is assumed to be due primarily to leading-edge separation.

The comparison between the experimental and theoretical sidewash angles below the unswept wing is shown in figure 10(b). As in the case of the swept wing, significant chordwise gradients exist under lifting conditions. The finite-step theory in which 10 spanwise and 4 chordwise horseshoe vortices were utilized is seen to underpredict the sidewash angles. Increasing the number of spanwise vortices from 10 to 20 and using the estimated surface sidewash velocity (see appendix A) in determining the sidewash velocity variation with vertical distance appear to provide better agreement with experiment over most of the chord. The disagreements existing ahead of the wing-chord leading edge at positive lifts are not fully understood, but some of the disagreement may be due to support-strut interference effects that have not been assessed.

The dynamic pressures (fig. 10(c)) appear to be well predicted throughout the lift-coefficient range investigated with the exception of the largest negative lift coefficient.

The effects of sweepback cannot be adequately determined throughout the lift-coefficient range by comparing the wings of the present investigation since several geometric differences exist other than the angle of sweep. If it is assumed, however, that, for the midsemispan locations, the zero-lift flow characteristics are essentially two dimensional, as indicated by the ability of two-dimensional theory to predict the flow characteristics, some insight is gained as to the effect of sweep. Comparison of the zero-lift downwash angles and dynamic pressure of the swept wing (fig. 8) with the comparable characteristics for the unswept wing (fig. 10) indicates that sweep has little effect on these parameters. The differences that do exist are felt to be due to the difference in thickness ratios. Examination of the sidewash angles (figs. 8(b) and 10(b)) indicates that the effect of wing sweep is to induce larger sidewash angles, at zero lift, in accordance with simple sweep theory. (See appendix A.)

Effects of Compressibility

In the foregoing discussion, the flow-field characteristics were for the incompressible case. It would now be desirable to examine briefly the effects of compressibility on the flow characteristics. Since no experimental data are available at the higher speeds, theoretical comparisons have been made in order to provide at least a qualitative indication of the effect of compressibility.

The calculated compressibility effects, for a subcritical Mach number of 0.80, on the flow characteristics at a distance 25 percent of the local wing chord beneath the midsemispan location of the swept wing are presented in figure 11 for three conditions. The effect of increasing the Mach number on the zero-lift flow characteristics is to cause increases in both the downwash and sidewash angularities as well as the dynamic-pressure ratio, although the basic-flow structure appears to be relatively unchanged. In considering Mach number effects for the lifting condition, as calculated by the finite-step method, it is convenient to examine the effects from two standpoints, namely, the case where α is held constant and the case where C_L is held constant. For the constant α case (fig. 11), the effect of increasing the Mach number is to cause large increases in the positive and negative magnitudes of the downwash angles over the complete chordwise range shown and particularly near the leading edge. Large increases in the region of the leading edge are also evident in the sidewash angles and large decreases occur in the dynamic pressure over the leading-edge portion of the chord; however, the rear 80 percent of the chord appears to be relatively unchanged. Some of these effects are due to the fact that the wing in compressible flow at constant α is generating more lift than the wing in incompressible flow. In order to eliminate these additional lift effects, the effects of compressibility at constant lift are also presented in figure 11. For this condition, the negative and positive magnitudes of the downwash angles are still increased over the incompressible conditions. In the case of the sidewash angles, however, although the compressible values are slightly higher at the leading edge, they are reduced over the chord proper. The compressible dynamic-pressure ratios still appear to be reduced at the leading edge, but to a lesser extent than for the constant α condition, and are actually increased beyond the quarter-chord locations.

CONCLUDING REMARKS

A theoretical and experimental investigation of the subsonic-flow fields beneath swept and unswept wings indicates the existence of significant chordwise gradients in the flow characteristics. These gradients diminish in severity as the distance from the wing chord plane is increased. Increasing the lift coefficient caused large changes in the local downwash and sidewash angles and in the dynamic-pressure ratios. The effect of wing sweep at zero lift was to cause increased sidewash angles.

The theoretical predictions of the flow-field characteristics were qualitatively correct in all cases considered, although there were indications that the magnitude of the downwash angles tended to be overpredicted as the tip of the swept wing was approached and that the sidewash angles ahead of the unswept wing were underpredicted.

The effects of compressibility, as calculated by first-order linear theory, indicated significant increases in the chordwise variations of flow angles and dynamic-pressure ratios for both the zero-lift and lifting cases. The effects of compressibility for the lifting case in which the lift coefficient was held constant were less severe than those for the constant-angle-of-attack case.

Langley Aeronautical Laboratory,
National Advisory Committee for Aeronautics,
Langley Field, Va., April 26, 1956.

APPENDIX A

DETAILED THEORETICAL CONSIDERATIONS

The purpose of this appendix is to present a more detailed description of the calculative procedure described briefly in the text.

The flow is assumed potential and planar, and, hence, the effects of boundary-layer separation and the rolling up and displacement of the trailing vortex wake are neglected. The effects of the presence of the fuselage have been neglected (see fig. 4) for the lateral locations of present interest $\left(y\Big/\frac{b}{2} = 0.5 \text{ and } 0.75\right)$. For regions closer to the fuselage, however, its presence may be considered by methods similar to those reported in references 4 and 7.

A well-established practice in two-dimensional-airfoil theory is to consider independently the effects of thickness and the effects of angle of attack (ref. 19). The present paper also employs this procedure in determining the flow-field characteristics but includes in the nonlifting case first-order three-dimensional effects incurred either by sweep or taper or both; and in the lifting case, both spanwise and chordwise distributions of vorticity are considered in an approximate manner.

Nonlifting Case

In two-dimensional flow, the nonlifting or thickness-induced perturbation velocities are primarily a function of thickness distribution. These perturbation velocities, that is, downwash in the vertical direction and backwash in the chordwise direction, may be calculated either by conformal mapping techniques, as reported in references 12 to 14, or by use of the appropriate singularity (source sink) distribution, as reported in references 5 and 15.

In three-dimensional flow, the problem of determining the perturbation velocities in the field surrounding the wing becomes considerably more complex and requires, in rigorous form, a representation of the wing by an infinite number of singularities which must be integrated over the wing surface (refs. 8 to 11).

Examination of the extensive theoretical investigations of the zero-lift longitudinal or backwash velocity distributions on unswept and swept-back wings reported in references 8 to 11 indicated that it is necessary to determine only the three-dimensional effects incurred either by sweep or taper or both, since the isobars tend to be parallel to lines of constant percent thickness (for regions not very close to the wing root or tip) and since the effect of aspect ratio on the local velocities is negligible (ref. 9) for the aspect ratios considered in the present paper. In view of the foregoing discussion, the following development (zero-lift case) will be primarily two dimensional in nature and will generally consider swept wings by use of simple sweep theory (ref. 6); but the procedure will also be applicable to unswept wings.

The original contribution of simple sweep theory (ref. 6) was to indicate a geometric device by which the critical Mach number of wings could be raised. Reference 6 points out that the wing pressure distribution was chiefly affected by the velocity component normal to the lines of constant percent thickness. In determining the zero-lift or thickness-induced velocities of a swept wing, it is, therefore, necessary to consider the thickness distributions of the airfoil sections normal to the lines of constant percent thickness. These airfoil sections will hereinafter be referred to as normal sections in order to differentiate them from the streamwise sections.

The geometric characteristics necessary in the calculation of the thickness-induced velocities is shown for the swept wing of the present investigation in figure 12. The streamwise chord locations at which the flow-field characteristics are desired are indicated by the data points. The normal sections were assumed to be two dimensional and, therefore, the perturbation velocities generated by these sections, in conjunction with the reduced velocity component $V \cos \Lambda$ could be calculated by either of the two-dimensional-flow techniques mentioned previously (conformal mapping or singularity solution). For the points ahead of the wing leading edge, the sweep angles of the normal sections generating the perturbation velocities at these points (as indicated by the dashed lines in fig. 12) were assumed constant and equal to the sweep angle of the leading edge.

Since the perturbation velocities along and perpendicular to the chords of the normal sections (u_n and w, respectively) have been determined, it is now necessary to determine the components of these velocities relative to the streamwise chord (fig. 12). The downwash velocity w remains unchanged since the effects of the increased normal-section thickness ratio relative to the streamwise-section thickness ratio are canceled by the reduced normal velocity component. The normal-section backwash velocity u_n must, however, be added to the normal-velocity component $V \cos \Lambda$ (fig. 12). These vectors are then combined with the parallel-velocity component $V \sin \Lambda$. This vector addition (fig. 12) determines the direction of the resultant-velocity vector V_R relative to the free-stream direction. This resultant-velocity direction is seen to be toward the plane of symmetry for regions of supervelocity ($V_R > V$) and toward the wing tip for regions of subvelocity ($V_R < V$).

The backwash and sidewash perturbation velocities relative to the free-stream direction are (from the vector diagram of fig. 12)

$$u = u_n \cos \Lambda \tag{A1}$$

$$v = u_n \sin \Lambda \tag{A2}$$

and the flow angles in the vertical and lateral directions are, respectively,

$$\epsilon = \tan^{-1} \frac{w/V}{1 + \frac{u}{V}} = \tan^{-1} \frac{w/V}{1 + \frac{u_n \cos \Lambda}{V}} \tag{A3}$$

$$\sigma = - \tan^{-1} \frac{v/V}{1 + \frac{u}{V}} = - \tan^{-1} \frac{\frac{u_n \sin \Lambda}{V}}{1 + \frac{u_n \cos \Lambda}{V}} \tag{A4}$$

The dynamic-pressure ratios are defined by

$$\frac{q_l}{q_o} = \frac{(V + u)^2 + w^2 + v^2}{V^2} \tag{A5}$$

or, since

$$(w^2 + v^2) \ll (V + u)^2$$

then

$$\frac{q_l}{q_o} \approx \frac{(V + u)^2}{V^2} \approx \left(1 + \frac{u_n \cos \Lambda}{V}\right)^2 \tag{A6}$$

In the foregoing development, it was assumed necessary, because of wing taper, to determine the thickness distributions of each of the sections normal to the lines of constant percent thickness, and then to calculate the perturbation velocities generated by these sections. It is obvious that fulfillment of this assumption would entail a prohibitive amount of computational labor. In order to reduce the computations to practical proportions, it is necessary to introduce certain simplifying assumptions. It was, therefore, assumed that the given tapered swept wing could be replaced by some equivalent infinite-span, swept, untapered wing. The effects of wing taper would be retained, however, in using the correct local sweep angles in equations (A1) and (A2).

In order to evaluate the changes in the airfoil thickness distribution incurred by the foregoing assumption, the thickness distributions of the normal sections (as indicated by sections 1 to 7 in fig. 12) were determined and were found to have maximum thickness ratios of 7.45 to 7.7 percent. These thickness distributions were then compared with the thickness distribution of the streamwise airfoil section which was increased so that its maximum thickness ratio was equivalent to the average maximum thickness ratios of the normal sections (7.6 percent). This comparison is presented in figure 13. It is evident from this figure that wing taper causes some small variations in the thickness distributions, particularly over the rear portion of the chord; however, when consideration is given to the fact that the maximum surface velocity induced on an NACA 65A008 airfoil section is only of the order of 10 percent greater than the free-stream velocity (for zero lift, see ref. 20), it may safely be assumed that these differences in thickness distributions, due to wing taper, are negligible.

Since it has been shown that the given swept wing can be approximated by an infinite-span, swept, untapered wing without incurring any appreciable differences in the airfoil-section thickness distributions, some useful relationships between the assumed infinite-span, swept, untapered wing and an infinite-span, unswept, untapered wing should be noted.

Comparison of an infinite-span, swept, untapered wing with an infinite-span, unswept, untapered wing of the same streamwise thickness ratio indicates that the normal-section thickness ratio of the swept wing is increased by $1/\cos\Lambda$ relative to the streamwise section and that the normal component of the imposed velocity is decreased by $\cos\Lambda$. (See the following sketch.)

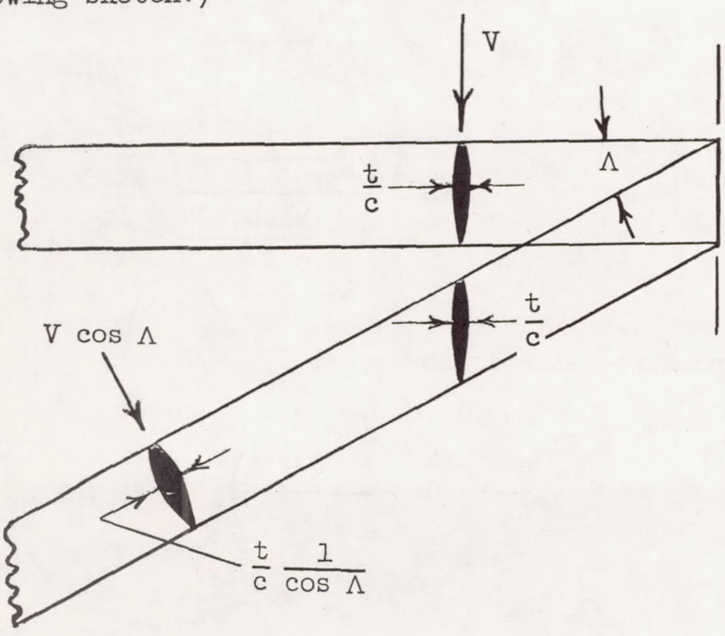

It can, therefore, be reasoned that, since the perturbation velocities are linear functions of thickness, for small thickness ratios (as indicated by an analysis similar to that of ref. 21), the increased thickness effects $\left(\frac{t}{c}\frac{1}{\cos\Lambda}\right)$ are canceled by the reduced velocity $V\cos\Lambda$. The perturbation velocities relative to the normal section of the swept wing are then approximately equal to the perturbation velocities relative to the streamwise section of the unswept, untapered wing; that is,

$$u_n \cong u_s \tag{A7}$$

where u_s is the backwash velocity generated by the streamwise thickness distribution in two-dimensional flow with a free-stream velocity equal to V.

Equations (A1) and (A2) may now be rewritten as

$$u = u_s \cos\Lambda \tag{A8}$$

$$v = u_s \sin\Lambda \tag{A9}$$

and the flow angles given by equations (A3) and (A4) may be rewritten as

$$\epsilon = \tan^{-1}\frac{w/V}{1 + \frac{u_s\cos\Lambda}{V}} \tag{A10}$$

$$\sigma = -\tan^{-1}\frac{\frac{u_s\sin\Lambda}{V}}{1 + \frac{u_s\cos\Lambda}{V}} \tag{A11}$$

The dynamic-pressure ratio is now

$$\frac{q_l}{q_o} \approx \left(1 + \frac{u_s\cos\Lambda}{V}\right)^2 \tag{A12}$$

The present paper utilized the singularity-distribution method of reference 5 in order to calculate the two-dimensional perturbation velocities in the field surrounding the NACA 65A-series airfoils of the swept and unswept wings. These velocities were then modified by the use of equations (A8) and (A9) to account for the three-dimensional-flow effects of either sweep or taper or both. The calculated velocities induced at the midsemispan location of the swept wing at zero lift are presented in figure 14, and the flow-field parameters determined from equations (A10) to (A12) are presented in figure 7(a) for comparison with experiment.

Lifting Case

The general practice of accounting for the wing lift-induced velocities, by employing a single lifting line (approximated by a number of horseshoe vortices), becomes increasingly inaccurate as the vortices are approached. (See ref. 1.) In order to obtain more realistic values of the lift-induced velocities for regions close to the wing, a more detailed accounting of the chordwise distribution of vorticity is required. It should be noted that, if the actual load distributions are known, they would probably greatly enhance the accuracy of the calculations. In the absence of these loadings for the wings of the present investigation, the spanwise loadings were determined by the method of reference 17 and the chordwise load distributions were assumed to be two dimensional in shape with the local circulation strength dictated by the span-load distribution.

The shape function of the two-dimensional chordwise vorticity accumulation ϕ_s is given by reference 16 and may be expressed, with a change in variable, as

$$\frac{d\,\frac{\pi\phi_s}{V\alpha c}}{d\,\frac{x}{c}} = \frac{1}{2}\sqrt{\frac{1 - \frac{x}{c}}{\frac{x}{c}}} \qquad \text{(A13)}$$

It was further assumed that this chordwise accumulation could be approximated by a finite number of vortices of equal strength since the stratagem was to determine where possible, the perturbation velocities, due to the vortices, at points in the field (in the immediate vicinity of the local chord) lying midway between any two adjacent vortex locations, thus effecting some cancellation of the objectionable effects of the single lifting line.

Integration of equation (A13) gives the chordwise accumulation of vorticity as

$$\frac{\pi\phi_s}{V\alpha c} = \frac{1}{2}\sqrt{\frac{x}{c} - \left(\frac{x}{c}\right)^2} + \sin^{-1}\sqrt{\frac{x}{c}}\Bigg|_{(x/c)_1}^{(x/c)_2} \tag{A14}$$

The chordwise limits necessary to insure equal circulation strengths $(x/c)_1$ and $(x/c)_2$ must be determined by trial and error. After these limits are determined, the centroidal locations of the vortices may be found by

$$\frac{\bar{x}}{c} = \frac{\int_{(x/c)_1}^{(x/c)_2} \frac{x}{c}\sqrt{\frac{1 - \frac{x}{c}}{\frac{x}{c}}}\, d\frac{x}{c}}{\int_{(x/c)_1}^{(x/c)_2} \sqrt{\frac{1 - \frac{x}{c}}{\frac{x}{c}}}\, d\frac{x}{c}} \tag{A15}$$

which upon integration gives

$$\frac{\bar{x}}{c} = \frac{\frac{2\frac{x}{c} - 1}{4}\sqrt{\frac{x}{c} - \left(\frac{x}{c}\right)^2} + \frac{1}{8}\sin^{-1}\left(2\frac{x}{c} - 1\right)}{\sqrt{\frac{x}{c} - \left(\frac{x}{c}\right)^2} + \sin^{-1}\sqrt{\frac{x}{c}}}\Bigg|_{(x/c)_1}^{(x/c)_2} \tag{A16}$$

A study of the number of two-dimensional-flow vortices needed to approximate the airfoil boundary conditions, that is, $\alpha = -w/V$, in which combinations of one, two, four, and eight vortices were considered, indicated that one and two vortices were insufficient. Utilization of eight vortices, of course, was found to give the best approximation of those investigated, although this was felt to raise the computations to the prohibitive level. Four chordwise vortices were, therefore, chosen as the best compromise between required labor and the approximation of the boundary conditions. The centroidal locations of these four vortices were found, from equations (A14) and (A16), to be approximately $x/c = 0.013$, 0.092, 0.272, and 0.621.

The vortex arrangements thus chosen to represent the wing plan form consisted of four chordwise horseshoe vortices at each of 10 spanwise stations. The vortex arrangement assumed to represent the swept wing is presented in figure 15.

The equations of the lift-induced perturbation velocities for the assumed vortex arrangement may be expressed as

$$\frac{u_a}{V} = \frac{1}{4\pi Vs} \sum_{n=1}^{n=10} \sum_{m=1}^{m=4} \frac{\Gamma}{4} F_u \tag{A17}$$

$$\frac{v_a}{V} = \frac{1}{4\pi Vs} \sum_{n=1}^{n=10} \sum_{m=1}^{m=4} \frac{\Gamma}{4} F_v \tag{A18}$$

$$\frac{w_a}{V} = \frac{1}{4\pi Vs} \sum_{n=1}^{n=10} \sum_{m=1}^{m=4} \frac{\Gamma}{4} F_w \tag{A19}$$

where F_u, F_v, and F_w are the geometric functions associated with a unit horseshoe vortex. The equations of these functions, as given in reference 16, with the appropriate sign changes and nondimensionalized with respect to the semiwidth s of the vortex, are presented in appendix B. The values of these functions over a wide range of distances are presented in tables III to V.

Since 10 spanwise vortices were assumed in the present investigation, the semiwidth of each horseshoe vortex is

$$s = \frac{b}{20} \tag{A20}$$

The circulation strength Γ may also be related to the local section lift coefficient by

$$\Gamma = \frac{c_l cV}{2} \tag{A21}$$

Equations (A17) to (A19) may now be expressed as

$$\frac{u_a}{VC_L} = \frac{5}{2\pi A} \sum_{n=1}^{n=10} \sum_{m=1}^{m=4} \frac{c_l c}{4C_L c_{av}} F_u \tag{A22}$$

$$\frac{v_a}{VC_L} = \frac{5}{2\pi A} \sum_{n=1}^{n=10} \sum_{m=1}^{m=4} \frac{c_l c}{4C_L c_{av}} F_v \tag{A23}$$

$$\frac{w_a}{VC_L} = \frac{5}{2\pi A} \sum_{n=1}^{n=10} \sum_{m=1}^{m=4} \frac{c_l c}{4C_L c_{av}} F_w \tag{A24}$$

The lift-induced velocities were computed for the wing plan forms of the present investigation by use of equations (A22) to (A24) by using the span-load distributions presented in figure 16 as determined by the method of reference 17. A sample calculation of the lift-induced velocities for each unit of lift coefficient for the swept wing is presented in table II. The velocities induced at several vertical locations below the midsemispan location of the swept wing are presented in figure 17.

A study of the lift-induced velocities indicated that the downwash and backwash velocities calculated by use of equations (A22) and (A24) (fig. 17) had the correct qualitative variation with vertical distance, whereas the sidewash velocities did not. Examination of the sidewash velocity factor F_V (see eq. (B6)) indicates that when a finite number of horseshoe vortices are used the sidewash velocity for small vertical distances must approach, at the surface, either zero or become infinite, depending on whether the point of interest lies between the trailing vortices or directly under a trailing-vortex segment. The points of interest in the present calculations were chosen midway between the trailing segments of the horseshoe vortices and, hence, approach zero as the wing chord plane is approached. In reality, this condition does not exist since the lateral gradient in loading or vorticity implies the existence of sidewash velocities at the wing surface. Clearly, then, sidewash velocities calculated by use of the finite-step method (eq. (A23)), where the sidewash velocity is zero at the wing surface, would yield much smaller values for points close to the wing (fig. 17) than would a method accounting for the finite sidewash at the wing surface.

Unpublished theoretical studies (eqs. (A25) to (A32)) made by Percy J. Bobbitt of the Langley Laboratory have indicated that a more realistic value of the sidewash velocity variation with vertical distance could be obtained by estimating the sidewash velocity at the wing chord plane due to the lateral gradient in the velocity potential (referred to herein as the chordwise accumulation of vorticity) and then by fairing the maximum sidewash velocity in the wing field, as calculated by equations (A23) and (B6), to this chord-plane velocity. The sidewash velocity at the wing chord plane may be determined from the lateral gradient in the chordwise accumulation of vorticity which may be expressed as

$$v_a = \frac{\partial \phi(x,y)}{\partial y} \tag{A25}$$

which may be nondimensionalized as

$$\frac{v_a}{VC_L} = \frac{\partial \dfrac{\phi(x,y)}{VC_L \frac{b}{2}}}{\partial \dfrac{y}{b/2}} \tag{A26}$$

In the absence of experimental information regarding the chordwise accumulation of vorticity ϕ for the wings of the present investigation, the two-dimensional vorticity accumulation given by equation (A14) was assumed. In order that the total circulation of the system be correct, the total chordwise circulation strengths must be corrected to agree with the strengths of spanwise vorticity distribution. Thus, equation (A14) may be expressed as

$$\frac{\phi_s}{VC_L \frac{b}{2}} = \frac{c}{\pi b C_{L_\alpha}}\left[\sqrt{\frac{x}{c} - \left(\frac{x}{c}\right)^2} + \sin^{-1}\sqrt{\frac{x}{c}}\right] \tag{A27}$$

Since

$$2\phi_{s,te} = \Gamma_s$$

evaluation of equation (A27) at the trailing edge of the chord $(x/c = 1.0)$ gives

$$\frac{\Gamma_s}{VC_L \frac{b}{2}} = \frac{c}{bC_{L_\alpha}} \tag{A28}$$

The three-dimensional vorticity equation given by equation (A21) may be nondimensionalized as

$$\frac{\Gamma}{VC_L \frac{b}{2}} = \frac{1}{A} \frac{c_l c}{C_L c_{av}} \tag{A29}$$

The two-dimensional circulation strength (eq. (A28)) may now be corrected to the three-dimensional value (eq. (A29)) by defining a correction factor K as the ratio of equation (A29) to (A28).

$$K = \frac{\Gamma}{\Gamma_s} = \frac{b}{cA} C_{L_\alpha} \frac{c_l c}{C_L c_{av}} \tag{A30}$$

Multiplying equation (A27) by the correction factor (eq. (A30)) gives

$$\frac{\phi(x,y)}{VC_L \frac{b}{2}} = \frac{1}{\pi A}\left(\frac{c_l c}{C_L c_{av}}\right)\left[\sqrt{\frac{x}{c} - \left(\frac{x}{c}\right)^2} + \sin^{-1}\sqrt{\frac{x}{c}}\right] \tag{A31}$$

which is the assumed chordwise vorticity accumulation in terms of the correct local total circulation strength.

An approximate expression for the sidewash velocity existing at the wing chord plane may now be obtained by substituting equation (A31) into equation (A26):

$$\frac{v_a}{VC_L} = \frac{\partial \dfrac{\phi(x,y)}{VC_L \dfrac{b}{2}}}{\partial \dfrac{y}{b/2}} \approx \frac{1}{\pi A} \frac{\partial \left\{ \dfrac{c_l c}{C_L c_{av}} \left[\sqrt{\dfrac{x}{c} - \left(\dfrac{x}{c}\right)^2} + \sin^{-1}\sqrt{\dfrac{x}{c}} \right] \right\}}{\partial \dfrac{y}{b/2}} \tag{A32}$$

Inasmuch as it is difficult to express the geometric characteristics of the swept wing in analytic terms amenable for use in equation (A32), the required differentiation may best be performed graphically. An illustrated example of this procedure is presented for the swept wing in figure 18, and the manner in which the sidewash velocities existing in the field are faired to the estimated chord-plane velocity is shown in figure 19.

Further studies of the sidewash-velocity variation with vertical distance made by increasing the number of spanwise horseshoe vortices also indicated more realistic characteristics except for vertical locations very close to the wing chord plane. These characteristics have previously been reported in reference 22 for somewhat different circumstances. The effects of increasing the number of spanwise horseshoe vortices on the variation of sidewash velocity with vertical distance are shown for the unswept wing in figure 20.

The flow-field characteristics due to the lift-induced velocities may now be determined by

$$\epsilon = \tan^{-1}\left(\frac{\dfrac{w_a}{VC_L} C_L}{1 + \dfrac{u_a}{VC_L} C_L}\right) \tag{A33}$$

$$\sigma = -\tan^{-1}\left(\frac{\dfrac{v_a}{VC_L} C_L}{1 + \dfrac{u_a}{VC_L} C_L}\right) \tag{A34}$$

$$\frac{q_l}{q_o} = \left(1 + \frac{u_a}{VC_L} C_L\right)^2 + \left(\frac{v_a}{VC_L} C_L\right)^2 + \left(\frac{w_a}{VC_L} C_L\right)^2 \tag{A35}$$

Combined Effects

In order to determine the total flow characteristics, it is necessary to combine the lifting and nonlifting velocities. The total flow-field characteristics may be written as

$$\epsilon = \tan^{-1}\left(\frac{\frac{w}{V} + \frac{w_a}{VC_L} C_L}{1 + \frac{u_s \cos \Lambda}{V} + \frac{u_a}{VC_L} C_L}\right) \tag{A36}$$

$$\sigma = - \tan^{-1}\left(\frac{\frac{u_s}{V} \sin \Lambda + \frac{v_a}{VC_L} C_L}{1 + \frac{u_s \cos \Lambda}{V} + \frac{u_a}{VC_L} C_L}\right) \tag{A37}$$

$$\frac{q_l}{q_o} = \left(1 + \frac{u_s}{V} \cos \Lambda + \frac{u_a}{VC_L} C_L\right)^2 + \left(\frac{w_a}{VC_L} C_L\right)^2 + \left(\frac{v_a}{VC_L} C_L\right)^2 \tag{A38}$$

In order to eliminate errors involved in estimating the lift-curve slopes of the wings under consideration, the comparisons of theory with experiment were made at the same lift coefficient. A comparison of the theoretical flow fields with experiment, under lifting conditions, beneath the midsemispan location of the sweptback wing as calculated by equations (A36) to (A38) is presented in figure 7(b).

Effects of Compressibility

In determining the first-order compressibility effects on the flow-field characteristics, the three-dimensional Prandtl-Glauert transformation, as given by reference 18, may be used. The general computational procedures involved in this transformation have been stated very simply by Dr. S. Katzoff of the Langley Laboratory and are presented in the subsequent discussion:

> The incremental velocities at a point P on the surface of a thin body B in compressible flow may be obtained in three steps:
>
> (1) The x-coordinates of all points of B are increased by the factor $1/\beta$, where $\beta = \sqrt{1 - M^2}$ and where the x-axis is in the stream direction. This transformation changes B into a stretched body B'.
>
> (2) The incremental velocities u', v', and w' in the direction of the x-, y-, and z-axes, respectively, at the point P' on B' corresponding to the point P on B are calculated as though B' were in an incompressible flow having the same free-stream velocity as the original compressible flow.
>
> (3) The values u, v, and w of the incremental velocities at the point P on the original unstretched body B in compressible flow are then found by the equations

$$u = \frac{1}{\beta^2} u' \tag{A39}$$

$$v = \frac{1}{\beta} v' \tag{A40}$$

$$w = \frac{1}{\beta} w' \tag{A41}$$

It is pertinent to note that the result of step (1), that is, stretching the wing chord, causes the transformed wing to have an increased angle of sweep, a decreased aspect ratio, a decreased thickness ratio, and a decreased angle of attack. The relationship between the geometric parameters of the given wing in compressible flow and its transformed equivalent wing in incompressible flow may be expressed as

$$\frac{x'}{c'} = \frac{x}{c} \tag{A42}$$

$$\frac{z'}{c'} = \beta \frac{z}{c} \tag{A43}$$

$$\frac{t'}{c'} = \beta \frac{t}{c} \tag{A44}$$

$$\frac{y'}{b'/2} = \frac{y}{b/2} \tag{A45}$$

$$A' = \beta A \tag{A46}$$

$$\Lambda' = \tan^{-1}\left(\frac{\tan \Lambda}{\beta}\right) \tag{A47}$$

$$\alpha' = \beta\alpha \tag{A48}$$

The perturbation velocities in the field due to the transformed wing in incompressible flow, as indicated by step (2), may now be calculated by the methods mentioned previously in this appendix. It should be noted, however, that, although the chordwise and spanwise locations of interest remain unchanged in the transformation, as indicated by equations (A42) and (A45), the vertical locations of interest move closer in percent of local chord to the equivalent transformed wing chord plane. (See eq. (A43).)

In accordance with step (3) of Katzoff's general directions, the perturbation velocities due to the transformed wing may now be resolved into their final form by equations (A39) to (A41).

A few specific observations, supplementary to the foregoing general procedure, are appropriate inasmuch as they may somewhat reduce the necessary computations.

Nonlifting case.- If the first step of the transformation, that is, stretching the plan form in the x-direction, which is shown for the swept wing in figure 21, is assumed to have been completed, it may be observed from equation (A44) that the thickness ratio is reduced by β. Also, if it is noted from equations (A39) to (A41) that the perturbation velocities must be increased by inverse functions of β, it is apparent that some beneficial (time saving) cancellation effects might be realized. Care must be taken, however, that the correct relationship between corresponding vertical locations are used (eq. (A43)).

In view of the foregoing discussion, it is readily seen that the downwash velocity w remains unchanged since the reduced thickness effects (eq. (A44)) are canceled by equation (A41). The downwash w at location $-\frac{1}{\beta}\frac{z}{c}$ below the wing in compressible flow is then equal to the downwash w at a location $-z/c$ below the wing in incompressible flow. This simple transformation of vertical locations is possible since the downwash velocity at zero lift is independent of the wing sweep angle (as shown previously in this appendix).

In the case of the backwash and sidewash velocities, although some cancellation of the thickness effects are realized, a simple transformation of vertical distances is not immediately possible since these velocities are also a function of the transformed wing sweep angle (eqs. (A8), (A9), and (A47)). Some saving is possible, however, by considering equations (A8), (A9), (A39), (A40), and (A47), and noting by use of equation (A44) that $u_s' = \beta u_s$, from which the following may be deduced:

$$v = u_s \sin \Lambda \frac{\sin \Lambda'}{\sin \Lambda} \tag{A49}$$

$$u = \frac{u_s \cos \Lambda}{\beta} \frac{\cos \Lambda'}{\cos \Lambda} \tag{A50}$$

where again the corresponding vertical locations in compressible and incompressible flow (as given by eq. (A43)) must be observed.

With the perturbation velocities now determined, the flow-field characteristics in compressible flow, for subcritical Mach numbers, for nonlifting conditions may be found by equations (A10) to (A12).

The calculated first-order zero-lift compressibility effects, for a subcritical Mach number of 0.8, on the flow-field characteristics beneath the midsemispan location of the swept wing are presented in figure 11.

Lifting case.- In calculating the effects of compressibility on the lift-induced perturbation velocities, it is necessary to follow only the general outlined procedure. The perturbation velocities at corresponding vertical locations (given by eq. (A43)) may then be expressed, by use of equations (A22) to (A24) and (A39) to (A41), as

$$\frac{u_a}{VC_L} = \frac{1}{\beta^2}\frac{u_a'}{VC_L'} \tag{A51}$$

$$\frac{v_a}{VC_L} = \frac{1}{\beta}\frac{v_a'}{VC_L'} \tag{A52}$$

$$\frac{w_a}{VC_L} = \frac{1}{\beta}\frac{w_a'}{VC_L'} \tag{A53}$$

If comparing the effects of compressibility on the flow-field characteristics on a constant α basis is desirable and the calculations are performed on the basis of unit lift coefficient, as it is generally convenient to do, some care must be exercised in the lift-coefficient reduction in order to obtain the proper α.

Since

$$C_L' = \left(C_{L_\alpha}\right)'\alpha' \tag{A54}$$

then substituting equation (A48) into equation (A54) gives

$$C_L' = \left(C_{L_\alpha}\right)'\beta\alpha \tag{A55}$$

where $\left(C_{L_\alpha}\right)'$ is the lift-curve slope of the equivalent transformed wing and is not to be confused with the true compressible lift-curve slope.

The equations for the perturbation velocities (A51) to (A53) for a constant α comparison may now be expressed by

$$\left(\frac{u_a}{V}\right)_{\alpha=\text{Constant}} = \frac{1}{\beta} \frac{u_a'}{VC_L'} \left(C_{L_\alpha}\right)'\alpha \qquad \text{(A56)}$$

$$\left(\frac{v_a}{V}\right)_{\alpha=\text{Constant}} = \frac{v_a'}{VC_L'}\left(C_{L_\alpha}\right)'\alpha \qquad \text{(A57)}$$

$$\left(\frac{w_a}{V}\right)_{\alpha=\text{Constant}} = \frac{w_a'}{VC_L'}\left(C_{L_\alpha}\right)'\alpha \qquad \text{(A58)}$$

The calculated compressibility effects, at constant α, on the flow-field characteristics beneath the midsemispan location of the swept wing calculated by the aforementioned equations and combined with the zero-lift perturbation effects are presented in figure 11.

If it is desired to determine the calculated effects of compressibility on the flow-field characteristics on the basis of constant lift coefficient, it is necessary to decrease only the lift-induced perturbation velocities at constant α, as given by equations (A56) to (A58), by the ratio of the incompressible lift-curve slope to the true compressible lift-curve slope.

The compressible lift-curve slope of the swept wing used in the present paper was determined from the equation

$$C_{L_{\alpha,M}} = \frac{c_{l_\alpha} A}{\frac{c_{l_\alpha}}{\pi} + \sqrt{\left(\frac{A}{\cos \Lambda_{c/2}}\right)^2 + \left(\frac{c_{l_\alpha}}{\pi}\right)^2 - (AM)^2}} \qquad \text{(A59)}$$

This expression, which was developed by Edward C. Polhamus of the Langley Laboratory in 1949, is an improved version, with regard to low aspect ratios and compressibility effects, of that presented in reference 23. Another, but somewhat more complicated, form of this equation has been independently developed in reference 24. With regard to the use of the sweep of the half-chord line in equation (A59), a recent unpublished analysis by Polhamus indicates that there is little effect of taper ratio for wings having the same half-chord-line sweep angles.

The calculated compressibility effects, at constant lift, on the flow-field characteristics beneath the midsemispan location of the swept wing are presented in figure 11.

APPENDIX B

DOWNWASH, SIDEWASH, AND BACKWASH FUNCTIONS DUE

TO A UNIT HORSESHOE VORTEX

The positive directions of distances and velocities used in determining the induction characteristics of a unit horseshoe vortex are defined in the following sketch:

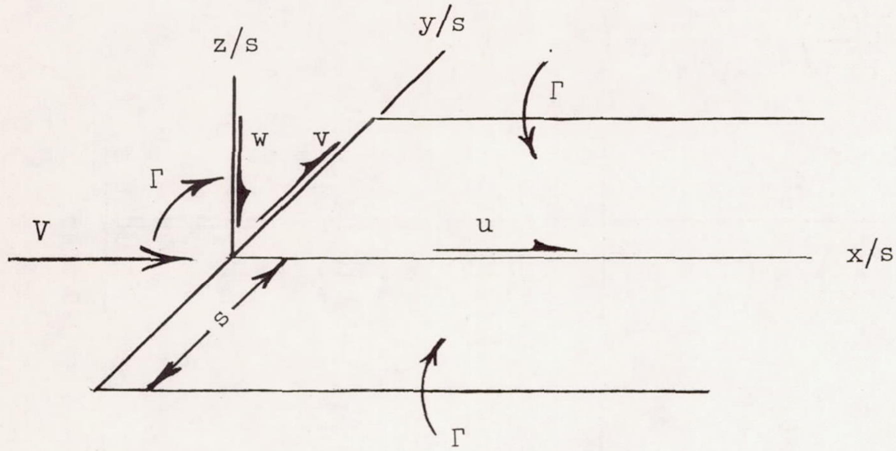

Downwash Equation

The downwash velocity induced at a point in space is given by the following equation:

$$\frac{w_a}{V} = \frac{\Gamma}{4\pi Vs} F_w \tag{B1}$$

where

$$F_W = \frac{\frac{\Delta x}{s}}{\left(\frac{\Delta x}{s}\right)^2 + \left(\frac{\Delta z}{s}\right)^2}\left[\frac{\frac{\Delta y}{s} + 1}{\sqrt{\left(\frac{\Delta x}{s}\right)^2 + \left(\frac{\Delta z}{s}\right)^2 + \left(\frac{\Delta y}{s} + 1\right)^2}} - \frac{\frac{\Delta y}{s} - 1}{\sqrt{\left(\frac{\Delta x}{s}\right)^2 + \left(\frac{\Delta z}{s}\right)^2 + \left(\frac{\Delta y}{s} - 1\right)^2}}\right] - \frac{\frac{\Delta y}{s} - 1}{\left(\frac{\Delta z}{s}\right)^2 + \left(\frac{\Delta y}{s} - 1\right)^2}\left[1 + \frac{\frac{\Delta x}{s}}{\sqrt{\left(\frac{\Delta x}{s}\right)^2 + \left(\frac{\Delta z}{s}\right)^2 + \left(\frac{\Delta y}{s} - 1\right)^2}}\right] + \frac{\frac{\Delta y}{s} + 1}{\left(\frac{\Delta z}{s}\right)^2 + \left(\frac{\Delta y}{s} + 1\right)^2}\left[1 + \frac{\frac{\Delta x}{s}}{\sqrt{\left(\frac{\Delta x}{s}\right)^2 + \left(\frac{\Delta z}{s}\right)^2 + \left(\frac{\Delta y}{s} + 1\right)^2}}\right] \tag{B2}$$

Some identities, due to the symmetry of the aforementioned equations, which increase the useful range of table III are given by

$$\left.\begin{aligned} F_W\left(\frac{\Delta x}{s}, \frac{\Delta y}{s}, \frac{\Delta z}{s}\right) &= F_W\left(\frac{\Delta x}{s}, -\frac{\Delta y}{s}, \frac{\Delta z}{s}\right) \\ &= F_W\left(\frac{\Delta x}{s}, -\frac{\Delta y}{s}, -\frac{\Delta z}{s}\right) \\ &= F_W\left(\frac{\Delta x}{s}, \frac{\Delta y}{s}, -\frac{\Delta z}{s}\right) \end{aligned}\right\} \tag{B3}$$

and

$$\left.\begin{aligned} F_W\left(-\frac{\Delta x}{s}, \frac{\Delta y}{s}, \frac{\Delta z}{s}\right) &= F_W\left(-\frac{\Delta x}{s}, -\frac{\Delta y}{s}, \frac{\Delta z}{s}\right) \\ &= F_W\left(-\frac{\Delta x}{s}, -\frac{\Delta y}{s}, -\frac{\Delta z}{s}\right) \\ &= F_W\left(-\frac{\Delta x}{s}, \frac{\Delta y}{s}, -\frac{\Delta z}{s}\right) \end{aligned}\right\} \tag{B4}$$

Sidewash Equation

The sidewash velocity induced at a point in space is given by the following equation:

$$\frac{v_a}{V} = \frac{\Gamma}{4\pi V s} F_V \tag{B5}$$

where

$$F_V = -\frac{\frac{\Delta z}{s}}{\left(\frac{\Delta z}{s}\right)^2 + \left(\frac{\Delta y}{s} - 1\right)^2}\left[1 + \frac{\frac{\Delta x}{s}}{\sqrt{\left(\frac{\Delta x}{s}\right)^2 + \left(\frac{\Delta z}{s}\right)^2 + \left(\frac{\Delta y}{s} - 1\right)^2}}\right] +$$

$$\frac{\frac{\Delta z}{s}}{\left(\frac{\Delta z}{s}\right)^2 + \left(\frac{\Delta y}{s} + 1\right)^2}\left[1 + \frac{\frac{\Delta x}{s}}{\sqrt{\left(\frac{\Delta x}{s}\right)^2 + \left(\frac{\Delta z}{s}\right)^2 + \left(\frac{\Delta y}{s} + 1\right)^2}}\right] \tag{B6}$$

Some identities, due to the symmetry of the aforementioned equations, which increase the useful range of table IV are given by

$$\left.\begin{aligned} F_V\left(\frac{\Delta x}{s}, \frac{\Delta y}{s}, \frac{\Delta z}{s}\right) &= F_V\left(\frac{\Delta x}{s}, -\frac{\Delta y}{s}, -\frac{\Delta z}{s}\right) \\ &= -F_V\left(\frac{\Delta x}{s}, -\frac{\Delta y}{s}, \frac{\Delta z}{s}\right) \\ &= -F_V\left(\frac{\Delta x}{s}, \frac{\Delta y}{s}, -\frac{\Delta z}{s}\right) \end{aligned}\right\} \tag{B7}$$

and

$$\left.\begin{aligned} F_V\left(-\frac{\Delta x}{s}, \frac{\Delta y}{s}, \frac{\Delta z}{s}\right) &= F_V\left(-\frac{\Delta x}{s}, -\frac{\Delta y}{s}, -\frac{\Delta z}{s}\right) \\ &= -F_V\left(-\frac{\Delta x}{s}, \frac{\Delta y}{s}, -\frac{\Delta z}{s}\right) \\ &= -F_V\left(-\frac{\Delta x}{s}, \frac{\Delta y}{s}, -\frac{\Delta z}{s}\right) \end{aligned}\right\} \tag{B8}$$

Backwash Equation

The backwash velocity induced at a point in space is given by the following equation:

$$\frac{u_a}{V} = \frac{\Gamma}{4\pi Vs} F_u \tag{B9}$$

where

$$F_u = \frac{\frac{\Delta z}{s}}{\left(\frac{\Delta x}{s}\right)^2 + \left(\frac{\Delta z}{s}\right)^2}\left[\frac{\frac{\Delta y}{s} + 1}{\sqrt{\left(\frac{\Delta x}{s}\right)^2 + \left(\frac{\Delta z}{s}\right)^2 + \left(\frac{\Delta y}{s} + 1\right)^2}} - \frac{\frac{\Delta y}{s} - 1}{\sqrt{\left(\frac{\Delta x}{s}\right)^2 + \left(\frac{\Delta z}{s}\right)^2 + \left(\frac{\Delta y}{s} - 1\right)^2}}\right] \tag{B10}$$

Some identities, due to the symmetry of the aforementioned equations, which increase the useful range of table V are given by

$$\left.\begin{aligned} F_u\left(\frac{\Delta x}{s}, \frac{\Delta y}{s}, \frac{\Delta z}{s}\right) &= F_u\left(-\frac{\Delta x}{s}, \frac{\Delta y}{s}, \frac{\Delta z}{s}\right) \\ &= F_u\left(-\frac{\Delta x}{s}, -\frac{\Delta y}{s}, \frac{\Delta z}{s}\right) \\ &= F_u\left(\frac{\Delta x}{s}, -\frac{\Delta y}{s}, \frac{\Delta z}{s}\right) \end{aligned}\right\} \tag{B11}$$

and

$$\left.\begin{aligned} F_u\left(\frac{\Delta x}{s}, \frac{\Delta y}{s}, -\frac{\Delta z}{s}\right) &= F_u\left(-\frac{\Delta x}{s}, -\frac{\Delta y}{s}, -\frac{\Delta z}{s}\right) \\ &= F_u\left(\frac{\Delta x}{s}, -\frac{\Delta y}{s}, -\frac{\Delta z}{s}\right) \\ &= -F_u\left(\frac{\Delta x}{s}, \frac{\Delta y}{s}, \frac{\Delta z}{s}\right) \end{aligned}\right\} \tag{B12}$$

REFERENCES

1. Silverstein, Abe, Katzoff, S., and Bullivant, W. Kenneth: Downwash and Wake Behind Plain and Flapped Airfoils. NACA Rep. 651, 1939.

2. Silverstein, Abe, and Katzoff, S.: Design Charts for Predicting Downwash angles and Wake Characteristics Behind Plain and Flapped Wings. NACA Rep. 648, 1939.

3. Diederich, Franklin W.: Charts and Tables for Use in Calculations of Downwash of Wings of Arbitrary Plan Form. NACA TN 2353, 1951.

4. Zlotnick, Martin, and Robinson, Samuel W., Jr.: A Simplified Mathematical Model for Calculating Aerodynamic Loading and Downwash for Wing-Fuselage Combinations With Wings of Arbitrary Plan Form. NACA TN 3057, 1954. (Supersedes NACA RM L52J27a.)

5. Smith, R. H.: Aerodynamic Theory and Test of Strut Forms - I. NACA Rep. 311, 1929.

6. Jones, Robert T.: Wing Plan Forms for High-Speed Flight. NACA Rep. 863, 1947. (Supersedes NACA TN 1033.)

7. Letko, William, and Danforth, Edward, C. B., III: Theoretical Investigation at Subsonic Speeds of the Flow Ahead of a Slender Inclined Parabolic-Arc Body of Revolution and Correlation With Experimental Data Obtained at Low Speeds. NACA TN 3205, 1954.

8. Neumark, S.: Velocity Distribution on Straight and Swept-Back Wings of Small Thickness and Infinite Aspect Ratio at Zero Incidence. R. & M. No. 2713, British A.R.C., May 1947.

9. Neumark, S., and Collingbourne, J.: Velocity Distribution on Untapered Sheared and Swept-Back Wings of Small Thickness and Finite Aspect Ratio at Zero Incidence. R. & M. No. 2717, British A.R.C., Mar. 1949.

10. Neumark, S.: Critical Mach Numbers for Thin Untapered Swept Wings at Zero Incidence. R. & M. No. 2821, British A.R.C., Nov. 1949.

11. Neumark, S.: Critical Mach Numbers for Swept-Back Wings. Aero. Quarterly, vol. II, pt. II, Aug. 1950, pp. 85-110.

12. Theordorsen, T., and Garrick, I. E.: General Potential Theory of Arbitrary Wing Sections. NACA Rep. 452, 1933.

13. Von Kármán, Th., and Burgers, J. M.: General Aerodynamic Theory - Perfect Fluids. Theory of Airplane Wings of Infinite Span. Vol. II of Aerodynamic Theory, div. E, ch. II, sec. 21, W. F. Durand, ed., Julius Springer (Berlin), 1935, p. 80. (Reprinted 1943.)

14. Chang, Kwei-Lien: The Potential Theory Around Given Wing Sections. Jour. Aero. Sci., vol. 16, no. 5, May 1949, pp. 306-310.

15. Keune, F.: Two-Dimensional Potential Flow Past an Ordinary Thick Wing Profile. NACA TM 1023, 1942.

16. Glauert, H.: The Elements of Aerofoil and Airscrew Theory. Second ed., Cambridge Univ. Press, 1947, pp. 158-159. (Reprinted 1948.)

17. Campbell, George S.: A Finite-Step Method for the Calculation of Span Loadings of Unusual Plan Forms. NACA RM L50L13, 1951.

18. Göthert, B.: Plane and Three-Dimensional Flow at High Subsonic Speeds. NACA TM 1105, 1946.

19. Abbott, Ira H., Von Doenhoff, Albert E., and Stivers, Louis S., Jr.: Summary of Airfoil Data. NACA Rep. 824, 1945. (Supersedes NACA WR L-560.)

20. Loftin, Laurence K., Jr.: Theoretical and Experimental Data for a Number of NACA 6A-Series Airfoil Sections. NACA Rep. 903, 1948. (Supersedes NACA TN 1368.)

21. Allen, H. Julian: General Theory of Airfoil Sections Having Arbitrary Shape or Pressure Distribution. NACA Rep. 833, 1945.

22. Michael, William H., Jr.: Analysis of the Effects of Wing Interference on the Tail Contributions to the Rolling Derivatives. NACA Rep. 1086, 1952. (Supersedes NACA TN 2332.)

23. Polhamus, Edward C.: A Simple Method of Estimating the Subsonic Lift and Damping in Roll of Sweptback Wings. NACA TN 1862, 1949.

24. Diederich, Franklin W.: A Plan-Form Parameter for Correlating Certain Aerodynamic Characteristics of Swept Wings. NACA TN 2335, 1951.

TABLE I.- FUSELAGE ORDINATES

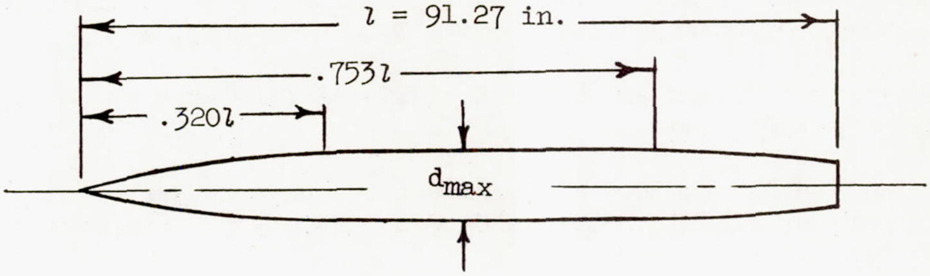

Ordinates, percent length	
Station	Radius
0	0
3.28	.91
6.57	1.71
9.86	2.41
13.15	3.00
16.43	3.50
19.72	3.90
23.01	4.21
26.29	4.43
29.58	4.53
32.00	4.57
75.34	4.57
76.69	4.54
79.98	4.38
83.26	4.18
86.55	3.95
89.84	3.72
93.13	3.49
96.41	3.26
100.00	3.02

TABLE II.- SAMPLE CALCULATION OF LIFT-INDUCED VELOCITIES

BENEATH THE SWEPT-WING MODEL BY USE OF

EQUATIONS (A22) TO (A24)

$\left[y \Big/ \frac{b}{2} = -0.5;\ \frac{x}{c} = 0.45;\ \frac{{}^{*}z}{c} = -0.10 \right]$

n	m	$\frac{c_l c}{4C_L c_{av}}$	$\frac{\Delta x}{s}$	$\frac{\Delta y}{s}$	F_w	(6) × (3)	F_v	(8) × (3)	F_u	(10) × (3)
(1)	(2)	(3)	(4)	(5)	(6)	(7)	(8)	(9)	(10)	(11)
1	1	0.1592	-2.40	4	-0.06089	-0.00969	0.00970	0.00154	-0.01037	-0.00165
	2	.1592	-2.60	4	-.05705	-.00908	.00862	.00137	-.00965	-.00154
	3	.1592	-3.10	4	-.04806	-.00765	.00615	.00098	-.00796	-.00127
	4	.1592	-4.10	4	-.03522	-.00561	.00341	.00054	-.00540	-.00086
2	1	0.2285	-0.10	2	-0.45168	-0.10321	0.31150	0.07118	-0.18147	-0.04147
	2	.2285	-.40	2	-.38099	-.08706	.21825	.04987	-.16563	-.03785
	3	.2285	-1.10	2	-.24501	-.05598	.08612	.01968	-.10022	-.02290
	4	.2285	-2.50	2	-.10915	-.02494	.01779	.00407	-.03335	-.00762
3	1	0.2695	2.20	0	3.38626	0.91260	0	0	-0.08891	-0.02396
	2	.2695	1.80	0	3.43737	.92637	0	0	-.13266	-.03575
	3	.2695	.90	0	3.78603	1.02034	0	0	-.67532	-.18200
	4	.2695	-.90	0	-.58603	-.15794	0	0	-.67532	-.18200
4	1	0.2915	4.40	-2	-0.90675	-0.26432	-0.68894	-0.20083	-0.00909	-0.00265
	2	.2915	3.90	-2	-.89736	-.26158	-.68762	-.20044	-.01197	-.00349
	3	.2915	2.80	-2	-.85954	-.25056	-.67932	-.19802	-.02599	-.00758
	4	.2915	.70	-2	-.63479	-.18504	-.54483	-.15882	-.13726	-.04001
5	1	0.2975	6.70	-4	-0.23453	-0.06977	-0.06754	-0.02009	-0.00221	-0.00066
	2	.2975	6.10	-4	-.23223	-.06909	-.06732	-.02003	-.00260	-.00077
	3	.2975	4.80	-4	-.22374	-.06656	-.06617	-.01969	-.00417	-.00124
	4	.2975	2.30	-4	-.18981	-.05647	-.05826	-.01733	-.01073	-.00319
6	1	0.2975	6.70	-6	-0.09739	-0.02897	-0.01831	-0.00545	-0.00143	-0.00043
	2	.2975	6.10	-6	-.09579	-.02850	-.01826	-.00543	-.00162	-.00048
	3	.2975	4.80	-6	-.09095	-.02706	-.01758	-.00523	-.00224	-.00067
	4	.2975	2.30	-6	-.07601	-.02261	-.01468	-.00437	-.00388	-.00115
7	1	0.2915	4.40	-8	-0.04652	-0.01356	-0.00668	-0.00195	-0.00133	-0.00039
	2	.2915	3.90	-8	-.04518	-.01317	-.00648	-.00189	-.00144	-.00042
	3	.2915	2.80	-8	-.04177	-.01218	-.00598	-.00174	-.00167	-.00049
	4	.2915	.70	-8	-.03412	-.00994	-.00452	-.00132	-.00198	-.00058
8	1	0.2695	2.20	-10	-0.02437	-0.00657	-0.00268	-0.00072	-0.00095	-0.00026
	2	.2695	1.80	-10	-.02377	-.00641	-.00257	-.00069	-.00097	-.00026
	3	.2695	.90	-10	-.02186	-.00589	-.00231	-.00062	-.00100	-.00027
	4	.2695	-.90	-10	-.01824	-.00492	-.00175	-.00047	-.00100	-.00027
9	1	0.2285	-0.10	-12	-0.01380	-0.00315	-0.00115	-0.00026	-0.00058	-0.00013
	2	.2285	-.40	-12	-.01345	-.00307	-.00111	-.00025	-.00058	-.00013
	3	.2285	-1.10	-12	-.01263	-.00289	-.00101	-.00023	-.00058	-.00013
	4	.2285	-2.50	-12	-.01107	-.00253	-.00081	-.00019	-.00054	-.00012
10	1	0.1592	-2.40	-14	-0.00849	-0.00135	-0.00058	-0.00009	-0.00036	-0.00006
	2	.1592	-2.60	-14	-.00835	-.00133	-.00054	-.00009	-.00035	-.00006
	3	.1592	-3.10	-14	-.00800	-.00127	-.00050	-.00008	-.00034	-.00005
	4	.1592	-4.10	-14	-.00744	-.00118	-.00043	-.00007	-.00033	-.00005

$\sum (7) = 0.9782$ $\qquad \sum (9) = -0.7172$ $\qquad \sum (11) = -0.6049$

$$\frac{w_a}{VC_L} = \frac{5}{8\pi} \sum (7) = 0.1946$$

$$\frac{u_a}{VC_L} = \frac{5}{8\pi} \sum (11) = -0.1203$$

$$\frac{v_a}{VC_L} = \frac{5}{8\pi} \sum (9) = -0.1427$$

*The vertical distance $z/c = -0.10$ is identical with $\Delta z/s = -0.5$ and is constant for this table.

TABLE III.- DOWNWASH FACTOR F_w FOR VARIOUS VALUES OF $\Delta z/s$

(a) $\Delta z/s = \pm 0.50$

$\Delta x/s$ \ $\Delta y/s$	+0	+2	+4	+6	+8	+10	+12	+14	+16	+18	+20
+ .00	+ 1.60000	- .47568	- .12630	- .05589	- .03136	- .02005	- .01391	- .01022	- .00782	- .00618	- .00500
+ .20	+ 3.09616	- .52367	- .13283	- .05778	- .03215	- .02045	- .01415	- .01036	- .00792	- .00625	- .00505
+ .40	+ 3.78220	- .57037	- .13929	- .05967	- .03294	- .02085	- .01438	- .01051	- .00802	- .00632	- .00510
+ .60	+ 3.90697	- .61451	- .14565	- .06154	- .03373	- .02126	- .01461	- .01066	- .00811	- .00638	- .00515
+ .80	+ 3.83874	- .65506	- .15186	- .06339	- .03451	- .02166	- .01484	- .01080	- .00821	- .00645	- .00520
+ 1.00	+ 3.73333	- .69141	- .15787	- .06522	- .03529	- .02205	- .01507	- .01095	- .00831	- .00652	- .00525
+ 1.40	+ 3.55740	- .75115	- .16917	- .06878	- .03682	- .02284	- .01553	- .01124	- .00850	- .00666	- .00535
+ 2.00	+ 3.40736	- .81332	- .18406	- .07380	- .03903	- .02400	- .01621	- .01167	- .00879	- .00686	- .00550
+ 3.00	+ 3.30187	- .87110	- .20322	- .08116	- .04246	- .02584	- .01730	- .01236	- .00926	- .00719	- .00575
+ 4.00	+ 3.25947	- .90028	- .21648	- .08715	- .04548	- .02753	- .01833	- .01303	- .00972	- .00752	- .00599
+ 5.00	+ 3.23874	- .91645	- .22556	- .09190	- .04807	- .02905	- .01928	- .01366	- .01016	- .00783	- .00622
+ 6.00	+ 3.22716	- .92616	- .23185	- .09560	- .05026	- .03040	- .02015	- .01425	- .01057	- .00813	- .00644
+ 8.00	+ 3.21543	- .93659	- .23952	- .10072	- .05360	- .03260	- .02165	- .01530	- .01132	- .00869	- .00686
+12.00	+ 3.20691	- .94458	- .24622	- .10593	- .05749	- .03547	- .02376	- .01687	- .01252	- .00961	- .00758
+14.00	+ 3.20508	- .94635	- .24782	- .10730	- .05862	- .03638	- .02449	- .01745	- .01297	- .00997	- .00787
+16.00	+ 3.20389	- .94750	- .24889	- .10825	- .05943	- .03706	- .02505	- .01791	- .01335	- .01028	- .00813
+18.00	+ 3.20308	- .94830	- .24964	- .10893	- .06004	- .03758	- .02549	- .01829	- .01367	- .01055	- .00835
+20.00	+ 3.20249	- .94887	- .25019	- .10944	- .06049	- .03799	- .02585	- .01859	- .01393	- .01077	- .00854
- .00	+ 1.60000	- .47568	- .12630	- .05589	- .03136	- .02005	- .01391	- .01022	- .00782	- .00618	- .00500
- .20	+ .10384	- .42768	- .11978	- .05400	- .03057	- .01964	- .01368	- .01007	- .00772	- .00611	- .00495
- .40	- .58220	- .38099	- .11331	- .05211	- .02978	- .01924	- .01345	- .00992	- .00762	- .00604	- .00490
- .60	- .70697	- .33684	- .10695	- .05024	- .02900	- .01884	- .01321	- .00978	- .00753	- .00597	- .00485
- .80	- .63874	- .29629	- .10075	- .04838	- .02821	- .01844	- .01298	- .00963	- .00743	- .00590	- .00480
- 1.00	- .53333	- .25994	- .09474	- .04656	- .02744	- .01804	- .01275	- .00949	- .00733	- .00583	- .00475
- 1.40	- .35740	- .20021	- .08343	- .04300	- .02591	- .01725	- .01229	- .00920	- .00714	- .00570	- .00465
- 2.00	- .20736	- .13804	- .06855	- .03797	- .02369	- .01609	- .01162	- .00877	- .00685	- .00549	- .00450
- 3.00	- .10187	- .08025	- .04939	- .03062	- .02027	- .01426	- .01052	- .00807	- .00638	- .00516	- .00426
- 4.00	- .05947	- .05107	- .03613	- .02462	- .01725	- .01257	- .00950	- .00740	- .00592	- .00484	- .00402
- 5.00	- .03874	- .03490	- .02705	- .01988	- .01465	- .01105	- .00854	- .00677	- .00548	- .00452	- .00379
- 6.00	- .02716	- .02519	- .02076	- .01618	- .01246	- .00970	- .00767	- .00618	- .00507	- .00422	- .00356
- 8.00	- .01543	- .01476	- .01309	- .01105	- .00912	- .00749	- .00618	- .00514	- .00432	- .00367	- .00314
-12.00	- .00691	- .00677	- .00639	- .00584	- .00523	- .00463	- .00406	- .00356	- .00312	- .00275	- .00243
-14.00	- .00508	- .00501	- .00479	- .00448	- .00411	- .00372	- .00334	- .00299	- .00267	- .00238	- .00213
-16.00	- .00389	- .00385	- .00372	- .00353	- .00329	- .00304	- .00277	- .00252	- .00229	- .00207	- .00188
-18.00	- .00308	- .00305	- .00297	- .00285	- .00269	- .00251	- .00233	- .00215	- .00197	- .00181	- .00165
-20.00	- .00249	- .00248	- .00242	- .00234	- .00223	- .00211	- .00198	- .00184	- .00171	- .00158	- .00146

TABLE III.- DOWNWASH FACTOR F_w FOR VARIOUS VALUES OF $\Delta z/s$ - Continued

(b) $\Delta z/s = \pm 1.00$

$\Delta x/s$ \ $\Delta y/s$	+0	+2	+4	+6	+8	+10	+12	+14	+16	+18	+20
+ .00	+ 1.00000	- .20000	- .10769	- .05231	- .03024	- .01959	- .01369	- .01010	- .00775	- .00613	- .00497
+ .20	+ 1.40931	- .20365	- .11274	- .05402	- .03099	- .01998	- .01392	- .01024	- .00785	- .00620	- .00502
+ .40	+ 1.74142	- .20851	- .11775	- .05572	- .03174	- .02037	- .01415	- .01039	- .00794	- .00627	- .00507
+ .60	+ 1.96493	- .21534	- .12270	- .05741	- .03248	- .02076	- .01437	- .01053	- .00804	- .00634	- .00512
+ .80	+ 2.09281	- .22419	- .12755	- .05909	- .03322	- .02115	- .01460	- .01067	- .00814	- .00641	- .00517
+ 1.00	+ 2.15470	- .23463	- .13228	- .06074	- .03396	- .02153	- .01483	- .01082	- .00823	- .00647	- .00522
+ 1.40	+ 2.17888	- .25770	- .14128	- .06397	- .03541	- .02229	- .01527	- .01110	- .00843	- .00661	- .00532
+ 2.00	+ 2.14310	- .29048	- .15339	- .06854	- .03751	- .02341	- .01594	- .01152	- .00871	- .00681	- .00547
+ 3.00	+ 2.08544	- .32977	- .16958	- .07530	- .04077	- .02519	- .01700	- .01221	- .00918	- .00714	- .00571
+ 4.00	+ 2.05373	- .35309	- .18124	- .08087	- .04365	- .02683	- .01801	- .01287	- .00963	- .00746	- .00595
+ 5.00	+ 2.03627	- .36707	- .18947	- .08532	- .04614	- .02831	- .01894	- .01349	- .01006	- .00777	- .00618
+ 6.00	+ 2.02594	- .37585	- .19530	- .08884	- .04825	- .02962	- .01980	- .01407	- .01047	- .00807	- .00640
+ 8.00	+ 2.01503	- .38560	- .20257	- .09375	- .05149	- .03178	- .02126	- .01510	- .01121	- .00862	- .00682
+12.00	+ 2.00683	- .39331	- .20907	- .09883	- .05530	- .03459	- .02335	- .01666	- .01239	- .00953	- .00753
+14.00	+ 2.00504	- .39504	- .21063	- .10017	- .05641	- .03549	- .02407	- .01723	- .01285	- .00990	- .00782
+16.00	+ 2.00387	- .39618	- .21169	- .10111	- .05721	- .03616	- .02462	- .01769	- .01322	- .01020	- .00808
+18.00	+ 2.00306	- .39697	- .21243	- .10178	- .05781	- .03668	- .02507	- .01806	- .01354	- .01047	- .00830
+20.00	+ 2.00248	- .39753	- .21297	- .10229	- .05826	- .03708	- .02542	- .01836	- .01380	- .01069	- .00849
- .00	+ 1.00000	- .20000	- .10769	- .05231	- .03024	- .01959	- .01369	- .01010	- .00775	- .00613	- .00497
- .20	+ .59069	- .19635	- .10265	- .05060	- .02950	- .01920	- .01347	- .00996	- .00765	- .00607	- .00493
- .40	+ .25858	- .19149	- .09763	- .04890	- .02875	- .01881	- .01324	- .00981	- .00756	- .00600	- .00488
- .60	+ .03507	- .18466	- .09269	- .04720	- .02800	- .01843	- .01301	- .00967	- .00746	- .00593	- .00483
- .80	- .09281	- .17581	- .08784	- .04553	- .02726	- .01804	- .01279	- .00952	- .00736	- .00586	- .00478
- 1.00	- .15470	- .16537	- .08311	- .04387	- .02653	- .01765	- .01256	- .00938	- .00727	- .00579	- .00473
- 1.40	- .17888	- .14230	- .07411	- .04065	- .02508	- .01689	- .01211	- .00910	- .00708	- .00566	- .00463
- 2.00	- .14310	- .10952	- .06199	- .03607	- .02298	- .01577	- .01145	- .00867	- .00679	- .00546	- .00448
- 3.00	- .08544	- .07023	- .04581	- .02932	- .01972	- .01399	- .01038	- .00799	- .00633	- .00513	- .00424
- 4.00	- .05373	- .04691	- .03415	- .02375	- .01684	- .01236	- .00938	- .00733	- .00587	- .00481	- .00400
- 5.00	- .03627	- .03293	- .02591	- .01929	- .01435	- .01088	- .00845	- .00671	- .00544	- .00450	- .00377
- 6.00	- .02594	- .02415	- .02008	- .01578	- .01224	- .00956	- .00759	- .00613	- .00503	- .00420	- .00355
- 8.00	- .01503	- .01440	- .01281	- .01086	- .00900	- .00741	- .00612	- .00510	- .00429	- .00365	- .00313
-12.00	- .00683	- .00669	- .00632	- .00579	- .00519	- .00459	- .00404	- .00354	- .00311	- .00274	- .00242
-14.00	- .00504	- .00496	- .00475	- .00445	- .00408	- .00370	- .00332	- .00297	- .00266	- .00237	- .00213
-16.00	- .00387	- .00382	- .00370	- .00351	- .00327	- .00302	- .00276	- .00251	- .00228	- .00206	- .00187
-18.00	- .00306	- .00304	- .00296	- .00283	- .00268	- .00250	- .00232	- .00214	- .00197	- .00180	- .00165
-20.00	- .00248	- .00247	- .00241	- .00233	- .00222	- .00210	- .00197	- .00184	- .00171	- .00158	- .00146

TABLE III.- DOWNWASH FACTOR F_W FOR VARIOUS VALUES OF $\Delta z/s$ - Continued

(c) $\Delta z/s = \pm 1.50$

$\Delta x/s$ \ $\Delta y/s$	+0	+2	+4	+6	+8	+10	+12	+14	+16	+18	+20
+ .00	+ .61538	- .04103	- .08318	- .04690	- .02848	- .01886	- .01334	- .00991	- .00764	- .00606	- .00493
+ .20	+ .77954	- .02925	- .08641	- .04834	- .02916	- .01923	- .01356	- .01005	- .00773	- .00613	- .00498
+ .40	+ .92845	- .01857	- .08964	- .04977	- .02984	- .01959	- .01377	- .01019	- .00783	- .00620	- .00503
+ .60	+ 1.05170	- .00982	- .09284	- .05120	- .03052	- .01996	- .01399	- .01032	- .00792	- .00626	- .00508
+ .80	+ 1.14570	- .00348	- .09601	- .05261	- .03119	- .02032	- .01421	- .01046	- .00802	- .00633	- .00512
+ 1.00	+ 1.21240	+ .00040	- .09913	- .05401	- .03186	- .02069	- .01443	- .01060	- .00811	- .00640	- .00517
+ 1.40	+ 1.28421	+ .00176	- .10521	- .05675	- .03319	- .02141	- .01486	- .01088	- .00830	- .00653	- .00527
+ 2.00	+ 1.31017	- .00602	- .11372	- .06066	- .03511	- .02247	- .01549	- .01129	- .00858	- .00673	- .00542
+ 3.00	+ 1.29524	- .02540	- .12586	- .06651	- .03811	- .02415	- .01652	- .01196	- .00903	- .00705	- .00565
+ 4.00	+ 1.27633	- .04120	- .13524	- .07143	- .04078	- .02570	- .01749	- .01260	- .00947	- .00737	- .00589
+ 5.00	+ 1.26333	- .05212	- .14222	- .07544	- .04310	- .02711	- .01839	- .01320	- .00990	- .00767	- .00612
+ 6.00	+ 1.25482	- .05952	- .14736	- .07866	- .04509	- .02837	- .01922	- .01377	- .01030	- .00797	- .00634
+ 8.00	+ 1.24517	- .06823	- .15400	- .08325	- .04816	- .03044	- .02064	- .01477	- .01103	- .00851	- .00675
+12.00	+ 1.23746	- .07549	- .16015	- .08810	- .05184	- .03318	- .02268	- .01630	- .01219	- .00941	- .00745
+14.00	+ 1.23574	- .07716	- .16167	- .08941	- .05292	- .03406	- .02338	- .01686	- .01264	- .00977	- .00774
+16.00	+ 1.23460	- .07827	- .16270	- .09033	- .05371	- .03472	- .02393	- .01732	- .01301	- .01007	- .00799
+18.00	+ 1.23381	- .07904	- .16343	- .09099	- .05430	- .03523	- .02437	- .01768	- .01332	- .01033	- .00821
+20.00	+ 1.23324	- .07960	- .16396	- .09149	- .05474	- .03563	- .02471	- .01798	- .01358	- .01055	- .00840
- .00	+ .61538	- .04103	- .08318	- .04690	- .02848	- .01886	- .01334	- .00991	- .00764	- .00606	- .00493
- .20	+ .45123	- .05280	- .07995	- .04546	- .02780	- .01849	- .01312	- .00977	- .00754	- .00600	- .00488
- .40	+ .30232	- .06348	- .07672	- .04403	- .02711	- .01812	- .01290	- .00963	- .00745	- .00593	- .00483
- .60	+ .17907	- .07223	- .07352	- .04260	- .02644	- .01776	- .01268	- .00949	- .00735	- .00586	- .00478
- .80	+ .08507	- .07857	- .07035	- .04119	- .02576	- .01739	- .01247	- .00935	- .00726	- .00580	- .00473
- 1.00	+ .01837	- .08245	- .06723	- .03979	- .02509	- .01703	- .01225	- .00921	- .00717	- .00573	- .00468
- 1.40	- .05344	- .08381	- .06115	- .03706	- .02377	- .01631	- .01182	- .00893	- .00698	- .00560	- .00459
- 2.00	- .07940	- .07604	- .05264	- .03315	- .02184	- .01525	- .01118	- .00852	- .00670	- .00540	- .00444
- 3.00	- .06447	- .05665	- .04051	- .02729	- .01885	- .01357	- .01016	- .00786	- .00624	- .00507	- .00420
- 4.00	- .04556	- .04085	- .03112	- .02237	- .01618	- .01201	- .00919	- .00722	- .00580	- .00476	- .00397
- 5.00	- .03256	- .02993	- .02414	- .01836	- .01385	- .01060	- .00829	- .00661	- .00538	- .00445	- .00374
- 6.00	- .02405	- .02254	- .01900	- .01514	- .01187	- .00935	- .00746	- .00605	- .00498	- .00416	- .00352
- 8.00	- .01440	- .01382	- .01236	- .01055	- .00879	- .00727	- .00603	- .00504	- .00425	- .00362	- .00311
-12.00	- .00669	- .00656	- .00621	- .00570	- .00512	- .00454	- .00400	- .00351	- .00308	- .00272	- .00240
-14.00	- .00497	- .00489	- .00469	- .00439	- .00404	- .00366	- .00329	- .00295	- .00264	- .00236	- .00211
-16.00	- .00383	- .00378	- .00366	- .00347	- .00325	- .00300	- .00274	- .00250	- .00227	- .00205	- .00186
-18.00	- .00304	- .00301	- .00293	- .00281	- .00266	- .00249	- .00231	- .00213	- .00196	- .00179	- .00164
-20.00	- .00247	- .00245	- .00240	- .00231	- .00221	- .00[illegible]	- .00196	- .00183	- .00170	- .00157	- .00146

TABLE III.- DOWNWASH FACTOR F_W FOR VARIOUS VALUES OF $\Delta z/s$ - Continued

(d) $\Delta z/s = \pm 2.00$

$\Delta x/s$ \ $\Delta y/s$	+0.	+2.	+4.	+6.	+8.	+10.	+12.	+14.	+16.	+18.	+20.
+.00	+.40000	+.03077	-.05836	-.04034	-.02619	-.01788	-.01286	-.00964	-.00748	-.00597	-.00486
+.20	+.47974	+.04481	-.05993	-.04146	-.02679	-.01822	-.01306	-.00978	-.00757	-.00603	-.00491
+.40	+.55509	+.05818	-.06152	-.04258	-.02739	-.01856	-.01327	-.00991	-.00766	-.00610	-.00496
+.60	+.62255	+.07033	-.06311	-.04370	-.02798	-.01890	-.01347	-.01004	-.00776	-.00616	-.00501
+.80	+.67994	+.08084	-.06471	-.04480	-.02858	-.01923	-.01368	-.01018	-.00785	-.00623	-.00506
+1.00	+.72660	+.08950	-.06634	-.04590	-.02917	-.01957	-.01388	-.01031	-.00794	-.00629	-.00510
+1.40	+.79034	+.10132	-.06962	-.04806	-.03033	-.02023	-.01429	-.01058	-.00812	-.00642	-.00520
+2.00	+.83333	+.10794	-.07457	-.05118	-.03203	-.02121	-.01489	-.01097	-.00839	-.00661	-.00534
+3.00	+.84407	+.10394	-.08247	-.05595	-.03469	-.02277	-.01587	-.01161	-.00883	-.00693	-.00558
+4.00	+.83644	+.09538	-.08930	-.06008	-.03708	-.02421	-.01679	-.01223	-.00926	-.00724	-.00581
+5.00	+.82811	+.08780	-.09482	-.06354	-.03919	-.02553	-.01764	-.01281	-.00967	-.00754	-.00603
+6.00	+.82167	+.08202	-.09911	-.06638	-.04101	-.02671	-.01843	-.01335	-.01006	-.00783	-.00624
+8.00	+.81356	+.07460	-.10494	-.07054	-.04388	-.02868	-.01980	-.01433	-.01077	-.00836	-.00665
+12.00	+.80652	+.06793	-.11065	-.07510	-.04737	-.03130	-.02177	-.01582	-.01191	-.00924	-.00734
+14.00	+.80487	+.06634	-.11211	-.07636	-.04841	-.03215	-.02246	-.01637	-.01235	-.00959	-.00763
+16.00	+.80377	+.06527	-.11310	-.07725	-.04918	-.03280	-.02300	-.01681	-.01272	-.00989	-.00788
+18.00	+.80300	+.06451	-.11381	-.07790	-.04976	-.03330	-.02342	-.01717	-.01302	-.01015	-.00809
+20.00	+.80244	+.06396	-.11434	-.07838	-.05020	-.03369	-.02377	-.01747	-.01328	-.01037	-.00828
-.00	+.40000	+.03077	-.05836	-.04034	-.02619	-.01788	-.01286	-.00964	-.00748	-.00597	-.00486
-.20	+.32026	+.01673	-.05678	-.03922	-.02559	-.01754	-.01265	-.00951	-.00739	-.00590	-.00482
-.40	+.24491	+.00335	-.05520	-.03810	-.02500	-.01721	-.01244	-.00937	-.00730	-.00584	-.00477
-.60	+.17745	-.00879	-.05360	-.03698	-.02440	-.01687	-.01224	-.00924	-.00721	-.00577	-.00472
-.80	+.12006	-.01930	-.05200	-.03587	-.02381	-.01653	-.01203	-.00911	-.00712	-.00570	-.00467
-1.00	+.07340	-.02796	-.05038	-.03477	-.02322	-.01620	-.01183	-.00897	-.00702	-.00564	-.00462
-1.40	+.00966	-.03978	-.04709	-.03261	-.02206	-.01553	-.01142	-.00871	-.00684	-.00551	-.00453
-2.00	-.03333	-.04641	-.04214	-.02950	-.02036	-.01456	-.01082	-.00831	-.00657	-.00532	-.00439
-3.00	-.04407	-.04240	-.03424	-.02473	-.01770	-.01300	-.00984	-.00767	-.00613	-.00500	-.00415
-4.00	-.03644	-.03384	-.02741	-.02060	-.01530	-.01155	-.00892	-.00706	-.00570	-.00469	-.00392
-5.00	-.02811	-.02626	-.02189	-.01714	-.01319	-.01023	-.00807	-.00648	-.00529	-.00439	-.00370
-6.00	-.02167	-.02048	-.01761	-.01430	-.01137	-.00905	-.00728	-.00593	-.00490	-.00411	-.00348
-8.00	-.01356	-.01306	-.01177	-.01013	-.00851	-.00709	-.00591	-.00496	-.00419	-.00358	-.00308
-12.00	-.00652	-.00639	-.00606	-.00557	-.00502	-.00446	-.00394	-.00347	-.00305	-.00269	-.00239
-14.00	-.00487	-.00480	-.00461	-.00432	-.00397	-.00361	-.00325	-.00292	-.00261	-.00234	-.00210
-16.00	-.00377	-.00373	-.00361	-.00343	-.00321	-.00296	-.00271	-.00247	-.00225	-.00204	-.00185
-18.00	-.00300	-.00297	-.00290	-.00278	-.00263	-.00246	-.00229	-.00211	-.00194	-.00178	-.00163
-20.00	-.00244	-.00243	-.00237	-.00229	-.00219	-.00207	-.00195	-.00182	-.00169	-.00156	-.00145

TABLE III.- DOWNWASH FACTOR F_w FOR VARIOUS VALUES OF $\Delta z/s$ - Continued

(e) $\Delta z/s = \pm 2.50$

$\Delta x/s$ \ $\Delta y/s$	+0	+2	+4	+6	+8	+10	+12	+14	+16	+18	+20
+ .00	+ .27586	+ .05879	- .03672	- .03330	- .02354	- .01671	- .01226	- .00931	- .00729	- .00584	- .00478
+ .20	+ .31985	+ .07125	- .03704	- .03410	- .02405	- .01701	- .01246	- .00944	- .00737	- .00591	- .00483
+ .40	+ .36225	+ .08333	- .03736	- .03490	- .02455	- .01732	- .01265	- .00957	- .00746	- .00597	- .00488
+ .60	+ .40167	+ .09468	- .03772	- .03570	- .02505	- .01762	- .01284	- .00970	- .00755	- .00603	- .00492
+ .80	+ .43710	+ .10503	- .03811	- .03650	- .02555	- .01792	- .01303	- .00982	- .00764	- .00610	- .00497
+ 1.00	+ .46795	+ .11420	- .03856	- .03729	- .02605	- .01822	- .01322	- .00995	- .00773	- .00616	- .00502
+ 1.40	+ .51550	+ .12867	- .03960	- .03886	- .02703	- .01882	- .01360	- .01020	- .00790	- .00628	- .00511
+ 2.00	+ .55670	+ .14146	- .04159	- .04116	- .02847	- .01970	- .01416	- .01058	- .00816	- .00647	- .00525
+ 3.00	+ .57876	+ .14703	- .04571	- .04479	- .03075	- .02111	- .01507	- .01118	- .00859	- .00678	- .00548
+ 4.00	+ .57927	+ .14432	- .05009	- .04805	- .03283	- .02243	- .01593	- .01177	- .00900	- .00708	- .00570
+ 5.00	+ .57509	+ .13987	- .05408	- .05090	- .03469	- .02364	- .01673	- .01232	- .00939	- .00737	- .00592
+ 6.00	+ .57073	+ .13574	- .05746	- .05331	- .03631	- .02473	- .01748	- .01285	- .00977	- .00765	- .00613
+ 8.00	+ .56429	+ .12973	- .06239	- .05698	- .03892	- .02656	- .01877	- .01378	- .01046	- .00816	- .00653
+12.00	+ .55802	+ .12376	- .06757	- .06119	- .04219	- .02905	- .02066	- .01522	- .01156	- .00902	- .00720
+14.00	+ .55647	+ .12226	- .06895	- .06238	- .04319	- .02987	- .02132	- .01575	- .01199	- .00937	- .00748
+16.00	+ .55542	+ .12124	- .06990	- .06324	- .04394	- .03050	- .02185	- .01619	- .01235	- .00967	- .00773
+18.00	+ .55468	+ .12051	- .07059	- .06387	- .04449	- .03098	- .02227	- .01654	- .01265	- .00992	- .00794
+20.00	+ .55414	+ .11998	- .07110	- .06434	- .04492	- .03136	- .02260	- .01683	- .01290	- .01013	- .00813
- .00	+ .27586	+ .05879	- .03672	- .03330	- .02354	- .01671	- .01226	- .00931	- .00729	- .00584	- .00478
- .20	+ .23187	+ .04633	- .03641	- .03250	- .02304	- .01640	- .01207	- .00919	- .00720	- .00578	- .00474
- .40	+ .18948	+ .03425	- .03608	- .03170	- .02254	- .01610	- .01188	- .00906	- .00711	- .00572	- .00469
- .60	+ .15005	+ .02290	- .03572	- .03090	- .02204	- .01580	- .01169	- .00893	- .00702	- .00565	- .00464
- .80	+ .11462	+ .01255	- .03533	- .03011	- .02154	- .01549	- .01150	- .00881	- .00693	- .00559	- .00460
- 1.00	+ .08378	+ .00338	- .03489	- .02932	- .02104	- .01519	- .01131	- .00868	- .00685	- .00553	- .00455
- 1.40	+ .03622	- .01109	- .03384	- .02775	- .02006	- .01459	- .01093	- .00843	- .00667	- .00540	- .00446
- 2.00	- .00498	- .02388	- .03135	- .02545	- .01862	- .01371	- .01037	- .00805	- .00641	- .00521	- .00432
- 3.00	- .02704	- .02945	- .02773	- .02182	- .01634	- .01230	- .00946	- .00745	- .00599	- .00491	- .00409
- 4.00	- .02755	- .02674	- .02336	- .01855	- .01426	- .01099	- .00860	- .00686	- .00558	- .00461	- .00386
- 5.00	- .02337	- .02229	- .01936	- .01571	- .01240	- .00978	- .00779	- .00631	- .00518	- .00432	- .00365
- 6.00	- .01901	- .01816	- .01599	- .01330	- .01077	- .00869	- .00705	- .00578	- .00480	- .00404	- .00344
- 8.00	- .01257	- .01215	- .01106	- .00962	- .00817	- .00686	- .00575	- .00485	- .00412	- .00352	- .00304
-12.00	- .00630	- .00618	- .00587	- .00542	- .00490	- .00437	- .00387	- .00341	- .00301	- .00266	- .00236
-14.00	- .00475	- .00468	- .00450	- .00422	- .00390	- .00355	- .00320	- .00288	- .00258	- .00232	- .00208
-16.00	- .00370	- .00366	- .00354	- .00337	- .00315	- .00292	- .00268	- .00244	- .00222	- .00202	- .00183
-18.00	- .00295	- .00293	- .00285	- .00274	- .00260	- .00243	- .00226	- .00209	- .00192	- .00177	- .00162
-20.00	- .00241	- .00240	- .00235	- .00227	- .00217	- .00205	- .00193	- .00180	- .00167	- .00155	- .00144

TABLE III.- DOWNWASH FACTOR F_W FOR VARIOUS VALUES OF $\Delta z/s$ - Continued

(f) $\Delta z/s = \pm 3.00$

$\Delta x/s$ \ $\Delta y/s$	+0	+2	+4	+6	+8	+10	+12	+14	+16	+18	+20
+ .00	+ .20000	+ .06667	- .01961	- .02637	- .02069	- .01538	- .01158	- .00893	- .00706	- .00570	- .00468
+ .20	+ .22659	+ .07685	- .01908	- .02687	- .02109	- .01565	- .01176	- .00905	- .00714	- .00576	- .00473
+ .40	+ .25250	+ .08680	- .01857	- .02738	- .02150	- .01592	- .01193	- .00917	- .00722	- .00582	- .00478
+ .60	+ .27711	+ .09633	- .01810	- .02788	- .02190	- .01618	- .01211	- .00929	- .00731	- .00588	- .00482
+ .80	+ .29993	+ .10525	- .01767	- .02839	- .02231	- .01645	- .01228	- .00941	- .00739	- .00594	- .00487
+ 1.00	+ .32060	+ .11343	- .01730	- .02890	- .02271	- .01671	- .01246	- .00953	- .00747	- .00600	- .00491
+ 1.40	+ .35484	+ .12725	- .01677	- .02991	- .02350	- .01724	- .01280	- .00976	- .00764	- .00612	- .00500
+ 2.00	+ .38914	+ .14156	- .01658	- .03144	- .02467	- .01801	- .01332	- .01011	- .00789	- .00630	- .00514
+ 3.00	+ .41412	+ .15206	- .01770	- .03397	- .02655	- .01926	- .01415	- .01068	- .00829	- .00660	- .00536
+ 4.00	+ .41965	+ .15349	- .01993	- .03638	- .02829	- .02043	- .01494	- .01123	- .00869	- .00688	- .00558
+ 5.00	+ .41875	+ .15165	- .02251	- .03859	- .02987	- .02151	- .01569	- .01176	- .00906	- .00716	- .00579
+ 6.00	+ .41625	+ .14906	- .02498	- .04056	- .03129	- .02250	- .01638	- .01225	- .00942	- .00743	- .00599
+ 8.00	+ .41148	+ .14448	- .02896	- .04370	- .03361	- .02418	- .01759	- .01314	- .01008	- .00793	- .00638
+12.00	+ .40604	+ .13927	- .03357	- .04750	- .03663	- .02651	- .01938	- .01452	- .01115	- .00877	- .00704
+14.00	+ .40460	+ .13787	- .03485	- .04863	- .03758	- .02730	- .02002	- .01503	- .01157	- .00910	- .00731
+16.00	+ .40361	+ .13690	- .03575	- .04944	- .03829	- .02790	- .02053	- .01545	- .01192	- .00939	- .00755
+18.00	+ .40290	+ .13621	- .03641	- .05004	- .03882	- .02837	- .02093	- .01580	- .01221	- .00964	- .00776
+20.00	+ .40238	+ .13569	- .03690	- .05050	- .03924	- .02874	- .02126	- .01608	- .01245	- .00985	- .00794
- .00	+ .20000	+ .06667	- .01961	- .02637	- .02069	- .01538	- .01158	- .00893	- .00706	- .00570	- .00468
- .20	+ .17341	+ .05649	- .02013	- .02586	- .02028	- .01512	- .01141	- .00881	- .00697	- .00563	- .00464
- .40	+ .14750	+ .04653	- .02064	- .02536	- .01988	- .01485	- .01123	- .00869	- .00689	- .00557	- .00459
- .60	+ .12289	+ .03700	- .02112	- .02485	- .01948	- .01459	- .01106	- .00857	- .00680	- .00551	- .00455
- .80	+ .10007	+ .02809	- .02155	- .02435	- .01907	- .01432	- .01088	- .00846	- .00672	- .00545	- .00450
- 1.00	+ .07940	+ .01991	- .02192	- .02384	- .01867	- .01406	- .01071	- .00834	- .00664	- .00539	- .00446
- 1.40	+ .04516	+ .00608	- .02245	- .02282	- .01788	- .01353	- .01036	- .00810	- .00647	- .00527	- .00437
- 2.00	+ .01086	- .00823	- .02264	- .02130	- .01671	- .01276	- .00985	- .00775	- .00622	- .00509	- .00423
- 3.00	- .01412	- .01872	- .02152	- .01877	- .01483	- .01151	- .00901	- .00718	- .00582	- .00480	- .00401
- 4.00	- .01965	- .02016	- .01928	- .01636	- .01309	- .01034	- .00822	- .00663	- .00543	- .00451	- .00379
- 5.00	- .01875	- .01832	- .01670	- .01414	- .01150	- .00925	- .00748	- .00610	- .00505	- .00423	- .00358
- 6.00	- .01625	- .01573	- .01424	- .01218	- .01009	- .00827	- .00678	- .00561	- .00469	- .00396	- .00338
- 8.00	- .01148	- .01114	- .01025	- .00904	- .00777	- .00659	- .00557	- .00472	- .00403	- .00346	- .00299
-12.00	- .00604	- .00594	- .00565	- .00523	- .00475	- .00426	- .00378	- .00335	- .00296	- .00262	- .00233
-14.00	- .00460	- .00454	- .00437	- .00411	- .00380	- .00347	- .00314	- .00283	- .00254	- .00229	- .00206
-16.00	- .00361	- .00357	- .00346	- .00330	- .00309	- .00287	- .00264	- .00241	- .00220	- .00200	- .00182
-18.00	- .00290	- .00287	- .00280	- .00269	- .00255	- .00240	- .00223	- .00206	- .00190	- .00175	- .00161
-20.00	- .00238	- .00236	- .00231	- .00224	- .00214	- .00203	- .00191	- .00178	- .00166	- .00154	- .00143

TABLE III.- DOWNWASH FACTOR F_w FOR VARIOUS VALUES OF $\Delta z/s$ - Continued

(g) $\Delta z/s = \pm 4.00$

$\Delta x/s$ \ $\Delta y/s$	+0.	+2.	+4.	+6.	+8.	+10.	+12.	+14.	+16.	+18.	+20.
+ .00	+.11765	+.06118	+.00195	-.01426	-.01491	-.01249	-.01002	-.00803	-.00650	-.00534	-.00445
+ .20	+.12939	+.06758	+.00322	-.01430	-.01513	-.01268	-.01016	-.00813	-.00658	-.00539	-.00449
+ .40	+.14096	+.07389	+.00447	-.01435	-.01534	-.01287	-.01030	-.00823	-.00665	-.00545	-.00453
+ .60	+.15219	+.08005	+.00570	-.01440	-.01556	-.01305	-.01044	-.00833	-.00672	-.00550	-.00457
+ .80	+.16295	+.08597	+.00688	-.01446	-.01578	-.01324	-.01058	-.00843	-.00680	-.00556	-.00461
+ 1.00	+.17311	+.09159	+.00801	-.01452	-.01600	-.01343	-.01071	-.00853	-.00687	-.00561	-.00466
+ 1.40	+.19128	+.10176	+.01007	-.01466	-.01643	-.01380	-.01099	-.00873	-.00702	-.00572	-.00474
+ 2.00	+.21264	+.11396	+.01257	-.01495	-.01709	-.01435	-.01140	-.00903	-.00724	-.00589	-.00486
+ 3.00	+.23393	+.12651	+.01506	-.01565	-.01818	-.01525	-.01206	-.00952	-.00759	-.00616	-.00507
+ 4.00	+.24309	+.13199	+.01582	-.01657	-.01925	-.01611	-.01270	-.00999	-.00794	-.00642	-.00527
+ 5.00	+.24605	+.13357	+.01547	-.01763	-.02028	-.01692	-.01331	-.01044	-.00828	-.00667	-.00546
+ 6.00	+.24631	+.13335	+.01458	-.01873	-.02125	-.01769	-.01388	-.01086	-.00860	-.00692	-.00565
+ 8.00	+.24444	+.13134	+.01240	-.02078	-.02297	-.01903	-.01491	-.01164	-.00919	-.00738	-.00601
+12.00	+.24073	+.12771	+.00904	-.02372	-.02541	-.02100	-.01647	-.01287	-.01017	-.00815	-.00663
+14.00	+.23955	+.12656	+.00797	-.02467	-.02624	-.02169	-.01705	-.01334	-.01055	-.00847	-.00689
+16.00	+.23869	+.12572	+.00717	-.02539	-.02687	-.02224	-.01751	-.01373	-.01088	-.00874	-.00712
+18.00	+.23806	+.12509	+.00658	-.02594	-.02736	-.02267	-.01789	-.01406	-.01116	-.00897	-.00732
+20.00	+.23758	+.12462	+.00613	-.02636	-.02775	-.02302	-.01819	-.01433	-.01139	-.00917	-.00750
- .00	+.11765	+.06118	+.00195	-.01426	-.01491	-.01249	-.01002	-.00803	-.00650	-.00534	-.00445
- .20	+.10591	+.05478	+.00068	-.01421	-.01469	-.01230	-.00988	-.00793	-.00643	-.00528	-.00440
- .40	+.09434	+.04846	-.00057	-.01417	-.01447	-.01212	-.00974	-.00783	-.00636	-.00523	-.00436
- .60	+.08310	+.04230	-.00179	-.01412	-.01426	-.01193	-.00961	-.00773	-.00628	-.00517	-.00432
- .80	+.07234	+.03639	-.00298	-.01406	-.01404	-.01174	-.00947	-.00763	-.00621	-.00512	-.00428
- 1.00	+.06219	+.03076	-.00411	-.01400	-.01382	-.01156	-.00933	-.00753	-.00613	-.00507	-.00424
- 1.40	+.04402	+.02060	-.00617	-.01385	-.01338	-.01119	-.00905	-.00733	-.00599	-.00496	-.00415
- 2.00	+.02266	+.00840	-.00867	-.01356	-.01273	-.01063	-.00865	-.00703	-.00577	-.00479	-.00403
- 3.00	+.00136	-.00416	-.01116	-.01287	-.01164	-.00974	-.00798	-.00654	-.00541	-.00452	-.00382
- 4.00	-.00779	-.00963	-.01191	-.01195	-.01057	-.00887	-.00734	-.00607	-.00506	-.00426	-.00362
- 5.00	-.01075	-.01122	-.01157	-.01089	-.00954	-.00806	-.00673	-.00562	-.00473	-.00401	-.00343
- 6.00	-.01101	-.01100	-.01067	-.00979	-.00856	-.00730	-.00616	-.00520	-.00441	-.00376	-.00324
- 8.00	-.00915	-.00898	-.00849	-.00774	-.00685	-.00596	-.00514	-.00442	-.00381	-.00330	-.00288
-12.00	-.00544	-.00536	-.00513	-.00480	-.00440	-.00398	-.00357	-.00319	-.00284	-.00253	-.00226
-14.00	-.00426	-.00421	-.00406	-.00385	-.00358	-.00329	-.00300	-.00272	-.00245	-.00221	-.00200
-16.00	-.00340	-.00337	-.00327	-.00313	-.00295	-.00274	-.00253	-.00232	-.00213	-.00194	-.00177
-18.00	-.00276	-.00274	-.00268	-.00258	-.00245	-.00231	-.00216	-.00200	-.00185	-.00171	-.00157
-20.00	-.00229	-.00227	-.00223	-.00216	-.00207	-.00196	-.00185	-.00173	-.00162	-.00150	-.00140

TABLE III.- DOWNWASH FACTOR F_w FOR VARIOUS VALUES OF $\Delta z/s$ - Continued

(h) $\Delta z/s = \pm 6.00$

$\Delta x/s$ \ $\Delta y/s$	+0.	+2.	+4.	+6.	+8.	+10.	+12.	+14.	+16.	+18.	+20.
+ .00	+ .05405	+ .03964	+ .01530	+ .00039	- .00543	- .00686	- .00665	- .00594	- .00516	- .00445	- .00383
+ .20	+ .05765	+ .04231	+ .01648	+ .00073	- .00539	- .00691	- .00671	- .00600	- .00521	- .00449	- .00387
+ .40	+ .06123	+ .04496	+ .01766	+ .00108	- .00535	- .00696	- .00678	- .00606	- .00526	- .00453	- .00390
+ .60	+ .06476	+ .04758	+ .01882	+ .00142	- .00531	- .00701	- .00685	- .00612	- .00532	- .00457	- .00393
+ .80	+ .06822	+ .05015	+ .01997	+ .00176	- .00527	- .00706	- .00691	- .00618	- .00537	- .00461	- .00397
+ 1.00	+ .07159	+ .05266	+ .02109	+ .00209	- .00524	- .00711	- .00698	- .00624	- .00542	- .00465	- .00400
+ 1.40	+ .07800	+ .05743	+ .02324	+ .00273	- .00517	- .00721	- .00711	- .00637	- .00552	- .00474	- .00407
+ 2.00	+ .08656	+ .06387	+ .02617	+ .00360	- .00509	- .00736	- .00730	- .00654	- .00567	- .00486	- .00416
+ 3.00	+ .09762	+ .07229	+ .03010	+ .00477	- .00503	- .00764	- .00763	- .00684	- .00591	- .00506	- .00433
+ 4.00	+ .10489	+ .07791	+ .03281	+ .00555	- .00508	- .00793	- .00796	- .00713	- .00616	- .00526	- .00449
+ 5.00	+ .10920	+ .08130	+ .03446	+ .00597	- .00521	- .00824	- .00828	- .00742	- .00640	- .00545	- .00464
+ 6.00	+ .11152	+ .08313	+ .03532	+ .00609	- .00543	- .00856	- .00860	- .00770	- .00663	- .00564	- .00480
+ 8.00	+ .11300	+ .08424	+ .03566	+ .00581	- .00602	- .00922	- .00921	- .00822	- .00706	- .00599	- .00509
+12.00	+ .11218	+ .08332	+ .03454	+ .00455	- .00730	- .01041	- .01025	- .00911	- .00781	- .00662	- .00560
+14.00	+ .11154	+ .08268	+ .03392	+ .00396	- .00784	- .01089	- .01068	- .00947	- .00812	- .00688	- .00582
+16.00	+ .11098	+ .08213	+ .03339	+ .00346	- .00829	- .01130	- .01104	- .00979	- .00839	- .00711	- .00602
+18.00	+ .11053	+ .08168	+ .03296	+ .00305	- .00867	- .01164	- .01134	- .01005	- .00862	- .00731	- .00620
+20.00	+ .11016	+ .08132	+ .03261	+ .00272	- .00898	- .01192	- .01160	- .01028	- .00882	- .00749	- .00635
- .00	+ .05405	+ .03964	+ .01530	+ .00039	- .00543	- .00686	- .00665	- .00594	- .00516	- .00445	- .00383
- .20	+ .05045	+ .03697	+ .01412	+ .00004	- .00547	- .00681	- .00658	- .00588	- .00511	- .00441	- .00380
- .40	+ .04688	+ .03432	+ .01294	- .00031	- .00551	- .00676	- .00652	- .00582	- .00506	- .00437	- .00377
- .60	+ .04335	+ .03170	+ .01178	- .00065	- .00555	- .00671	- .00645	- .00576	- .00501	- .00433	- .00373
- .80	+ .03989	+ .02913	+ .01063	- .00099	- .00559	- .00666	- .00639	- .00570	- .00496	- .00428	- .00370
- 1.00	+ .03652	+ .02662	+ .00951	- .00132	- .00562	- .00661	- .00632	- .00564	- .00491	- .00424	- .00367
- 1.40	+ .03011	+ .02184	+ .00736	- .00196	- .00569	- .00651	- .00619	- .00552	- .00481	- .00416	- .00360
- 2.00	+ .02155	+ .01541	+ .00443	- .00283	- .00577	- .00635	- .00599	- .00534	- .00466	- .00404	- .00350
- 3.00	+ .01049	+ .00699	+ .00050	- .00400	- .00583	- .00608	- .00567	- .00505	- .00441	- .00384	- .00334
- 4.00	+ .00322	+ .00137	- .00220	- .00478	- .00578	- .00579	- .00534	- .00475	- .00417	- .00364	- .00318
- 5.00	- .00109	- .00202	- .00386	- .00519	- .00565	- .00548	- .00502	- .00447	- .00393	- .00345	- .00302
- 6.00	- .00341	- .00385	- .00472	- .00532	- .00543	- .00516	- .00470	- .00419	- .00370	- .00326	- .00287
- 8.00	- .00490	- .00496	- .00506	- .00504	- .00484	- .00450	- .00409	- .00367	- .00327	- .00290	- .00258
-12.00	- .00407	- .00404	- .00394	- .00378	- .00356	- .00331	- .00305	- .00278	- .00252	- .00228	- .00206
-14.00	- .00343	- .00340	- .00332	- .00319	- .00302	- .00283	- .00262	- .00241	- .00221	- .00202	- .00184
-16.00	- .00287	- .00285	- .00279	- .00269	- .00257	- .00242	- .00226	- .00210	- .00194	- .00179	- .00165
-18.00	- .00242	- .00240	- .00236	- .00228	- .00219	- .00208	- .00196	- .00183	- .00171	- .00159	- .00147
-20.00	- .00205	- .00204	- .00200	- .00195	- .00188	- .00179	- .00170	- .00161	- .00151	- .00141	- .00132

TABLE III.- DOWNWASH FACTOR F_W FOR VARIOUS VALUES OF $\Delta z/s$ - Concluded

(i) $\Delta z/s = \pm 8.00$

$\Delta x/s$ \ $\Delta y/s$	+0.	+2.	+4.	+6.	+8.	+10.	+12.	+14.	+16.	+18.	+20.
+ .00	+ .03077	+ .02571	+ .01508	+ .00577	+ .00012	- .00261	- .00367	- .00389	- .00374	- .00345	- .00312
+ .20	+ .03231	+ .02700	+ .01587	+ .00614	+ .00027	- .00257	- .00367	- .00392	- .00377	- .00348	- .00315
+ .40	+ .03384	+ .02829	+ .01666	+ .00652	+ .00041	- .00254	- .00368	- .00394	- .00380	- .00351	- .00317
+ .60	+ .03536	+ .02956	+ .01744	+ .00689	+ .00055	- .00251	- .00369	- .00396	- .00383	- .00353	- .00319
+ .80	+ .03686	+ .03082	+ .01821	+ .00726	+ .00069	- .00247	- .00370	- .00399	- .00386	- .00356	- .00322
+ 1.00	+ .03834	+ .03207	+ .01897	+ .00763	+ .00083	- .00244	- .00371	- .00401	- .00388	- .00358	- .00324
+ 1.40	+ .04122	+ .03449	+ .02046	+ .00834	+ .00110	- .00237	- .00373	- .00406	- .00394	- .00364	- .00329
+ 2.00	+ .04526	+ .03789	+ .02256	+ .00935	+ .00149	- .00228	- .00376	- .00414	- .00402	- .00372	- .00336
+ 3.00	+ .05105	+ .04280	+ .02564	+ .01086	+ .00206	- .00216	- .00383	- .00426	- .00416	- .00385	- .00347
+ 4.00	+ .05556	+ .04664	+ .02809	+ .01207	+ .00252	- .00207	- .00390	- .00439	- .00430	- .00398	- .00359
+ 5.00	+ .05883	+ .04946	+ .02992	+ .01299	+ .00286	- .00203	- .00399	- .00453	- .00444	- .00410	- .00370
+ 6.00	+ .06108	+ .05141	+ .03121	+ .01364	+ .00308	- .00203	- .00409	- .00466	- .00458	- .00423	- .00381
+ 8.00	+ .06345	+ .05348	+ .03258	+ .01430	+ .00324	- .00215	- .00433	- .00494	- .00485	- .00448	- .00403
+12.00	+ .06429	+ .05418	+ .03292	+ .01426	+ .00292	- .00264	- .00488	- .00548	- .00535	- .00493	- .00442
+14.00	+ .06410	+ .05397	+ .03269	+ .01401	+ .00264	- .00292	- .00515	- .00573	- .00557	- .00513	- .00460
+16.00	+ .06383	+ .05370	+ .03242	+ .01373	+ .00237	- .00318	- .00539	- .00596	- .00578	- .00531	- .00475
+18.00	+ .06355	+ .05343	+ .03215	+ .01347	+ .00212	- .00342	- .00562	- .00616	- .00596	- .00547	- .00490
+20.00	+ .06330	+ .05318	+ .03190	+ .01323	+ .00189	- .00363	- .00581	- .00634	- .00612	- .00561	- .00503
- .00	+ .03077	+ .02571	+ .01508	+ .00577	+ .00012	- .00261	- .00367	- .00389	- .00374	- .00345	- .00312
- .20	+ .02923	+ .02442	+ .01430	+ .00539	- .00002	- .00264	- .00366	- .00387	- .00372	- .00343	- .00310
- .40	+ .02770	+ .02314	+ .01351	+ .00502	- .00016	- .00268	- .00365	- .00384	- .00369	- .00340	- .00307
- .60	+ .02618	+ .02186	+ .01273	+ .00464	- .00031	- .00271	- .00364	- .00382	- .00366	- .00337	- .00305
- .80	+ .02468	+ .02060	+ .01196	+ .00427	- .00045	- .00275	- .00363	- .00379	- .00363	- .00335	- .00303
- 1.00	+ .02319	+ .01936	+ .01120	+ .00391	- .00059	- .00278	- .00362	- .00377	- .00361	- .00332	- .00300
- 1.40	+ .02032	+ .01694	+ .00971	+ .00320	- .00086	- .00285	- .00360	- .00372	- .00355	- .00327	- .00296
- 2.00	+ .01628	+ .01353	+ .00761	+ .00218	- .00125	- .00294	- .00357	- .00364	- .00347	- .00319	- .00289
- 3.00	+ .01048	+ .00862	+ .00453	+ .00068	- .00182	- .00306	- .00351	- .00352	- .00333	- .00306	- .00277
- 4.00	+ .00598	+ .00478	+ .00208	- .00054	- .00228	- .00315	- .00343	- .00339	- .00319	- .00293	- .00266
- 5.00	+ .00271	+ .00196	+ .00025	- .00146	- .00262	- .00319	- .00334	- .00326	- .00305	- .00280	- .00254
- 6.00	+ .00046	+ .00001	- .00104	- .00211	- .00284	- .00318	- .00324	- .00312	- .00291	- .00267	- .00243
- 8.00	- .00191	- .00206	- .00241	- .00277	- .00300	- .00307	- .00300	- .00284	- .00264	- .00243	- .00222
-12.00	- .00275	- .00275	- .00275	- .00273	- .00267	- .00258	- .00245	- .00230	- .00214	- .00198	- .00182
-14.00	- .00256	- .00255	- .00252	- .00247	- .00240	- .00230	- .00218	- .00205	- .00192	- .00178	- .00165
-16.00	- .00229	- .00228	- .00225	- .00220	- .00213	- .00204	- .00194	- .00183	- .00171	- .00160	- .00149
-18.00	- .00202	- .00201	- .00198	- .00193	- .00187	- .00180	- .00171	- .00162	- .00153	- .00144	- .00134
-20.00	- .00177	- .00176	- .00174	- .00170	- .00165	- .00159	- .00152	- .00145	- .00137	- .00129	- .00121

TABLE IV.- SIDEWASH FACTOR F_V FOR VARIOUS VALUES OF $\Delta z/s$

(a) $\Delta z/s = 0.50$

$\Delta x/s$ \ $\Delta y/s$	+0	+2	+4	+6	+8	+10	+12	+14	+16	+18	+20
- .00	- .00000	- .34595	- .03425	- .00965	- .00400	- .00203	- .00117	- .00073	- .00049	- .00034	- .00025
+ .20	- .00000	- .41284	- .03701	- .01015	- .00415	- .00209	- .00120	- .00075	- .00050	- .00035	- .00025
+ .40	- .00000	- .47364	- .03973	- .01064	- .00430	- .00215	- .00123	- .00077	- .00051	- .00036	- .00026
+ .60	- .00000	- .52463	- .04237	- .01113	- .00445	- .00221	- .00126	- .00078	- .00052	- .00036	- .00026
+ .80	- .00000	- .56496	- .04489	- .01161	- .00460	- .00228	- .00129	- .00080	- .00053	- .00037	- .00027
+ 1.00	- .00000	- .59573	- .04727	- .01208	- .00475	- .00234	- .00132	- .00081	- .00054	- .00037	- .00027
+ 1.40	- .00000	- .63591	- .05154	- .01298	- .00504	- .00245	- .00137	- .00084	- .00056	- .00038	- .00028
+ 2.00	- .00000	- .66540	- .05663	- .01419	- .00545	- .00263	- .00146	- .00089	- .00058	- .00040	- .00029
+ 3.00	- .00000	- .68280	- .06206	- .01581	- .00605	- .00289	- .00159	- .00096	- .00063	- .00043	- .00031
+ 4.00	- .00000	- .68815	- .06495	- .01696	- .00653	- .00312	- .00171	- .00103	- .00067	- .00046	- .00032
+ 5.00	- .00000	- .69012	- .06647	- .01773	- .00690	- .00331	- .00181	- .00109	- .00071	- .00048	- .00034
+ 6.00	- .00000	- .69096	- .06728	- .01823	- .00719	- .00347	- .00191	- .00115	- .00074	- .00050	- .00036
+ 8.00	- .00000	- .69157	- .06801	- .01879	- .00755	- .00369	- .00205	- .00124	- .00080	- .00054	- .00038
+12.00	- .00000	- .69182	- .06838	- .01915	- .00784	- .00391	- .00220	- .00135	- .00088	- .00060	- .00043
+14.00	- .00000	- .69185	- .06844	- .01921	- .00790	- .00396	- .00225	- .00138	- .00091	- .00062	- .00044
+16.00	- .00000	- .69187	- .06846	- .01924	- .00793	- .00399	- .00227	- .00141	- .00093	- .00064	- .00046
+18.00	- .00000	- .69188	- .06848	- .01926	- .00795	- .00401	- .00229	- .00142	- .00094	- .00065	- .00047
+20.00	- .00000	- .69188	- .06849	- .01928	- .00797	- .00403	- .00231	- .00144	- .00095	- .00066	- .00047
- .00	- .00000	- .34595	- .03425	- .00965	- .00400	- .00203	- .00117	- .00073	- .00049	- .00034	- .00025
- .20	- .00000	- .27906	- .03149	- .00915	- .00385	- .00197	- .00114	- .00072	- .00048	- .00034	- .00025
- .40	- .00000	- .21825	- .02877	- .00866	- .00369	- .00191	- .00111	- .00070	- .00047	- .00033	- .00024
- .60	- .00000	- .16726	- .02614	- .00817	- .00354	- .00185	- .00108	- .00069	- .00046	- .00033	- .00024
- .80	- .00000	- .12693	- .02361	- .00769	- .00339	- .00178	- .00105	- .00067	- .00045	- .00032	- .00024
- 1.00	- .00000	- .09616	- .02123	- .00722	- .00324	- .00172	- .00102	- .00066	- .00045	- .00032	- .00023
- 1.40	- .00000	- .05599	- .01696	- .00632	- .00296	- .00161	- .00097	- .00062	- .00043	- .00030	- .00022
- 2.00	- .00000	- .02650	- .01188	- .00511	- .00255	- .00143	- .00088	- .00058	- .00040	- .00029	- .00021
- 3.00	- .00000	- .00909	- .00644	- .00349	- .00195	- .00117	- .00075	- .00051	- .00036	- .00026	- .00020
- 4.00	- .00000	- .00374	- .00356	- .00234	- .00147	- .00094	- .00063	- .00044	- .00032	- .00023	- .00018
- 5.00	- .00000	- .00177	- .00204	- .00157	- .00109	- .00075	- .00052	- .00038	- .00028	- .00021	- .00016
- 6.00	- .00000	- .00093	- .00122	- .00107	- .00081	- .00059	- .00043	- .00032	- .00024	- .00019	- .00015
- 8.00	- .00000	- .00032	- .00049	- .00051	- .00045	- .00037	- .00029	- .00023	- .00018	- .00015	- .00012
-12.00	- .00000	- .00007	- .00012	- .00015	- .00016	- .00015	- .00013	- .00012	- .00010	- .00009	- .00007
-14.00	- .00000	- .00004	- .00007	- .00009	- .00010	- .00010	- .00009	- .00008	- .00008	- .00007	- .00006
-16.00	- .00000	- .00002	- .00004	- .00005	- .00006	- .00007	- .00006	- .00006	- .00006	- .00005	- .00005
-18.00	- .00000	- .00001	- .00003	- .00004	- .00004	- .00005	- .00005	- .00005	- .00004	- .00004	- .00004
-20.00	- .00000	- .00001	- .00002	- .00002	- .00003	- .00003	- .00003	- .00003	- .00003	- .00003	- .00003

TABLE IV.- SIDEWASH FACTOR F_V FOR VARIOUS VALUES OF $\Delta z/s$ - Continued

(b) $\Delta z/s = 1.00$

$\Delta x/s$ \ $\Delta y/s$	+0	+2	+4	+6	+8	+10	+12	+14	+16	+18	+20
- .00	-.00000	-.40000	-.06154	-.01846	-.00780	-.00400	-.00231	-.00146	-.00098	-.00069	-.00050
+ .20	-.00000	-.46370	-.06634	-.01940	-.00810	-.00412	-.00237	-.00149	-.00099	-.00070	-.00051
+ .40	-.00000	-.52353	-.07108	-.02034	-.00840	-.00424	-.00243	-.00152	-.00101	-.00071	-.00052
+ .60	-.00000	-.57664	-.07568	-.02127	-.00869	-.00436	-.00249	-.00155	-.00103	-.00072	-.00052
+ .80	-.00000	-.62166	-.08010	-.02217	-.00898	-.00448	-.00255	-.00158	-.00105	-.00073	-.00053
+ 1.00	-.00000	-.65852	-.08429	-.02306	-.00927	-.00460	-.00260	-.00161	-.00107	-.00074	-.00054
+ 1.40	-.00000	-.71128	-.09184	-.02476	-.00983	-.00483	-.00272	-.00168	-.00110	-.00077	-.00055
+ 2.00	-.00000	-.75480	-.10095	-.02706	-.01062	-.00517	-.00288	-.00177	-.00116	-.00080	-.00057
+ 3.00	-.00000	-.78344	-.11086	-.03015	-.01178	-.00569	-.00314	-.00191	-.00124	-.00085	-.00061
+ 4.00	-.00000	-.79296	-.11625	-.03235	-.01272	-.00613	-.00338	-.00205	-.00133	-.00091	-.00065
+ 5.00	-.00000	-.79661	-.11913	-.03384	-.01346	-.00651	-.00359	-.00217	-.00140	-.00096	-.00068
+ 6.00	-.00000	-.79820	-.12070	-.03483	-.01401	-.00682	-.00377	-.00228	-.00147	-.00100	-.00071
+ 8.00	-.00000	-.79937	-.12210	-.03591	-.01472	-.00726	-.00405	-.00246	-.00159	-.00108	-.00077
+12.00	-.00000	-.79986	-.12284	-.03663	-.01530	-.00770	-.00436	-.00268	-.00175	-.00120	-.00085
+14.00	-.00000	-.79993	-.12294	-.03675	-.01542	-.00780	-.00444	-.00275	-.00180	-.00124	-.00088
+16.00	-.00000	-.79996	-.12300	-.03681	-.01548	-.00787	-.00450	-.00279	-.00184	-.00127	-.00091
+18.00	-.00000	-.79997	-.12302	-.03685	-.01553	-.00791	-.00454	-.00283	-.00187	-.00129	-.00093
+20.00	-.00000	-.79998	-.12304	-.03687	-.01555	-.00793	-.00456	-.00285	-.00189	-.00131	-.00094
- .00	-.00000	-.40000	-.06154	-.01846	-.00780	-.00400	-.00231	-.00146	-.00098	-.00069	-.00050
- .20	-.00000	-.33630	-.05673	-.01752	-.00751	-.00388	-.00226	-.00143	-.00096	-.00067	-.00049
- .40	-.00000	-.27647	-.05200	-.01658	-.00721	-.00376	-.00220	-.00139	-.00094	-.00066	-.00048
- .60	-.00000	-.22336	-.04739	-.01566	-.00692	-.00364	-.00214	-.00136	-.00092	-.00065	-.00048
- .80	-.00000	-.17834	-.04297	-.01475	-.00663	-.00352	-.00208	-.00133	-.00090	-.00064	-.00047
- 1.00	-.00000	-.14148	-.03879	-.01386	-.00634	-.00340	-.00203	-.00130	-.00088	-.00063	-.00046
- 1.40	-.00000	-.08872	-.03124	-.01216	-.00578	-.00317	-.00191	-.00124	-.00085	-.00061	-.00045
- 2.00	-.00000	-.04520	-.02213	-.00986	-.00499	-.00283	-.00175	-.00115	-.00080	-.00057	-.00043
- 3.00	-.00000	-.01656	-.01222	-.00677	-.00383	-.00231	-.00148	-.00100	-.00071	-.00052	-.00039
- 4.00	-.00000	-.00704	-.00683	-.00457	-.00289	-.00186	-.00125	-.00087	-.00063	-.00047	-.00035
- 5.00	-.00000	-.00339	-.00395	-.00308	-.00215	-.00148	-.00104	-.00075	-.00055	-.00042	-.00032
- 6.00	-.00000	-.00180	-.00233	-.00209	-.00160	-.00118	-.00086	-.00064	-.00048	-.00037	-.00029
- 8.00	-.00000	-.00063	-.00097	-.00101	-.00089	-.00073	-.00058	-.00046	-.00036	-.00029	-.00023
-12.00	-.00000	-.00014	-.00024	-.00029	-.00031	-.00029	-.00027	-.00023	-.00020	-.00017	-.00015
-14.00	-.00000	-.00007	-.00014	-.00017	-.00019	-.00019	-.00018	-.00017	-.00015	-.00013	-.00012
-16.00	-.00000	-.00004	-.00008	-.00011	-.00012	-.00013	-.00013	-.00012	-.00011	-.00010	-.00009
-18.00	-.00000	-.00003	-.00005	-.00007	-.00008	-.00009	-.00009	-.00009	-.00009	-.00008	-.00007
-20.00	-.00000	-.00002	-.00003	-.00005	-.00006	-.00006	-.00007	-.00007	-.00006	-.00006	-.00006

TABLE IV.- SIDEWASH FACTOR F_V FOR VARIOUS VALUES OF $\Delta z/s$ - Continued

(c) $\Delta z/s = 1.50$

$\Delta y/s$ / $\Delta x/s$	+0	+2	+4	+6	+8	+10	+12	+14	+16	+18	+20
- .00	-.00000	-.32821	-.07829	-.02578	-.01125	-.00585	-.00341	-.00216	-.00145	-.00102	-.00075
+ .20	-.00000	-.37116	-.08412	-.02707	-.01167	-.00602	-.00350	-.00220	-.00148	-.00104	-.00076
+ .40	-.00000	-.41239	-.08987	-.02835	-.01209	-.00620	-.00358	-.00225	-.00150	-.00105	-.00077
+ .60	-.00000	-.45048	-.09548	-.02962	-.01251	-.00637	-.00367	-.00230	-.00153	-.00107	-.00078
+ .80	-.00000	-.48448	-.10088	-.03087	-.01293	-.00655	-.00375	-.00234	-.00156	-.00109	-.00079
+ 1.00	-.00000	-.51399	-.10603	-.03209	-.01334	-.00672	-.00384	-.00239	-.00159	-.00111	-.00080
+ 1.40	-.00000	-.55993	-.11539	-.03442	-.01413	-.00706	-.00400	-.00248	-.00164	-.00114	-.00082
+ 2.00	-.00000	-.60274	-.12688	-.03760	-.01527	-.00755	-.00425	-.00261	-.00172	-.00119	-.00086
+ 3.00	-.00000	-.63492	-.13975	-.04189	-.01693	-.00830	-.00463	-.00283	-.00185	-.00127	-.00091
+ 4.00	-.00000	-.64681	-.14698	-.04498	-.01829	-.00896	-.00498	-.00303	-.00197	-.00135	-.00096
+ 5.00	-.00000	-.65166	-.15094	-.04709	-.01935	-.00951	-.00528	-.00321	-.00208	-.00142	-.00101
+ 6.00	-.00000	-.65384	-.15314	-.04851	-.02015	-.00996	-.00555	-.00337	-.00218	-.00149	-.00106
+ 8.00	-.00000	-.65549	-.15515	-.05007	-.02118	-.01061	-.00596	-.00363	-.00236	-.00161	-.00114
+12.00	-.00000	-.65621	-.15622	-.05112	-.02204	-.01126	-.00642	-.00397	-.00260	-.00178	-.00127
+14.00	-.00000	-.65630	-.15637	-.05130	-.02221	-.01141	-.00655	-.00407	-.00268	-.00184	-.00132
+16.00	-.00000	-.65634	-.15645	-.05139	-.02231	-.01150	-.00663	-.00413	-.00273	-.00189	-.00135
+18.00	-.00000	-.65637	-.15650	-.05145	-.02238	-.01156	-.00669	-.00418	-.00277	-.00192	-.00138
+20.00	-.00000	-.65638	-.15652	-.05148	-.02241	-.01160	-.00672	-.00422	-.00280	-.00195	-.00140
- .00	-.00000	-.32821	-.07829	-.02578	-.01125	-.00585	-.00341	-.00216	-.00145	-.00102	-.00075
- .20	-.00000	-.28525	-.07246	-.02449	-.01083	-.00567	-.00333	-.00211	-.00142	-.00100	-.00073
- .40	-.00000	-.24402	-.06670	-.02320	-.01041	-.00550	-.00324	-.00207	-.00140	-.00099	-.00072
- .60	-.00000	-.20593	-.06109	-.02194	-.00999	-.00532	-.00316	-.00202	-.00137	-.00097	-.00071
- .80	-.00000	-.17193	-.05569	-.02069	-.00957	-.00515	-.00307	-.00197	-.00134	-.00095	-.00070
- 1.00	-.00000	-.14242	-.05055	-.01947	-.00916	-.00498	-.00299	-.00193	-.00131	-.00094	-.00069
- 1.40	-.00000	-.09648	-.04119	-.01714	-.00837	-.00464	-.00282	-.00184	-.00126	-.00090	-.00067
- 2.00	-.00000	-.05367	-.02969	-.01396	-.00723	-.00415	-.00258	-.00170	-.00118	-.00085	-.00063
- 3.00	-.00000	-.02149	-.01683	-.00966	-.00557	-.00339	-.00219	-.00149	-.00105	-.00077	-.00058
- 4.00	-.00000	-.00960	-.00960	-.00657	-.00421	-.00274	-.00185	-.00129	-.00093	-.00069	-.00053
- 5.00	-.00000	-.00475	-.00564	-.00446	-.00315	-.00219	-.00154	-.00111	-.00082	-.00062	-.00048
- 6.00	-.00000	-.00257	-.00343	-.00305	-.00235	-.00173	-.00128	-.00095	-.00072	-.00055	-.00043
- 8.00	-.00000	-.00092	-.00142	-.00149	-.00132	-.00108	-.00086	-.00068	-.00054	-.00043	-.00035
-12.00	-.00000	-.00020	-.00035	-.00044	-.00046	-.00044	-.00040	-.00035	-.00030	-.00026	-.00022
-14.00	-.00000	-.00011	-.00020	-.00026	-.00029	-.00029	-.00027	-.00025	-.00023	-.00020	-.00017
-16.00	-.00000	-.00007	-.00012	-.00016	-.00019	-.00019	-.00019	-.00018	-.00017	-.00015	-.00014
-18.00	-.00000	-.00004	-.00008	-.00011	-.00013	-.00014	-.00014	-.00013	-.00013	-.00012	-.00011
-20.00	-.00000	-.00003	-.00005	-.00007	-.00009	-.00010	-.00010	-.00010	-.00010	-.00009	-.00009

TABLE IV.- SIDEWASH FACTOR F_V FOR VARIOUS VALUES OF $\Delta z/s$ - Continued

(d) $\Delta z/s$ = 2.00

$\Delta x/s$ \ $\Delta y/s$	+0	+2	+4	+6	+8	+10	+12	+14	+16	+18	+20
+ .00	- .00000	- .24615	- .08488	- .03123	- .01421	- .00753	- .00444	- .00283	- .00191	- .00135	- .00099
+ .20	- .00000	- .27327	- .09084	- .03275	- .01473	- .00775	- .00455	- .00289	- .00194	- .00137	- .00100
+ .40	- .00000	- .29963	- .09674	- .03427	- .01526	- .00798	- .00466	- .00295	- .00198	- .00139	- .00101
+ .60	- .00000	- .32456	- .10250	- .03577	- .01578	- .00820	- .00477	- .00301	- .00201	- .00141	- .00103
+ .80	- .00000	- .34757	- .10807	- .03724	- .01629	- .00842	- .00488	- .00307	- .00205	- .00144	- .00104
+ 1.00	- .00000	- .36834	- .11341	- .03869	- .01680	- .00864	- .00499	- .00313	- .00209	- .00146	- .00106
+ 1.40	- .00000	- .40273	- .12321	- .04146	- .01780	- .00907	- .00520	- .00325	- .00216	- .00150	- .00109
+ 2.00	- .00000	- .43819	- .13550	- .04524	- .01921	- .00970	- .00552	- .00342	- .00226	- .00157	- .00113
+ 3.00	- .00000	- .46847	- .14972	- .05042	- .02130	- .01066	- .00602	- .00370	- .00243	- .00167	- .00120
+ 4.00	- .00000	- .48103	- .15803	- .05418	- .02301	- .01150	- .00647	- .00396	- .00259	- .00178	- .00127
+ 5.00	- .00000	- .48652	- .16274	- .05679	- .02435	- .01221	- .00686	- .00419	- .00273	- .00187	- .00134
+ 6.00	- .00000	- .48910	- .16542	- .05855	- .02537	- .01280	- .00721	- .00441	- .00287	- .00196	- .00140
+ 8.00	- .00000	- .49113	- .16793	- .06053	- .02670	- .01364	- .00774	- .00475	- .00310	- .00212	- .00151
+12.00	- .00000	- .49205	- .16930	- .06189	- .02781	- .01448	- .00835	- .00519	- .00342	- .00235	- .00168
+14.00	- .00000	- .49216	- .16950	- .06212	- .02804	- .01468	- .00852	- .00532	- .00352	- .00243	- .00174
+16.00	- .00000	- .49222	- .16960	- .06224	- .02817	- .01480	- .00862	- .00541	- .00359	- .00249	- .00179
+18.00	- .00000	- .49225	- .16966	- .06232	- .02825	- .01488	- .00870	- .00548	- .00365	- .00254	- .00183
+20.00	- .00000	- .49227	- .16969	- .06236	- .02830	- .01493	- .00875	- .00552	- .00369	- .00257	- .00186
- .00	- .00000	- .24615	- .08488	- .03123	- .01421	- .00753	- .00444	- .00283	- .00191	- .00135	- .00099
- .20	- .00000	- .21904	- .07892	- .02971	- .01368	- .00731	- .00433	- .00277	- .00187	- .00132	- .00097
- .40	- .00000	- .19268	- .07303	- .02819	- .01316	- .00708	- .00422	- .00271	- .00184	- .00130	- .00096
- .60	- .00000	- .16774	- .06726	- .02669	- .01263	- .00686	- .00411	- .00265	- .00180	- .00128	- .00094
- .80	- .00000	- .14473	- .06169	- .02522	- .01212	- .00664	- .00400	- .00259	- .00177	- .00126	- .00093
- 1.00	- .00000	- .12397	- .05635	- .02377	- .01161	- .00642	- .00389	- .00253	- .00173	- .00123	- .00091
- 1.40	- .00000	- .08957	- .04655	- .02100	- .01061	- .00598	- .00367	- .00241	- .00166	- .00119	- .00088
- 2.00	- .00000	- .05411	- .03427	- .01722	- .00920	- .00536	- .00336	- .00223	- .00156	- .00112	- .00084
- 3.00	- .00000	- .02384	- .02004	- .01204	- .00711	- .00440	- .00286	- .00195	- .00139	- .00102	- .00077
- 4.00	- .00000	- .01128	- .01173	- .00828	- .00540	- .00355	- .00241	- .00170	- .00123	- .00092	- .00070
- 5.00	- .00000	- .00579	- .00702	- .00567	- .00406	- .00284	- .00202	- .00146	- .00108	- .00082	- .00063
- 6.00	- .00000	- .00321	- .00434	- .00390	- .00304	- .00226	- .00167	- .00125	- .00095	- .00073	- .00057
- 8.00	- .00000	- .00118	- .00183	- .00193	- .00172	- .00142	- .00114	- .00090	- .00072	- .00057	- .00046
-12.00	- .00000	- .00026	- .00046	- .00057	- .00060	- .00058	- .00052	- .00046	- .00040	- .00034	- .00029
-14.00	- .00000	- .00015	- .00026	- .00034	- .00038	- .00038	- .00036	- .00033	- .00030	- .00026	- .00023
-16.00	- .00000	- .00009	- .00016	- .00021	- .00025	- .00026	- .00025	- .00024	- .00022	- .00020	- .00018
-18.00	- .00000	- .00005	- .00010	- .00014	- .00017	- .00018	- .00018	- .00018	- .00017	- .00016	- .00014
-20.00	- .00000	- .00004	- .00007	- .00010	- .00012	- .00013	- .00013	- .00013	- .00013	- .00012	- .00012

TABLE IV.- SIDEWASH FACTOR F_V FOR VARIOUS VALUES OF $\Delta z/s$ - Continued

(e) $\Delta z/s = 2.50$

$\Delta x/s$ \ $\Delta y/s$	+0	+2	+4	+6	+8	+10	+12	+14	+16	+18	+20
+ .00	-.00000	-.18089	-.08393	-.03475	-.01660	-.00901	-.00538	-.00345	-.00234	-.00166	-.00122
+ .20	-.00000	-.19805	-.08946	-.03639	-.01720	-.00927	-.00551	-.00353	-.00239	-.00169	-.00124
+ .40	-.00000	-.21486	-.09493	-.03803	-.01780	-.00954	-.00565	-.00360	-.00243	-.00172	-.00125
+ .60	-.00000	-.23100	-.10029	-.03965	-.01840	-.00980	-.00578	-.00367	-.00247	-.00174	-.00127
+ .80	-.00000	-.24620	-.10550	-.04124	-.01899	-.01006	-.00591	-.00375	-.00252	-.00177	-.00129
+ 1.00	-.00000	-.26028	-.11051	-.04281	-.01958	-.01032	-.00604	-.00382	-.00256	-.00180	-.00131
+ 1.40	-.00000	-.28464	-.11982	-.04581	-.02072	-.01083	-.00630	-.00396	-.00265	-.00185	-.00134
+ 2.00	-.00000	-.31178	-.13171	-.04994	-.02235	-.01158	-.00668	-.00418	-.00277	-.00193	-.00140
+ 3.00	-.00000	-.33765	-.14598	-.05565	-.02477	-.01272	-.00728	-.00451	-.00298	-.00206	-.00149
+ 4.00	-.00000	-.34965	-.15468	-.05986	-.02676	-.01372	-.00782	-.00483	-.00317	-.00219	-.00157
+ 5.00	-.00000	-.35530	-.15980	-.06283	-.02833	-.01457	-.00830	-.00512	-.00335	-.00231	-.00165
+ 6.00	-.00000	-.35810	-.16280	-.06486	-.02953	-.01527	-.00872	-.00538	-.00352	-.00242	-.00173
+ 8.00	-.00000	-.36039	-.16568	-.06718	-.03111	-.01628	-.00937	-.00580	-.00380	-.00261	-.00186
+12.00	-.00000	-.36147	-.16730	-.06880	-.03245	-.01730	-.01011	-.00634	-.00419	-.00290	-.00207
+14.00	-.00000	-.36161	-.16754	-.06908	-.03273	-.01754	-.01031	-.00650	-.00432	-.00299	-.00215
+16.00	-.00000	-.36168	-.16767	-.06924	-.03289	-.01770	-.01045	-.00661	-.00441	-.00307	-.00221
+18.00	-.00000	-.36172	-.16774	-.06933	-.03299	-.01779	-.01054	-.00669	-.00448	-.00312	-.00226
+20.00	-.00000	-.36174	-.16778	-.06938	-.03305	-.01786	-.01060	-.00674	-.00453	-.00317	-.00229
- .00	-.00000	-.18089	-.08393	-.03475	-.01660	-.00901	-.00538	-.00345	-.00234	-.00166	-.00122
- .20	-.00000	-.16374	-.07841	-.03311	-.01599	-.00874	-.00525	-.00338	-.00230	-.00163	-.00120
- .40	-.00000	-.14693	-.07294	-.03147	-.01539	-.00848	-.00512	-.00331	-.00226	-.00161	-.00118
- .60	-.00000	-.13079	-.06758	-.02985	-.01479	-.00821	-.00498	-.00323	-.00221	-.00158	-.00116
- .80	-.00000	-.11558	-.06237	-.02826	-.01420	-.00795	-.00485	-.00316	-.00217	-.00155	-.00115
- 1.00	-.00000	-.10151	-.05735	-.02670	-.01361	-.00769	-.00472	-.00309	-.00213	-.00152	-.00113
- 1.40	-.00000	-.07714	-.04805	-.02369	-.01247	-.00718	-.00446	-.00295	-.00204	-.00147	-.00109
- 2.00	-.00000	-.05001	-.03616	-.01956	-.01084	-.00644	-.00408	-.00273	-.00191	-.00139	-.00104
- 3.00	-.00000	-.02414	-.02189	-.01386	-.00842	-.00529	-.00348	-.00239	-.00171	-.00126	-.00095
- 4.00	-.00000	-.01214	-.01319	-.00964	-.00643	-.00429	-.00294	-.00208	-.00151	-.00113	-.00087
- 5.00	-.00000	-.00649	-.00807	-.00667	-.00486	-.00345	-.00246	-.00179	-.00133	-.00101	-.00079
- 6.00	-.00000	-.00369	-.00507	-.00464	-.00366	-.00275	-.00204	-.00153	-.00117	-.00090	-.00071
- 8.00	-.00000	-.00140	-.00219	-.00232	-.00209	-.00173	-.00139	-.00111	-.00088	-.00071	-.00057
-12.00	-.00000	-.00032	-.00056	-.00070	-.00074	-.00071	-.00065	-.00057	-.00049	-.00042	-.00036
-14.00	-.00000	-.00018	-.00032	-.00042	-.00047	-.00047	-.00045	-.00041	-.00037	-.00033	-.00029
-16.00	-.00000	-.00011	-.00020	-.00026	-.00030	-.00032	-.00032	-.00030	-.00028	-.00025	-.00023
-18.00	-.00000	-.00007	-.00013	-.00017	-.00021	-.00022	-.00023	-.00022	-.00021	-.00020	-.00018
-20.00	-.00000	-.00004	-.00009	-.00012	-.00014	-.00016	-.00016	-.00016	-.00016	-.00015	-.00014

TABLE IV.- SIDEWASH FACTOR F_V FOR VARIOUS VALUES OF $\Delta z/s$ - Continued

(f) $\Delta z/s$ = 3.00

$\Delta x/s$ \ $\Delta y/s$	+0	+2	+4	+6	+8	+10	+12	+14	+16	+18	+20
+ .00	-.00000	-.13333	-.07843	-.03651	-.01839	-.01026	-.00622	-.00403	-.00275	-.00196	-.00144
+ .20	-.00000	-.14442	-.08325	-.03818	-.01905	-.01055	-.00638	-.00412	-.00280	-.00199	-.00146
+ .40	-.00000	-.15534	-.08804	-.03984	-.01970	-.01085	-.00653	-.00420	-.00286	-.00202	-.00148
+ .60	-.00000	-.16592	-.09274	-.04148	-.02035	-.01115	-.00668	-.00429	-.00291	-.00206	-.00151
+ .80	-.00000	-.17603	-.09732	-.04310	-.02099	-.01144	-.00683	-.00437	-.00296	-.00209	-.00153
+ 1.00	-.00000	-.18555	-.10175	-.04469	-.02163	-.01173	-.00698	-.00446	-.00301	-.00212	-.00155
+ 1.40	-.00000	-.20255	-.11006	-.04776	-.02288	-.01231	-.00728	-.00462	-.00311	-.00218	-.00159
+ 2.00	-.00000	-.22262	-.12087	-.05200	-.02465	-.01315	-.00771	-.00487	-.00326	-.00228	-.00165
+ 3.00	-.00000	-.24358	-.13429	-.05792	-.02730	-.01443	-.00840	-.00526	-.00350	-.00243	-.00176
+ 4.00	-.00000	-.25434	-.14285	-.06237	-.02949	-.01557	-.00902	-.00563	-.00372	-.00258	-.00186
+ 5.00	-.00000	-.25980	-.14808	-.06556	-.03124	-.01653	-.00958	-.00596	-.00394	-.00272	-.00195
+ 6.00	-.00000	-.26265	-.15124	-.06778	-.03258	-.01733	-.01006	-.00626	-.00413	-.00285	-.00204
+ 8.00	-.00000	-.26509	-.15437	-.07035	-.03437	-.01849	-.01081	-.00676	-.00446	-.00308	-.00220
+12.00	-.00000	-.26629	-.15620	-.07220	-.03591	-.01968	-.01168	-.00739	-.00492	-.00341	-.00245
+14.00	-.00000	-.26646	-.15648	-.07253	-.03623	-.01996	-.01192	-.00758	-.00507	-.00353	-.00254
+16.00	-.00000	-.26654	-.15663	-.07271	-.03642	-.02014	-.01207	-.00771	-.00518	-.00362	-.00261
+18.00	-.00000	-.26659	-.15671	-.07282	-.03654	-.02025	-.01218	-.00780	-.00526	-.00368	-.00267
+20.00	-.00000	-.26661	-.15676	-.07288	-.03661	-.02033	-.01225	-.00787	-.00532	-.00374	-.00271
- .00	-.00000	-.13333	-.07843	-.03651	-.01839	-.01026	-.00622	-.00403	-.00275	-.00196	-.00144
- .20	-.00000	-.12225	-.07361	-.03484	-.01774	-.00996	-.00607	-.00395	-.00270	-.00193	-.00142
- .40	-.00000	-.11133	-.06883	-.03319	-.01708	-.00966	-.00592	-.00386	-.00265	-.00189	-.00140
- .60	-.00000	-.10075	-.06413	-.03154	-.01643	-.00937	-.00577	-.00378	-.00260	-.00186	-.00138
- .80	-.00000	-.09064	-.05954	-.02992	-.01579	-.00907	-.00562	-.00369	-.00255	-.00183	-.00136
- 1.00	-.00000	-.08112	-.05511	-.02833	-.01515	-.00878	-.00547	-.00361	-.00250	-.00180	-.00133
- 1.40	-.00000	-.06411	-.04680	-.02526	-.01391	-.00820	-.00517	-.00344	-.00240	-.00173	-.00129
- 2.00	-.00000	-.04404	-.03599	-.02102	-.01213	-.00737	-.00473	-.00320	-.00225	-.00164	-.00123
- 3.00	-.00000	-.02308	-.02257	-.01510	-.00948	-.00608	-.00405	-.00280	-.00201	-.00148	-.00113
- 4.00	-.00000	-.01233	-.01401	-.01065	-.00729	-.00495	-.00342	-.00244	-.00178	-.00134	-.00103
- 5.00	-.00000	-.00687	-.00879	-.00746	-.00555	-.00398	-.00287	-.00210	-.00157	-.00120	-.00093
- 6.00	-.00000	-.00402	-.00563	-.00524	-.00420	-.00319	-.00239	-.00180	-.00138	-.00107	-.00084
- 8.00	-.00000	-.00158	-.00249	-.00267	-.00242	-.00202	-.00164	-.00131	-.00104	-.00084	-.00068
-12.00	-.00000	-.00037	-.00066	-.00082	-.00087	-.00084	-.00076	-.00068	-.00059	-.00050	-.00043
-14.00	-.00000	-.00021	-.00038	-.00049	-.00055	-.00056	-.00053	-.00049	-.00044	-.00039	-.00034
-16.00	-.00000	-.00013	-.00023	-.00031	-.00036	-.00038	-.00037	-.00036	-.00033	-.00030	-.00027
-18.00	-.00000	-.00008	-.00015	-.00021	-.00024	-.00026	-.00027	-.00026	-.00025	-.00023	-.00021
-20.00	-.00000	-.00005	-.00010	-.00014	-.00017	-.00019	-.00020	-.00020	-.00019	-.00018	-.00017

TABLE IV.- SIDEWASH FACTOR F_v FOR VARIOUS VALUES OF $\Delta z/s$ - Continued

(g) $\Delta z/s = 4.00$

$\Delta x/s$ \ $\Delta y/s$	+0	+2	+4	+6	+8	+10	+12	+14	+16	+18	+20
+ .00	- .00000	- .07529	- .06244	- .03602	- .02030	- .01204	- .00758	- .00502	- .00348	- .00250	- .00186
+ .20	- .00000	- .08030	- .06579	- .03754	- .02099	- .01238	- .00776	- .00513	- .00355	- .00255	- .00188
+ .40	- .00000	- .08526	- .06912	- .03906	- .02168	- .01272	- .00794	- .00523	- .00361	- .00259	- .00191
+ .60	- .00000	- .09011	- .07240	- .04056	- .02236	- .01305	- .00812	- .00534	- .00367	- .00263	- .00194
+ .80	- .00000	- .09483	- .07562	- .04204	- .02304	- .01339	- .00830	- .00544	- .00374	- .00267	- .00197
+ 1.00	- .00000	- .09937	- .07876	- .04350	- .02371	- .01372	- .00848	- .00554	- .00380	- .00271	- .00199
+ 1.40	- .00000	- .10781	- .08474	- .04633	- .02503	- .01438	- .00883	- .00575	- .00393	- .00279	- .00205
+ 2.00	- .00000	- .11856	- .09277	- .05029	- .02691	- .01533	- .00935	- .00605	- .00411	- .00291	- .00213
+ 3.00	- .00000	- .13141	- .10337	- .05595	- .02975	- .01681	- .01017	- .00653	- .00441	- .00310	- .00226
+ 4.00	- .00000	- .13918	- .11070	- .06036	- .03213	- .01812	- .01092	- .00698	- .00470	- .00329	- .00239
+ 5.00	- .00000	- .14369	- .11553	- .06363	- .03407	- .01924	- .01159	- .00740	- .00496	- .00347	- .00251
+ 6.00	- .00000	- .14630	- .11865	- .06599	- .03559	- .02018	- .01217	- .00777	- .00521	- .00363	- .00262
+ 8.00	- .00000	- .14876	- .12195	- .06885	- .03765	- .02156	- .01309	- .00838	- .00562	- .00392	- .00283
+12.00	- .00000	- .15013	- .12406	- .07102	- .03951	- .02301	- .01417	- .00918	- .00621	- .00435	- .00315
+14.00	- .00000	- .15032	- .12440	- .07142	- .03990	- .02337	- .01447	- .00942	- .00640	- .00450	- .00327
+16.00	- .00000	- .15043	- .12458	- .07164	- .04014	- .02359	- .01467	- .00959	- .00654	- .00462	- .00336
+18.00	- .00000	- .15049	- .12468	- .07178	- .04029	- .02374	- .01480	- .00971	- .00664	- .00470	- .00343
+20.00	- .00000	- .15052	- .12475	- .07186	- .04038	- .02384	- .01490	- .00979	- .00672	- .00477	- .00349
- .00	- .00000	- .07529	- .06244	- .03602	- .02030	- .01204	- .00758	- .00502	- .00348	- .00250	- .00186
- .20	- .00000	- .07029	- .05909	- .03450	- .01961	- .01170	- .00739	- .00492	- .00342	- .00246	- .00183
- .40	- .00000	- .06533	- .05576	- .03299	- .01893	- .01136	- .00721	- .00482	- .00336	- .00242	- .00180
- .60	- .00000	- .06047	- .05248	- .03149	- .01824	- .01103	- .00703	- .00471	- .00329	- .00238	- .00178
- .80	- .00000	- .05575	- .04926	- .03000	- .01756	- .01069	- .00685	- .00461	- .00323	- .00234	- .00175
- 1.00	- .00000	- .05121	- .04611	- .02854	- .01689	- .01036	- .00668	- .00451	- .00317	- .00230	- .00172
- 1.40	- .00000	- .04278	- .04014	- .02571	- .01558	- .00970	- .00632	- .00430	- .00304	- .00222	- .00167
- 2.00	- .00000	- .03203	- .03210	- .02175	- .01369	- .00875	- .00580	- .00400	- .00285	- .00210	- .00159
- 3.00	- .00000	- .01918	- .02151	- .01609	- .01086	- .00727	- .00498	- .00352	- .00255	- .00190	- .00145
- 4.00	- .00000	- .01141	- .01418	- .01168	- .00847	- .00596	- .00423	- .00307	- .00227	- .00172	- .00133
- 5.00	- .00000	- .00690	- .00935	- .00841	- .00653	- .00484	- .00357	- .00265	- .00200	- .00154	- .00120
- 6.00	- .00000	- .00429	- .00623	- .00605	- .00502	- .00390	- .00298	- .00228	- .00176	- .00138	- .00109
- 8.00	- .00000	- .00182	- .00293	- .00320	- .00296	- .00252	- .00206	- .00167	- .00134	- .00108	- .00088
-12.00	- .00000	- .00046	- .00082	- .00103	- .00110	- .00107	- .00098	- .00087	- .00076	- .00066	- .00056
-14.00	- .00000	- .00026	- .00048	- .00063	- .00070	- .00071	- .00068	- .00063	- .00057	- .00051	- .00045
-16.00	- .00000	- .00016	- .00030	- .00040	- .00046	- .00049	- .00048	- .00046	- .00043	- .00039	- .00035
-18.00	- .00000	- .00010	- .00019	- .00027	- .00032	- .00034	- .00035	- .00034	- .00033	- .00031	- .00028
-20.00	- .00000	- .00007	- .00013	- .00018	- .00022	- .00024	- .00026	- .00026	- .00025	- .00024	- .00022

TABLE IV.- SIDEWASH FACTOR F_V FOR VARIOUS VALUES OF $\Delta z/s$ - Continued

(h) $\Delta z/s = 6.00$

$\Delta x/s$ \ $\Delta y/s$	+0	+2	+4	+6	+8	+10	+12	+14	+16	+18	+20
+ .00	- .00000	- .02883	- .03497	- .02777	- .01931	- .01307	- .00895	- .00628	- .00453	- .00335	- .00253
+ .20	- .00000	- .03018	- .03643	- .02876	- .01989	- .01340	- .00915	- .00640	- .00461	- .00340	- .00257
+ .40	- .00000	- .03153	- .03788	- .02974	- .02047	- .01374	- .00935	- .00653	- .00469	- .00345	- .00261
+ .60	- .00000	- .03287	- .03932	- .03072	- .02105	- .01408	- .00955	- .00665	- .00477	- .00351	- .00264
+ .80	- .00000	- .03419	- .04074	- .03169	- .02163	- .01441	- .00975	- .00678	- .00485	- .00356	- .00268
+ 1.00	- .00000	- .03548	- .04214	- .03265	- .02220	- .01475	- .00995	- .00690	- .00492	- .00361	- .00272
+ 1.40	- .00000	- .03796	- .04486	- .03453	- .02332	- .01540	- .01034	- .00714	- .00508	- .00372	- .00279
+ 2.00	- .00000	- .04138	- .04867	- .03721	- .02495	- .01637	- .01092	- .00750	- .00532	- .00387	- .00290
+ 3.00	- .00000	- .04612	- .05414	- .04120	- .02744	- .01787	- .01184	- .00808	- .00569	- .00413	- .00307
+ 4.00	- .00000	- .04964	- .05842	- .04451	- .02961	- .01923	- .01270	- .00863	- .00605	- .00437	- .00324
+ 5.00	- .00000	- .05212	- .06162	- .04715	- .03144	- .02042	- .01346	- .00913	- .00639	- .00460	- .00341
+ 6.00	- .00000	- .05382	- .06394	- .04919	- .03293	- .02144	- .01414	- .00959	- .00670	- .00482	- .00356
+ 8.00	- .00000	- .05575	- .06676	- .05189	- .03507	- .02299	- .01524	- .01035	- .00724	- .00521	- .00384
+12.00	- .00000	- .05709	- .06892	- .05423	- .03719	- .02472	- .01658	- .01137	- .00800	- .00578	- .00427
+14.00	- .00000	- .05732	- .06932	- .05472	- .03768	- .02517	- .01696	- .01169	- .00826	- .00598	- .00444
+16.00	- .00000	- .05744	- .06954	- .05500	- .03798	- .02546	- .01723	- .01191	- .00845	- .00614	- .00456
+18.00	- .00000	- .05752	- .06968	- .05518	- .03818	- .02566	- .01741	- .01208	- .00859	- .00626	- .00467
+20.00	- .00000	- .05756	- .06976	- .05529	- .03830	- .02579	- .01754	- .01220	- .00870	- .00635	- .00475
- .00	- .00000	- .02883	- .03497	- .02777	- .01931	- .01307	- .00895	- .00628	- .00453	- .00335	- .00253
- .20	- .00000	- .02747	- .03352	- .02679	- .01872	- .01273	- .00875	- .00616	- .00445	- .00330	- .00250
- .40	- .00000	- .02612	- .03207	- .02580	- .01814	- .01239	- .00855	- .00603	- .00437	- .00324	- .00246
- .60	- .00000	- .02479	- .03063	- .02482	- .01756	- .01205	- .00835	- .00591	- .00429	- .00319	- .00243
- .80	- .00000	- .02347	- .02921	- .02385	- .01699	- .01172	- .00815	- .00578	- .00421	- .00314	- .00239
- 1.00	- .00000	- .02218	- .02781	- .02289	- .01642	- .01138	- .00795	- .00566	- .00413	- .00308	- .00235
- 1.40	- .00000	- .01970	- .02509	- .02102	- .01529	- .01073	- .00755	- .00542	- .00397	- .00298	- .00228
- 2.00	- .00000	- .01627	- .02128	- .01834	- .01367	- .00977	- .00697	- .00506	- .00374	- .00282	- .00217
- 3.00	- .00000	- .01153	- .01581	- .01435	- .01117	- .00826	- .00605	- .00447	- .00336	- .00257	- .00200
- 4.00	- .00000	- .00802	- .01152	- .01103	- .00900	- .00690	- .00520	- .00393	- .00300	- .00232	- .00183
- 5.00	- .00000	- .00554	- .00832	- .00839	- .00717	- .00571	- .00443	- .00343	- .00266	- .00209	- .00166
- 6.00	- .00000	- .00384	- .00601	- .00635	- .00568	- .00470	- .00375	- .00297	- .00235	- .00188	- .00151
- 8.00	- .00000	- .00191	- .00319	- .00365	- .00354	- .00314	- .00266	- .00221	- .00181	- .00149	- .00123
-12.00	- .00000	- .00057	- .00103	- .00131	- .00142	- .00141	- .00132	- .00119	- .00105	- .00092	- .00079
-14.00	- .00000	- .00034	- .00063	- .00083	- .00093	- .00096	- .00093	- .00087	- .00080	- .00071	- .00063
-16.00	- .00000	- .00021	- .00040	- .00054	- .00063	- .00067	- .00067	- .00065	- .00061	- .00056	- .00051
-18.00	- .00000	- .00014	- .00027	- .00037	- .00044	- .00047	- .00049	- .00048	- .00046	- .00044	- .00040
-20.00	- .00000	- .00010	- .00018	- .00026	- .00031	- .00034	- .00036	- .00036	- .00036	- .00034	- .00032

TABLE IV.- SIDEWASH FACTOR F_V FOR VARIOUS VALUES OF $\Delta z/s$ - Concluded

(i) $\Delta z/s$ = 8.00

$\Delta x/s$ \ $\Delta y/s$	+0	+2	+4	+6	+8	+10	+12	+14	+16	+18	+20
+ .00	-.00000	-.01349	-.01970	-.01909	-.01562	-.01193	-.00891	-.00665	-.00502	-.00384	-.00298
+ .20	-.00000	-.01398	-.02036	-.01966	-.01604	-.01221	-.00909	-.00678	-.00510	-.00390	-.00302
+ .40	-.00000	-.01446	-.02102	-.02024	-.01645	-.01249	-.00928	-.00690	-.00519	-.00396	-.00307
+ .60	-.00000	-.01495	-.02167	-.02081	-.01687	-.01277	-.00947	-.00703	-.00527	-.00402	-.00311
+ .80	-.00000	-.01542	-.02232	-.02137	-.01728	-.01305	-.00965	-.00715	-.00536	-.00407	-.00315
+ 1.00	-.00000	-.01590	-.02297	-.02194	-.01769	-.01332	-.00983	-.00727	-.00544	-.00413	-.00319
+ 1.40	-.00000	-.01682	-.02423	-.02304	-.01850	-.01387	-.01020	-.00752	-.00561	-.00425	-.00327
+ 2.00	-.00000	-.01814	-.02604	-.02464	-.01967	-.01468	-.01074	-.00788	-.00585	-.00442	-.00340
+ 3.00	-.00000	-.02010	-.02877	-.02710	-.02152	-.01595	-.01160	-.00846	-.00626	-.00470	-.00360
+ 4.00	-.00000	-.02172	-.03108	-.02925	-.02316	-.01712	-.01241	-.00902	-.00664	-.00497	-.00379
+ 5.00	-.00000	-.02300	-.03296	-.03105	-.02460	-.01817	-.01314	-.00953	-.00700	-.00523	-.00398
+ 6.00	-.00000	-.02399	-.03444	-.03253	-.02582	-.01908	-.01380	-.01000	-.00734	-.00547	-.00416
+ 8.00	-.00000	-.02528	-.03647	-.03466	-.02766	-.02054	-.01489	-.01080	-.00793	-.00591	-.00448
+12.00	-.00000	-.02638	-.03831	-.03676	-.02967	-.02227	-.01630	-.01191	-.00878	-.00657	-.00499
+14.00	-.00000	-.02660	-.03870	-.03725	-.03018	-.02274	-.01672	-.01226	-.00908	-.00681	-.00518
+16.00	-.00000	-.02673	-.03894	-.03755	-.03051	-.02306	-.01701	-.01252	-.00930	-.00699	-.00533
+18.00	-.00000	-.02681	-.03909	-.03775	-.03073	-.02329	-.01722	-.01271	-.00947	-.00714	-.00546
+20.00	-.00000	-.02686	-.03918	-.03787	-.03087	-.02344	-.01737	-.01286	-.00959	-.00725	-.00556
- .00	-.00000	-.01349	-.01970	-.01909	-.01562	-.01193	-.00891	-.00665	-.00502	-.00384	-.00298
- .20	-.00000	-.01300	-.01904	-.01852	-.01521	-.01165	-.00872	-.00653	-.00493	-.00378	-.00294
- .40	-.00000	-.01251	-.01838	-.01795	-.01479	-.01137	-.00854	-.00640	-.00485	-.00372	-.00290
- .60	-.00000	-.01203	-.01773	-.01738	-.01438	-.01109	-.00835	-.00628	-.00477	-.00366	-.00286
- .80	-.00000	-.01155	-.01708	-.01681	-.01397	-.01081	-.00817	-.00616	-.00468	-.00361	-.00282
- 1.00	-.00000	-.01108	-.01644	-.01625	-.01356	-.01053	-.00798	-.00603	-.00460	-.00355	-.00277
- 1.40	-.00000	-.01015	-.01518	-.01514	-.01275	-.00999	-.00762	-.00579	-.00443	-.00343	-.00269
- 2.00	-.00000	-.00883	-.01337	-.01354	-.01157	-.00918	-.00708	-.00543	-.00418	-.00326	-.00257
- 3.00	-.00000	-.00687	-.01064	-.01108	-.00973	-.00791	-.00622	-.00484	-.00378	-.00298	-.00237
- 4.00	-.00000	-.00525	-.00832	-.00894	-.00808	-.00674	-.00541	-.00429	-.00340	-.00271	-.00217
- 5.00	-.00000	-.00397	-.00644	-.00713	-.00665	-.00569	-.00468	-.00378	-.00304	-.00245	-.00199
- 6.00	-.00000	-.00299	-.00496	-.00565	-.00543	-.00478	-.00402	-.00331	-.00270	-.00221	-.00181
- 8.00	-.00000	-.00170	-.00293	-.00353	-.00358	-.00332	-.00292	-.00250	-.00211	-.00177	-.00149
-12.00	-.00000	-.00060	-.00109	-.00142	-.00158	-.00159	-.00152	-.00140	-.00125	-.00111	-.00097
-14.00	-.00000	-.00038	-.00070	-.00093	-.00107	-.00112	-.00110	-.00104	-.00096	-.00087	-.00078
-16.00	-.00000	-.00025	-.00046	-.00063	-.00074	-.00079	-.00080	-.00078	-.00074	-.00069	-.00063
-18.00	-.00000	-.00017	-.00031	-.00044	-.00052	-.00057	-.00059	-.00059	-.00057	-.00054	-.00051
-20.00	-.00000	-.00012	-.00022	-.00031	-.00038	-.00042	-.00044	-.00045	-.00044	-.00043	-.00041

TABLE V.- BACKWASH FACTOR F_u FOR VARIOUS VALUES OF $\Delta z/s$

(a) $\Delta z/s = 0.50$

$\Delta x/s$ \ $\Delta y/s$	+0	+2	+4	+6	+8	+10	+12	+14	+16	+18	+20
+ .00	+ 3.57771	+ .18393	+ .01729	+ .00484	+ .00200	+ .00102	+ .00059	+ .00037	+ .00025	+ .00017	+ .00013
+ .20	+ 3.03604	+ .17900	+ .01721	+ .00483	+ .00200	+ .00102	+ .00058	+ .00037	+ .00025	+ .00017	+ .00013
+ .40	+ 2.05403	+ .16563	+ .01698	+ .00481	+ .00200	+ .00101	+ .00058	+ .00037	+ .00025	+ .00017	+ .00013
+ .60	+ 1.29199	+ .14724	+ .01662	+ .00477	+ .00199	+ .00101	+ .00058	+ .00037	+ .00025	+ .00017	+ .00013
+ .80	+ .81730	+ .12728	+ .01613	+ .00471	+ .00197	+ .00101	+ .00058	+ .00037	+ .00024	+ .00017	+ .00013
+ 1.00	+ .53333	+ .10815	+ .01554	+ .00463	+ .00196	+ .00100	+ .00058	+ .00036	+ .00024	+ .00017	+ .00013
+ 1.40	+ .25255	+ .07644	+ .01414	+ .00445	+ .00191	+ .00099	+ .00057	+ .00036	+ .00024	+ .00017	+ .00012
+ 2.00	+ .10269	+ .04562	+ .01180	+ .00409	+ .00182	+ .00096	+ .00056	+ .00036	+ .00024	+ .00017	+ .00012
+ 3.00	+ .03377	+ .02108	+ .00822	+ .00340	+ .00163	+ .00089	+ .00053	+ .00034	+ .00023	+ .00017	+ .00012
+ 4.00	+ .01482	+ .01096	+ .00558	+ .00271	+ .00142	+ .00081	+ .00050	+ .00033	+ .00022	+ .00016	+ .00012
+ 5.00	+ .00773	+ .00629	+ .00382	+ .00212	+ .00120	+ .00072	+ .00046	+ .00031	+ .00021	+ .00015	+ .00011
+ 6.00	+ .00452	+ .00389	+ .00266	+ .00165	+ .00101	+ .00063	+ .00042	+ .00028	+ .00020	+ .00015	+ .00011
+ 8.00	+ .00193	+ .00176	+ .00139	+ .00100	+ .00069	+ .00048	+ .00033	+ .00024	+ .00018	+ .00013	+ .00010
+12.00	+ .00058	+ .00055	+ .00049	+ .00041	+ .00033	+ .00026	+ .00020	+ .00016	+ .00013	+ .00010	+ .00008
+14.00	+ .00036	+ .00035	+ .00032	+ .00028	+ .00024	+ .00020	+ .00016	+ .00013	+ .00010	+ .00008	+ .00007
+16.00	+ .00024	+ .00024	+ .00022	+ .00020	+ .00017	+ .00015	+ .00013	+ .00010	+ .00009	+ .00007	+ .00006
+18.00	+ .00017	+ .00017	+ .00016	+ .00015	+ .00013	+ .00011	+ .00010	+ .00008	+ .00007	+ .00006	+ .00005
+20.00	+ .00012	+ .00012	+ .00012	+ .00011	+ .00010	+ .00009	+ .00008	+ .00007	+ .00006	+ .00005	+ .00004

(b) $\Delta z/s = 1.00$

+ .00	+ 1.41421	+ .24158	+ .03190	+ .00937	+ .00393	+ .00201	+ .00116	+ .00073	+ .00049	+ .00034	+ .00025
+ .20	+ 1.34642	+ .23717	+ .03177	+ .00935	+ .00393	+ .00201	+ .00116	+ .00073	+ .00049	+ .00034	+ .00025
+ .40	+ 1.17313	+ .22480	+ .03137	+ .00930	+ .00392	+ .00200	+ .00116	+ .00073	+ .00049	+ .00034	+ .00025
+ .60	+ .95727	+ .20670	+ .03074	+ .00922	+ .00390	+ .00200	+ .00116	+ .00073	+ .00049	+ .00034	+ .00025
+ .80	+ .75056	+ .18552	+ .02989	+ .00911	+ .00387	+ .00199	+ .00115	+ .00073	+ .00049	+ .00034	+ .00025
+ 1.00	+ .57735	+ .16359	+ .02886	+ .00897	+ .00384	+ .00198	+ .00115	+ .00073	+ .00049	+ .00034	+ .00025
+ 1.40	+ .33954	+ .12330	+ .02639	+ .00862	+ .00376	+ .00195	+ .00114	+ .00072	+ .00048	+ .00034	+ .00025
+ 2.00	+ .16330	+ .07871	+ .02222	+ .00794	+ .00358	+ .00189	+ .00111	+ .00071	+ .00048	+ .00034	+ .00025
+ 3.00	+ .06030	+ .03867	+ .01569	+ .00662	+ .00321	+ .00176	+ .00106	+ .00068	+ .00046	+ .00033	+ .00024
+ 4.00	+ .02773	+ .02074	+ .01077	+ .00530	+ .00279	+ .00160	+ .00099	+ .00065	+ .00045	+ .00032	+ .00024
+ 5.00	+ .01480	+ .01210	+ .00742	+ .00416	+ .00238	+ .00143	+ .00091	+ .00061	+ .00042	+ .00031	+ .00023
+ 6.00	+ .00877	+ .00757	+ .00521	+ .00324	+ .00199	+ .00126	+ .00083	+ .00057	+ .00040	+ .00029	+ .00022
+ 8.00	+ .00379	+ .00347	+ .00274	+ .00198	+ .00137	+ .00095	+ .00067	+ .00048	+ .00035	+ .00026	+ .00020
+12.00	+ .00114	+ .00110	+ .00098	+ .00082	+ .00066	+ .00052	+ .00041	+ .00032	+ .00025	+ .00020	+ .00016
+14.00	+ .00072	+ .00070	+ .00064	+ .00056	+ .00047	+ .00039	+ .00032	+ .00026	+ .00021	+ .00017	+ .00014
+16.00	+ .00048	+ .00047	+ .00044	+ .00040	+ .00035	+ .00030	+ .00025	+ .00021	+ .00017	+ .00014	+ .00012
+18.00	+ .00034	+ .00033	+ .00032	+ .00029	+ .00026	+ .00023	+ .00020	+ .00017	+ .00014	+ .00012	+ .00010
+20.00	+ .00025	+ .00025	+ .00023	+ .00022	+ .00020	+ .00018	+ .00016	+ .00014	+ .00012	+ .00010	+ .00009

TABLE V.- BACKWASH FACTOR F_u FOR VARIOUS VALUES OF $\Delta z/s$ - Continued

(c) $\Delta z/s = 1.50$

$\Delta x/s$ \ $\Delta y/s$	+0	+2	+4	+6	+8	+10	+12	+14	+16	+18	+20
+ .00	+ .73960	+ .22648	+ .04227	+ .01332	+ .00573	+ .00296	+ .00172	+ .00109	+ .00073	+ .00051	+ .00037
+ .20	+ .72225	+ .22371	+ .04211	+ .01329	+ .00572	+ .00296	+ .00172	+ .00109	+ .00073	+ .00051	+ .00037
+ .40	+ .67410	+ .21573	+ .04163	+ .01323	+ .00571	+ .00295	+ .00172	+ .00108	+ .00073	+ .00051	+ .00037
+ .60	+ .60496	+ .20353	+ .04087	+ .01312	+ .00568	+ .00294	+ .00171	+ .00108	+ .00073	+ .00051	+ .00037
+ .80	+ .52632	+ .18841	+ .03984	+ .01297	+ .00564	+ .00293	+ .00171	+ .00108	+ .00073	+ .00051	+ .00037
+ 1.00	+ .44776	+ .17173	+ .03857	+ .01278	+ .00559	+ .00291	+ .00170	+ .00108	+ .00072	+ .00051	+ .00037
+ 1.40	+ .31219	+ .13799	+ .03553	+ .01229	+ .00547	+ .00287	+ .00168	+ .00107	+ .00072	+ .00051	+ .00037
+ 2.00	+ .17827	+ .09524	+ .03029	+ .01136	+ .00523	+ .00279	+ .00165	+ .00105	+ .00071	+ .00050	+ .00037
+ 3.00	+ .07619	+ .05079	+ .02184	+ .00952	+ .00470	+ .00260	+ .00157	+ .00101	+ .00069	+ .00049	+ .00036
+ 4.00	+ .03747	+ .02850	+ .01525	+ .00767	+ .00409	+ .00237	+ .00147	+ .00096	+ .00066	+ .00048	+ .00035
+ 5.00	+ .02071	+ .01707	+ .01065	+ .00605	+ .00349	+ .00211	+ .00135	+ .00091	+ .00063	+ .00046	+ .00034
+ 6.00	+ .01252	+ .01086	+ .00754	+ .00473	+ .00293	+ .00186	+ .00123	+ .00084	+ .00060	+ .00044	+ .00033
+ 8.00	+ .00552	+ .00507	+ .00402	+ .00291	+ .00203	+ .00141	+ .00099	+ .00071	+ .00052	+ .00039	+ .00030
+12.00	+ .00169	+ .00162	+ .00145	+ .00122	+ .00099	+ .00078	+ .00061	+ .00048	+ .00037	+ .00029	+ .00024
+14.00	+ .00107	+ .00104	+ .00096	+ .00084	+ .00071	+ .00058	+ .00047	+ .00038	+ .00031	+ .00025	+ .00021
+16.00	+ .00072	+ .00071	+ .00066	+ .00059	+ .00052	+ .00044	+ .00037	+ .00031	+ .00026	+ .00021	+ .00018
+18.00	+ .00051	+ .00050	+ .00047	+ .00043	+ .00039	+ .00034	+ .00029	+ .00025	+ .00021	+ .00018	+ .00015
+20.00	+ .00037	+ .00037	+ .00035	+ .00033	+ .00030	+ .00027	+ .00024	+ .00021	+ .00018	+ .00015	+ .00013

(d) $\Delta z/s = 2.00$

+ .00	+ .44721	+ .19242	+ .04821	+ .01652	+ .00733	+ .00384	+ .00225	+ .00143	+ .00096	+ .00068	+ .00050
+ .20	+ .44103	+ .19076	+ .04805	+ .01650	+ .00732	+ .00384	+ .00225	+ .00143	+ .00096	+ .00068	+ .00049
+ .40	+ .42329	+ .18594	+ .04757	+ .01642	+ .00730	+ .00383	+ .00225	+ .00143	+ .00096	+ .00068	+ .00049
+ .60	+ .39627	+ .17836	+ .04679	+ .01629	+ .00727	+ .00382	+ .00224	+ .00142	+ .00096	+ .00068	+ .00049
+ .80	+ .36300	+ .16863	+ .04573	+ .01611	+ .00723	+ .00381	+ .00224	+ .00142	+ .00096	+ .00068	+ .00049
+ 1.00	+ .32660	+ .15741	+ .04443	+ .01588	+ .00717	+ .00379	+ .00223	+ .00142	+ .00096	+ .00067	+ .00049
+ 1.40	+ .25440	+ .13308	+ .04127	+ .01531	+ .00701	+ .00373	+ .00221	+ .00141	+ .00095	+ .00067	+ .00049
+ 2.00	+ .16667	+ .09857	+ .03570	+ .01420	+ .00671	+ .00362	+ .00216	+ .00139	+ .00094	+ .00067	+ .00049
+ 3.00	+ .08223	+ .05728	+ .02639	+ .01198	+ .00604	+ .00338	+ .00206	+ .00134	+ .00091	+ .00065	+ .00048
+ 4.00	+ .04364	+ .03389	+ .01883	+ .00973	+ .00528	+ .00308	+ .00192	+ .00127	+ .00088	+ .00063	+ .00047
+ 5.00	+ .02518	+ .02097	+ .01336	+ .00774	+ .00452	+ .00276	+ .00177	+ .00119	+ .00084	+ .00061	+ .00045
+ 6.00	+ .01562	+ .01362	+ .00958	+ .00609	+ .00381	+ .00244	+ .00162	+ .00111	+ .00079	+ .00058	+ .00044
+ 8.00	+ .00708	+ .00651	+ .00519	+ .00378	+ .00265	+ .00185	+ .00130	+ .00094	+ .00069	+ .00052	+ .00040
+12.00	+ .00221	+ .00213	+ .00190	+ .00160	+ .00130	+ .00103	+ .00080	+ .00063	+ .00049	+ .00039	+ .00031
+14.00	+ .00141	+ .00137	+ .00126	+ .00110	+ .00093	+ .00077	+ .00063	+ .00051	+ .00041	+ .00033	+ .00027
+16.00	+ .00095	+ .00093	+ .00087	+ .00078	+ .00069	+ .00059	+ .00049	+ .00041	+ .00034	+ .00028	+ .00024
+18.00	+ .00067	+ .00066	+ .00063	+ .00058	+ .00052	+ .00045	+ .00039	+ .00033	+ .00028	+ .00024	+ .00020
+20.00	+ .00049	+ .00048	+ .00046	+ .00043	+ .00039	+ .00035	+ .00031	+ .00027	+ .00024	+ .00020	+ .00018

TABLE V.- BACKWASH FACTOR F_u FOR VARIOUS VALUES OF $\Delta z/s$ - Continued

(e) $\Delta z/s$ = 2.50

$\Delta y/s$ / $\Delta x/s$	+0	+2	+4	+6	+8	+10	+12	+14	+16	+18	+20
+ .00	+ .29711	+ .15873	+ .05048	+ .01893	+ .00871	+ .00465	+ .00275	+ .00175	+ .00119	+ .00084	+ .00061
+ .20	+ .29441	+ .15773	+ .05033	+ .01890	+ .00870	+ .00464	+ .00275	+ .00175	+ .00119	+ .00084	+ .00061
+ .40	+ .28655	+ .15478	+ .04989	+ .01881	+ .00868	+ .00464	+ .00274	+ .00175	+ .00118	+ .00084	+ .00061
+ .60	+ .27421	+ .15008	+ .04917	+ .01867	+ .00864	+ .00462	+ .00274	+ .00175	+ .00118	+ .00084	+ .00061
+ .80	+ .25835	+ .14390	+ .04819	+ .01848	+ .00859	+ .00460	+ .00273	+ .00175	+ .00118	+ .00084	+ .00061
+ 1.00	+ .24011	+ .13657	+ .04698	+ .01824	+ .00852	+ .00458	+ .00272	+ .00174	+ .00118	+ .00083	+ .00061
+ 1.40	+ .20068	+ .11987	+ .04399	+ .01761	+ .00835	+ .00452	+ .00270	+ .00173	+ .00117	+ .00083	+ .00061
+ 2.00	+ .14544	+ .09405	+ .03863	+ .01640	+ .00799	+ .00439	+ .00264	+ .00170	+ .00116	+ .00082	+ .00060
+ 3.00	+ .08133	+ .05920	+ .02933	+ .01396	+ .00722	+ .00410	+ .00252	+ .00164	+ .00113	+ .00080	+ .00059
+ 4.00	+ .04660	+ .03700	+ .02143	+ .01145	+ .00634	+ .00375	+ .00236	+ .00156	+ .00108	+ .00078	+ .00058
+ 5.00	+ .02817	+ .02374	+ .01550	+ .00918	+ .00545	+ .00336	+ .00217	+ .00147	+ .00103	+ .00075	+ .00056
+ 6.00	+ .01799	+ .01580	+ .01128	+ .00728	+ .00461	+ .00297	+ .00198	+ .00137	+ .00098	+ .00072	+ .00054
+ 8.00	+ .00843	+ .00778	+ .00624	+ .00458	+ .00323	+ .00226	+ .00160	+ .00116	+ .00085	+ .00064	+ .00049
+12.00	+ .00271	+ .00260	+ .00233	+ .00197	+ .00160	+ .00127	+ .00099	+ .00078	+ .00061	+ .00049	+ .00039
+14.00	+ .00173	+ .00168	+ .00155	+ .00136	+ .00115	+ .00095	+ .00078	+ .00063	+ .00051	+ .00041	+ .00034
+16.00	+ .00118	+ .00115	+ .00108	+ .00097	+ .00085	+ .00073	+ .00061	+ .00051	+ .00042	+ .00035	+ .00029
+18.00	+ .00083	+ .00082	+ .00078	+ .00071	+ .00064	+ .00056	+ .00048	+ .00041	+ .00035	+ .00030	+ .00025
+20.00	+ .00061	+ .00060	+ .00058	+ .00054	+ .00049	+ .00044	+ .00039	+ .00034	+ .00029	+ .00025	+ .00022

(f) $\Delta z/s$ = 3.00

+ .00	+ .21082	+ .13029	+ .05013	+ .02055	+ .00985	+ .00536	+ .00321	+ .00206	+ .00140	+ .00099	+ .00073
+ .20	+ .20947	+ .12967	+ .05000	+ .02052	+ .00984	+ .00536	+ .00321	+ .00206	+ .00140	+ .00099	+ .00073
+ .40	+ .20550	+ .12781	+ .04962	+ .02044	+ .00981	+ .00535	+ .00320	+ .00206	+ .00140	+ .00099	+ .00073
+ .60	+ .19916	+ .12483	+ .04899	+ .02029	+ .00977	+ .00533	+ .00320	+ .00206	+ .00140	+ .00099	+ .00073
+ .80	+ .19081	+ .12084	+ .04813	+ .02010	+ .00971	+ .00531	+ .00319	+ .00205	+ .00140	+ .00099	+ .00073
+ 1.00	+ .18091	+ .11602	+ .04707	+ .01985	+ .00964	+ .00529	+ .00318	+ .00205	+ .00139	+ .00099	+ .00073
+ 1.40	+ .15830	+ .10465	+ .04443	+ .01922	+ .00945	+ .00522	+ .00315	+ .00203	+ .00139	+ .00098	+ .00072
+ 2.00	+ .12335	+ .08592	+ .03958	+ .01798	+ .00906	+ .00507	+ .00309	+ .00200	+ .00137	+ .00098	+ .00072
+ 3.00	+ .07647	+ .05799	+ .03086	+ .01545	+ .00822	+ .00475	+ .00294	+ .00193	+ .00133	+ .00095	+ .00071
+ 4.00	+ .04707	+ .03821	+ .02311	+ .01280	+ .00725	+ .00435	+ .00276	+ .00184	+ .00128	+ .00093	+ .00069
+ 5.00	+ .02983	+ .02545	+ .01707	+ .01036	+ .00626	+ .00391	+ .00255	+ .00173	+ .00122	+ .00089	+ .00067
+ 6.00	+ .01966	+ .01739	+ .01262	+ .00829	+ .00532	+ .00347	+ .00233	+ .00161	+ .00116	+ .00085	+ .00064
+ 8.00	+ .00955	+ .00884	+ .00714	+ .00529	+ .00376	+ .00265	+ .00189	+ .00137	+ .00101	+ .00076	+ .00059
+12.00	+ .00316	+ .00304	+ .00273	+ .00231	+ .00188	+ .00149	+ .00118	+ .00092	+ .00073	+ .00058	+ .00046
+14.00	+ .00204	+ .00198	+ .00182	+ .00160	+ .00136	+ .00113	+ .00092	+ .00075	+ .00061	+ .00049	+ .00040
+16.00	+ .00139	+ .00136	+ .00127	+ .00115	+ .00101	+ .00086	+ .00073	+ .00061	+ .00051	+ .00042	+ .00035
+18.00	+ .00099	+ .00097	+ .00092	+ .00085	+ .00076	+ .00067	+ .00058	+ .00049	+ .00042	+ .00036	+ .00030
+20.00	+ .00072	+ .00071	+ .00068	+ .00064	+ .00058	+ .00052	+ .00046	+ .00040	+ .00035	+ .00030	+ .00026

TABLE V.- BACKWASH FACTOR F_u FOR VARIOUS VALUES OF $\Delta z/s$ - Continued

(g) $\Delta z/s$ = 4.00

$\Delta x/s$ \ $\Delta y/s$	+0	+2	+4	+6	+8	+10	+12	+14	+16	+18	+20
+ .00	+.12127	+.08937	+.04522	+.02184	+.01139	+.00650	+.00400	+.00261	+.00180	+.00128	+.00095
+ .20	+.12082	+.08909	+.04513	+.02182	+.01138	+.00649	+.00399	+.00261	+.00180	+.00128	+.00095
+ .40	+.11951	+.08829	+.04487	+.02174	+.01136	+.00648	+.00399	+.00261	+.00179	+.00128	+.00095
+ .60	+.11736	+.08697	+.04443	+.02161	+.01131	+.00646	+.00398	+.00261	+.00179	+.00128	+.00095
+ .80	+.11447	+.08518	+.04384	+.02143	+.01125	+.00644	+.00397	+.00260	+.00179	+.00128	+.00095
+ 1.00	+.11092	+.08298	+.04310	+.02121	+.01118	+.00641	+.00396	+.00260	+.00179	+.00128	+.00094
+ 1.40	+.10230	+.07753	+.04122	+.02062	+.01097	+.00633	+.00392	+.00258	+.00178	+.00127	+.00094
+ 2.00	+.08729	+.06777	+.03765	+.01947	+.01057	+.00617	+.00385	+.00254	+.00176	+.00126	+.00093
+ 3.00	+.06276	+.05094	+.03082	+.01706	+.00967	+.00579	+.00368	+.00245	+.00171	+.00123	+.00092
+ 4.00	+.04352	+.03681	+.02422	+.01444	+.00861	+.00533	+.00346	+.00234	+.00165	+.00120	+.00089
+ 5.00	+.03011	+.02634	+.01865	+.01194	+.00751	+.00482	+.00320	+.00221	+.00157	+.00115	+.00087
+ 6.00	+.02113	+.01898	+.01428	+.00975	+.00645	+.00430	+.00294	+.00206	+.00149	+.00110	+.00084
+ 8.00	+.01111	+.01034	+.00850	+.00642	+.00465	+.00333	+.00240	+.00175	+.00130	+.00099	+.00076
+12.00	+.00394	+.00380	+.00342	+.00291	+.00239	+.00191	+.00151	+.00119	+.00095	+.00075	+.00061
+14.00	+.00259	+.00251	+.00232	+.00205	+.00175	+.00145	+.00119	+.00097	+.00079	+.00065	+.00053
+16.00	+.00178	+.00174	+.00163	+.00148	+.00130	+.00112	+.00094	+.00079	+.00066	+.00055	+.00046
+18.00	+.00127	+.00125	+.00119	+.00110	+.00098	+.00087	+.00075	+.00065	+.00055	+.00047	+.00040
+20.00	+.00094	+.00093	+.00089	+.00083	+.00076	+.00068	+.00060	+.00053	+.00046	+.00040	+.00034

(h) $\Delta z/s$ = 6.00

+ .00	+.05480	+.04714	+.03216	+.01985	+.01213	+.00764	+.00501	+.00342	+.00242	+.00177	+.00132
+ .20	+.05471	+.04707	+.03212	+.01983	+.01212	+.00764	+.00501	+.00342	+.00242	+.00177	+.00132
+ .40	+.05444	+.04685	+.03201	+.01978	+.01210	+.00763	+.00500	+.00342	+.00242	+.00176	+.00132
+ .60	+.05400	+.04651	+.03183	+.01969	+.01207	+.00761	+.00500	+.00341	+.00241	+.00176	+.00132
+ .80	+.05338	+.04603	+.03157	+.01958	+.01201	+.00759	+.00498	+.00341	+.00241	+.00176	+.00132
+ 1.00	+.05261	+.04542	+.03124	+.01943	+.01195	+.00756	+.00497	+.00340	+.00241	+.00176	+.00132
+ 1.40	+.05065	+.04387	+.03040	+.01905	+.01178	+.00748	+.00493	+.00338	+.00239	+.00175	+.00131
+ 2.00	+.04685	+.04086	+.02874	+.01827	+.01143	+.00731	+.00485	+.00333	+.00237	+.00174	+.00131
+ 3.00	+.03932	+.03477	+.02525	+.01658	+.01064	+.00693	+.00465	+.00323	+.00231	+.00170	+.00128
+ 4.00	+.03170	+.02847	+.02143	+.01462	+.00968	+.00645	+.00440	+.00309	+.00223	+.00165	+.00125
+ 5.00	+.02498	+.02278	+.01776	+.01262	+.00864	+.00591	+.00411	+.00293	+.00214	+.00160	+.00122
+ 6.00	+.01951	+.01802	+.01453	+.01072	+.00760	+.00535	+.00380	+.00275	+.00203	+.00153	+.00117
+ 8.00	+.01194	+.01127	+.00959	+.00757	+.00573	+.00426	+.00316	+.00237	+.00179	+.00138	+.00108
+12.00	+.00496	+.00480	+.00437	+.00378	+.00315	+.00256	+.00206	+.00165	+.00132	+.00106	+.00086
+14.00	+.00339	+.00330	+.00307	+.00273	+.00236	+.00199	+.00165	+.00136	+.00112	+.00092	+.00076
+16.00	+.00240	+.00235	+.00222	+.00202	+.00179	+.00155	+.00132	+.00111	+.00094	+.00079	+.00066
+18.00	+.00175	+.00173	+.00164	+.00152	+.00137	+.00122	+.00106	+.00092	+.00079	+.00067	+.00057
+20.00	+.00132	+.00130	+.00125	+.00117	+.00107	+.00097	+.00086	+.00076	+.00066	+.00057	+.00050

TABLE V.- BACKWASH FACTOR F_u FOR VARIOUS VALUES OF $\Delta z/s$ - Concluded

(i) $\Delta z/s$ = 8.00

$\Delta x/s$ \ $\Delta y/s$	+0	+2	+4	+6	+8	+10	+12	+14	+16	+18	+20
+ .00	+ .03101	+ .02839	+ .02236	+ .01606	+ .01111	+ .00767	+ .00537	+ .00384	+ .00281	+ .00210	+ .00161
+ .20	+ .03098	+ .02836	+ .02234	+ .01605	+ .01111	+ .00766	+ .00536	+ .00384	+ .00281	+ .00210	+ .00161
+ .40	+ .03089	+ .02829	+ .02229	+ .01602	+ .01109	+ .00765	+ .00536	+ .00383	+ .00281	+ .00210	+ .00161
+ .60	+ .03075	+ .02816	+ .02221	+ .01598	+ .01107	+ .00764	+ .00535	+ .00383	+ .00280	+ .00210	+ .00160
+ .80	+ .03055	+ .02799	+ .02209	+ .01591	+ .01103	+ .00762	+ .00534	+ .00382	+ .00280	+ .00210	+ .00160
+ 1.00	+ .03030	+ .02777	+ .02195	+ .01582	+ .01098	+ .00760	+ .00533	+ .00381	+ .00280	+ .00209	+ .00160
+ 1.40	+ .02964	+ .02720	+ .02156	+ .01560	+ .01086	+ .00753	+ .00529	+ .00379	+ .00278	+ .00209	+ .00160
+ 2.00	+ .02833	+ .02606	+ .02078	+ .01514	+ .01061	+ .00739	+ .00521	+ .00375	+ .00276	+ .00207	+ .00159
+ 3.00	+ .02548	+ .02357	+ .01904	+ .01410	+ .01003	+ .00707	+ .00503	+ .00364	+ .00269	+ .00203	+ .00156
+ 4.00	+ .02222	+ .02069	+ .01700	+ .01284	+ .00930	+ .00666	+ .00480	+ .00351	+ .00261	+ .00198	+ .00153
+ 5.00	+ .01895	+ .01777	+ .01485	+ .01147	+ .00848	+ .00618	+ .00452	+ .00334	+ .00251	+ .00191	+ .00148
+ 6.00	+ .01592	+ .01503	+ .01279	+ .01010	+ .00764	+ .00568	+ .00421	+ .00315	+ .00239	+ .00184	+ .00144
+ 8.00	+ .01101	+ .01052	+ .00924	+ .00762	+ .00602	+ .00466	+ .00358	+ .00275	+ .00213	+ .00167	+ .00132
+12.00	+ .00532	+ .00517	+ .00477	+ .00420	+ .00357	+ .00296	+ .00243	+ .00197	+ .00160	+ .00131	+ .00107
+14.00	+ .00381	+ .00372	+ .00348	+ .00314	+ .00274	+ .00234	+ .00197	+ .00165	+ .00137	+ .00114	+ .00095
+16.00	+ .00279	+ .00274	+ .00259	+ .00238	+ .00213	+ .00186	+ .00160	+ .00137	+ .00116	+ .00098	+ .00083
+18.00	+ .00209	+ .00206	+ .00197	+ .00183	+ .00166	+ .00148	+ .00130	+ .00113	+ .00098	+ .00084	+ .00072
+20.00	+ .00160	+ .00158	+ .00152	+ .00143	+ .00132	+ .00119	+ .00107	+ .00094	+ .00083	+ .00072	+ .00063

Wing Geometry

Symbol	Swept	Unswept
S	6.25 sq ft	6.25 sq ft
b	5.00 ft	4.33 ft
$\bar{c}$	1.37 ft	1.49 ft
A	4.0	3.0
λ	0.3	0.5
Λ	45°	0°
	@$c/4$	@$c/2$
Airfoil section	65A006	65A004

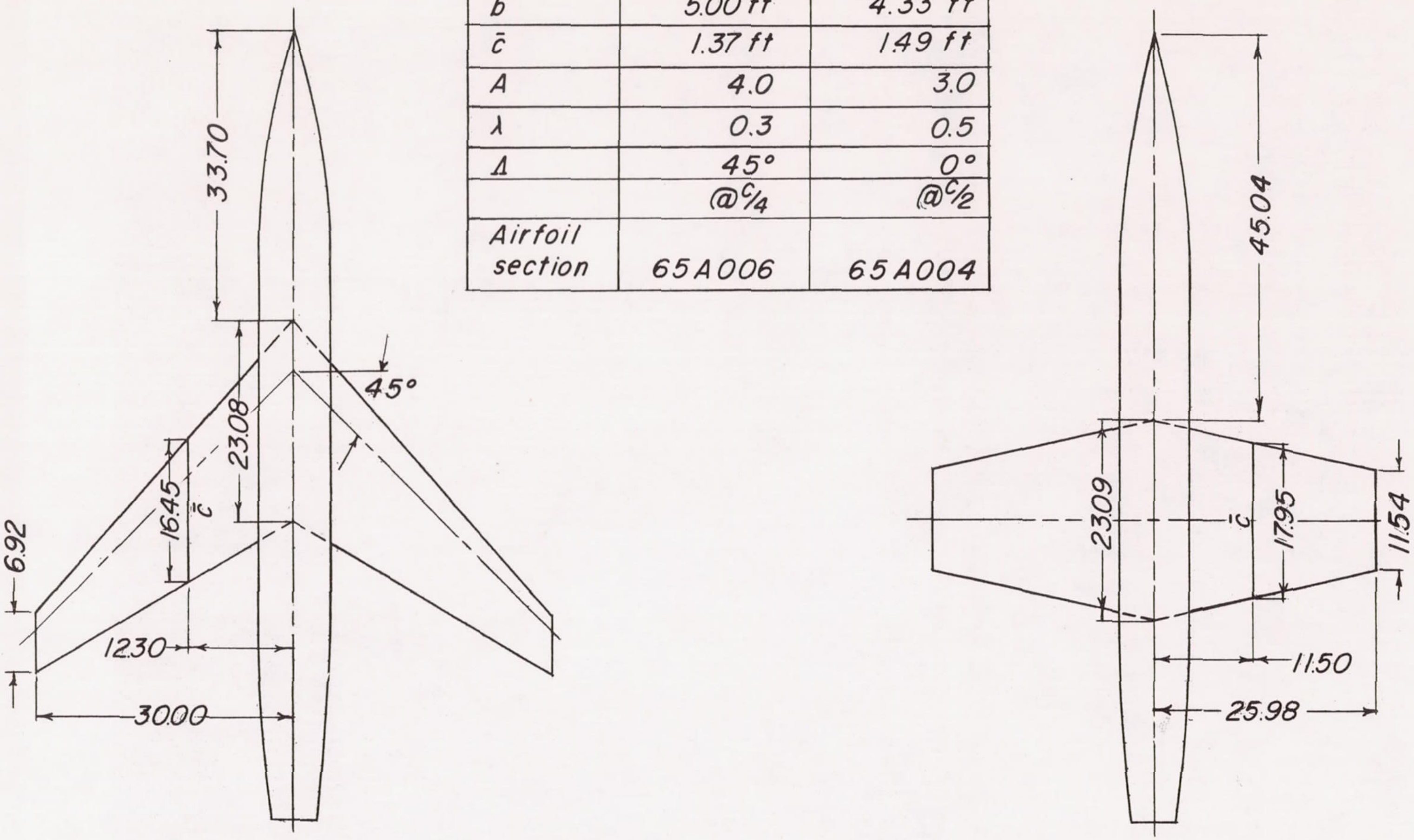

Figure 1.- Geometric characteristics of test models. All dimensions are in inches.

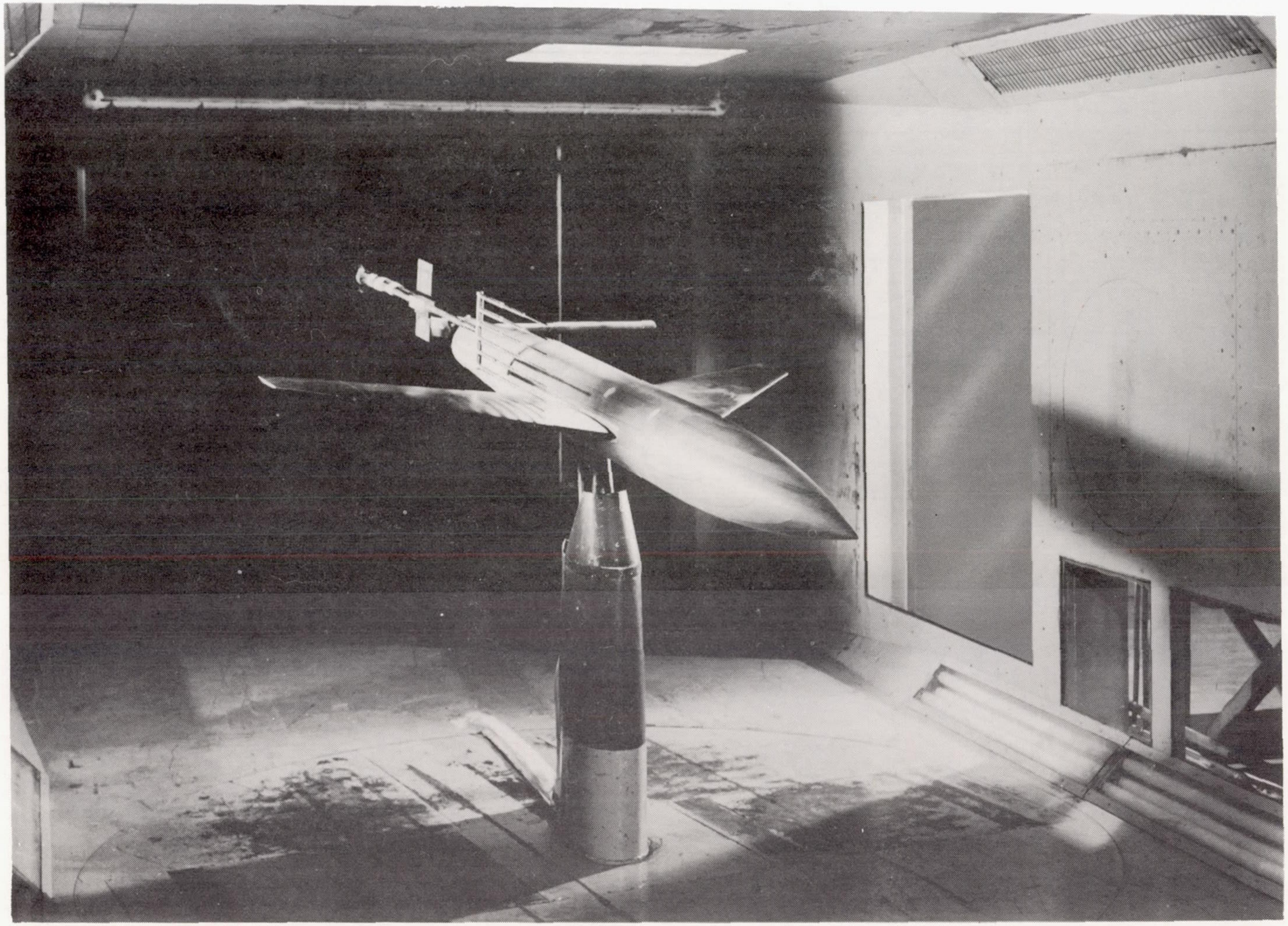

L-80760.1

Figure 2.- Photograph of swept-wing model with angularity survey rake installed.

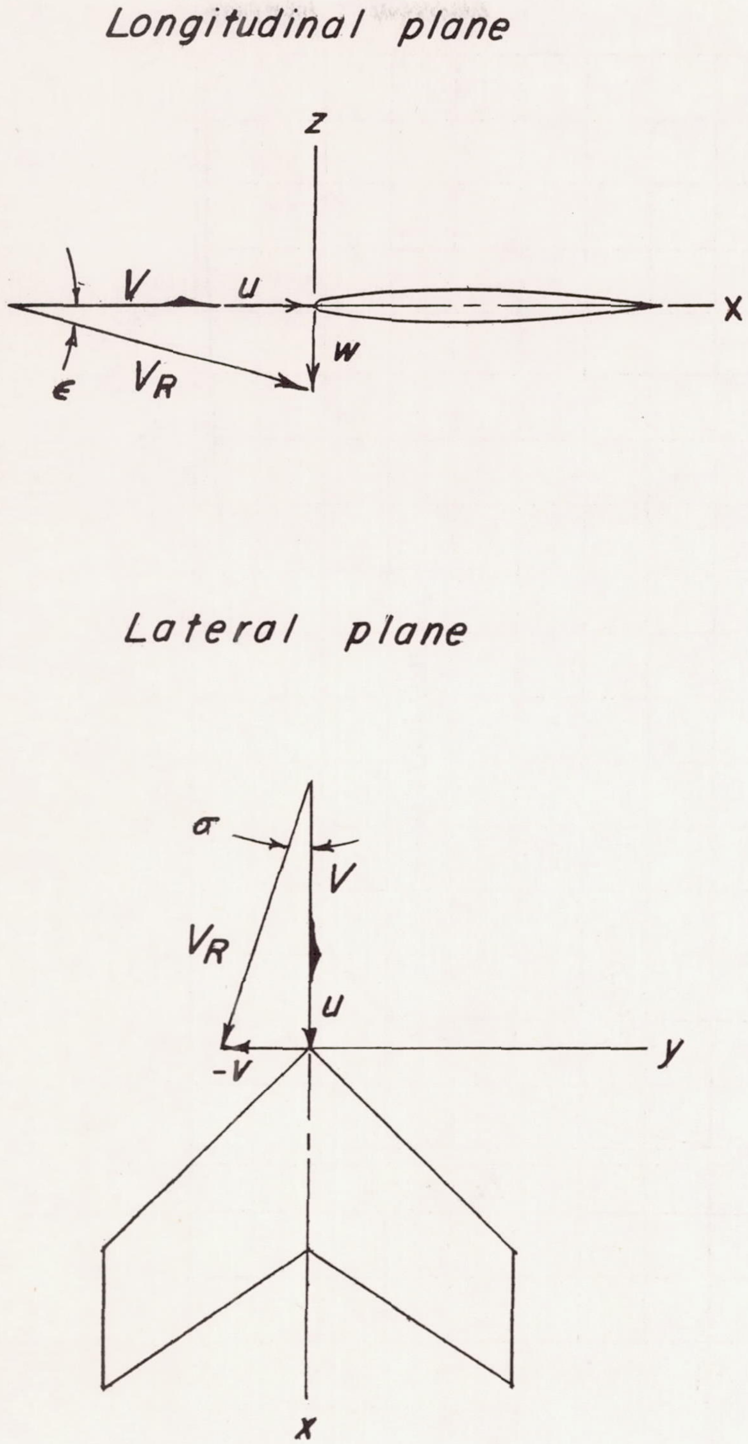

Figure 3.- Sketch showing coordinate system and positive directions of velocities and angles.

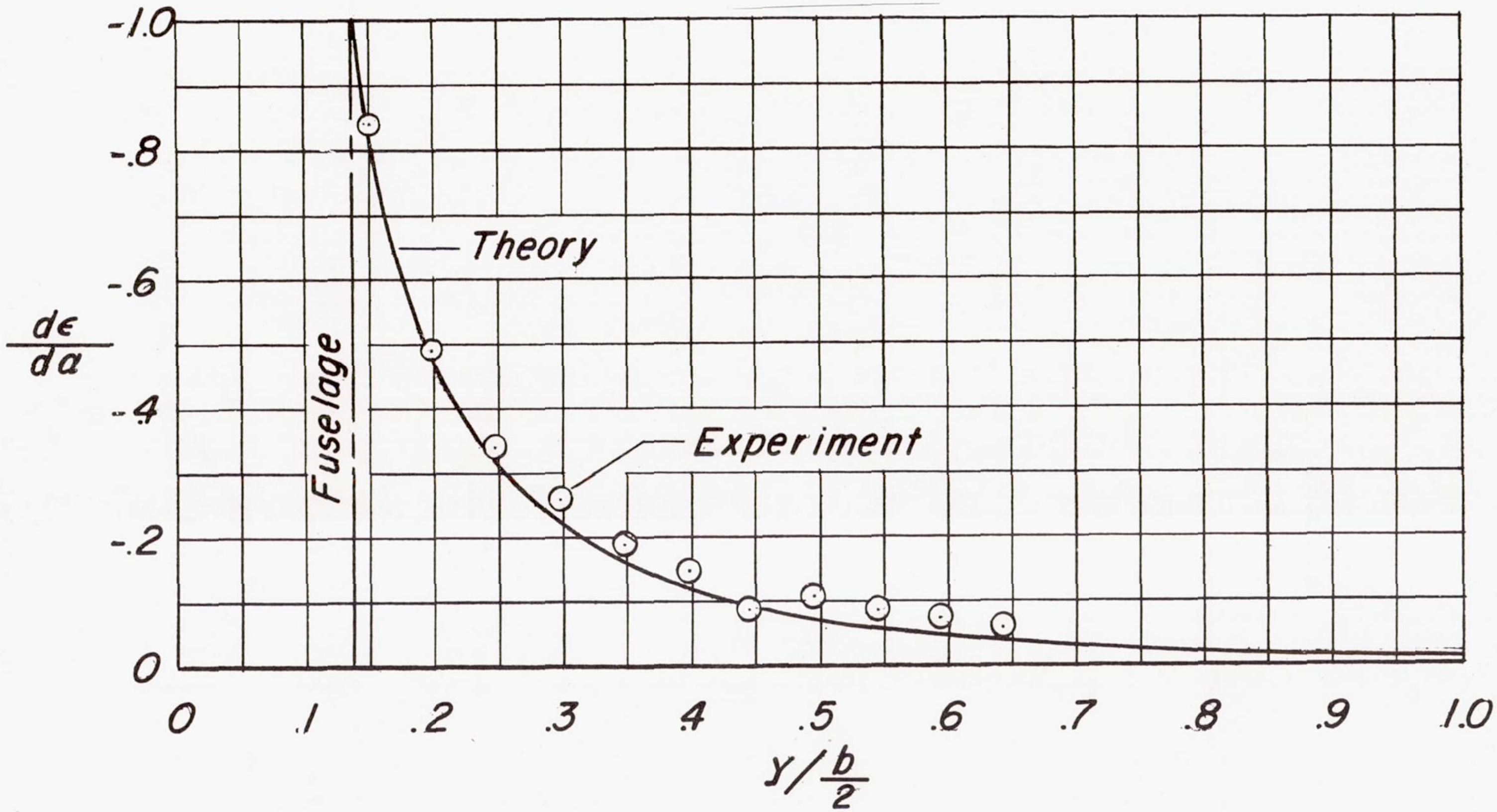

Figure 4.- Downwash induced by circular-cross-section fuselage alone based on swept-wing semispan. $z = 0$; $x/l = 0.5$.

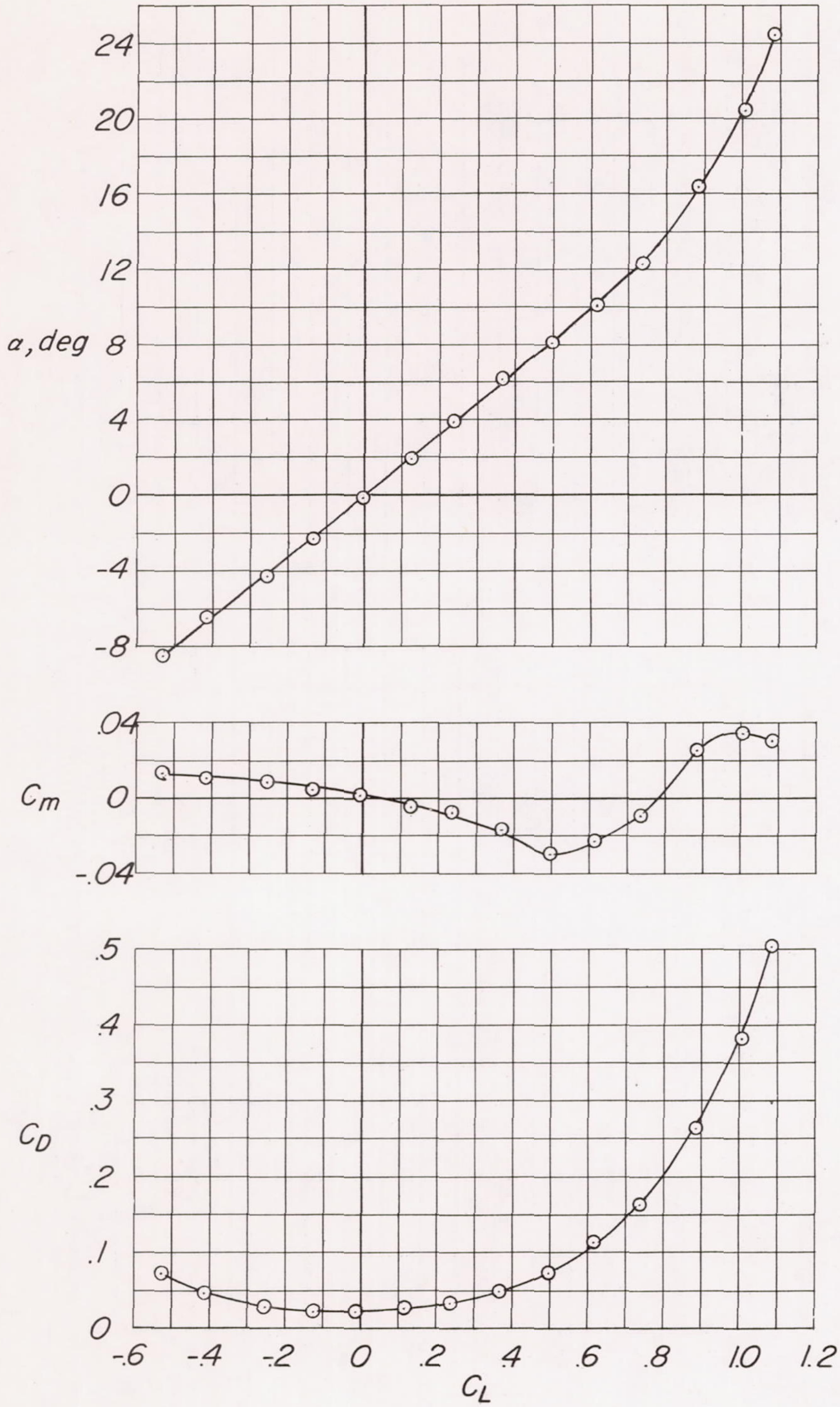

Figure 5.- Lift, drag, and pitching-moment characteristics of the swept-wing—fuselage configuration.

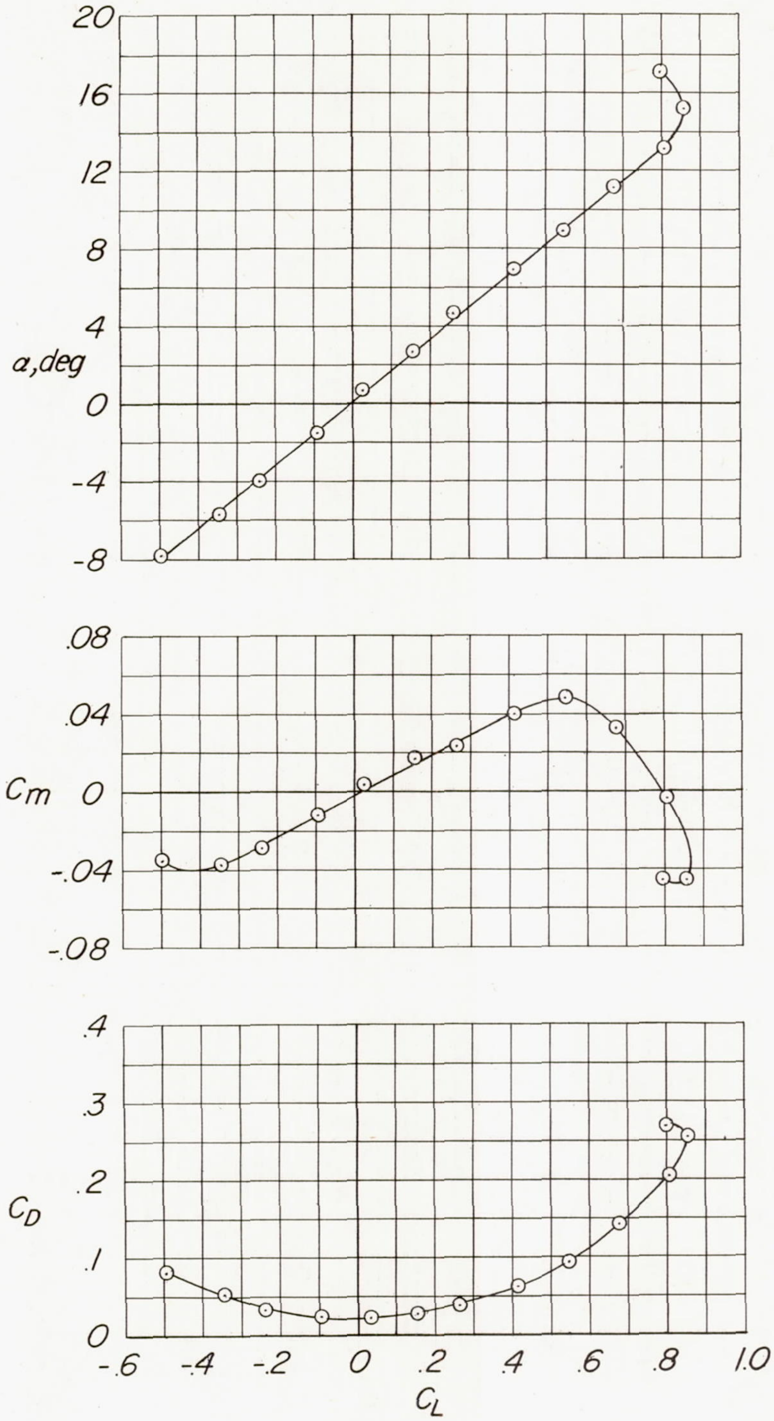

Figure 6.- Lift, drag, and pitching-moment characteristics of the unswept-wing—fuselage configuration.

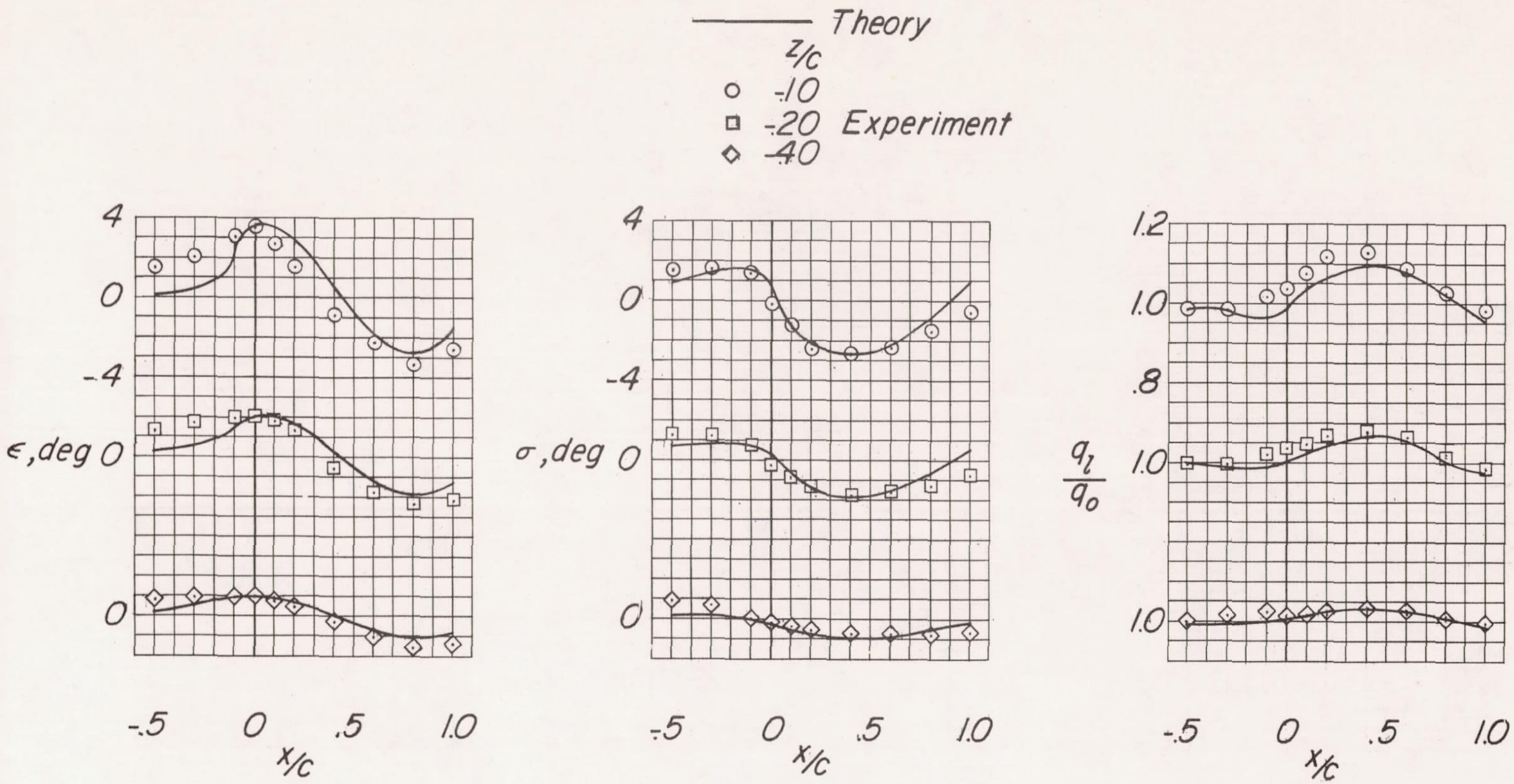

(a) $C_L = 0$.

Figure 7.- Flow characteristics at the midsemispan location of the swept wing for several vertical heights.

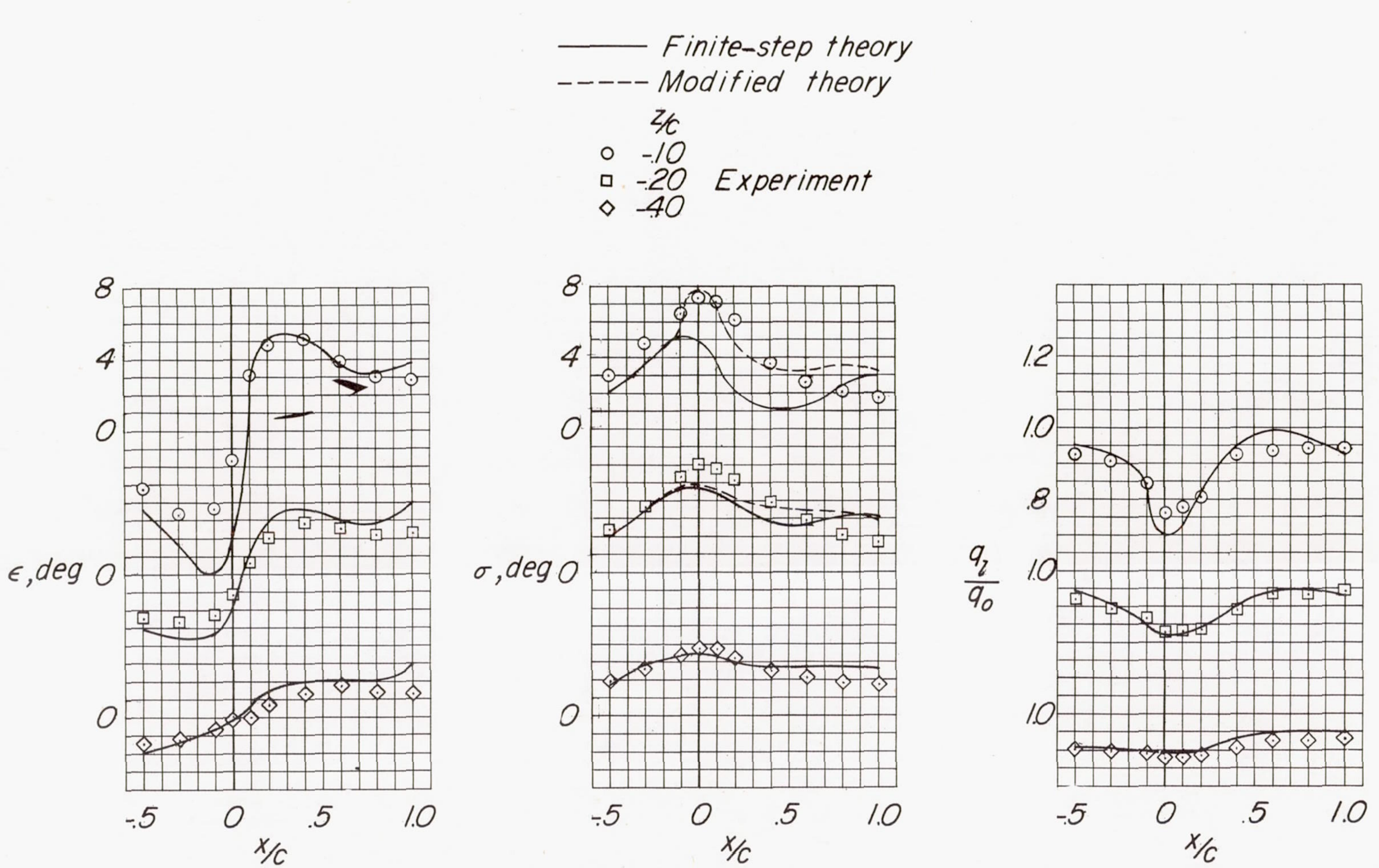

(b) $C_L = 0.49$.

Figure 7.- Concluded.

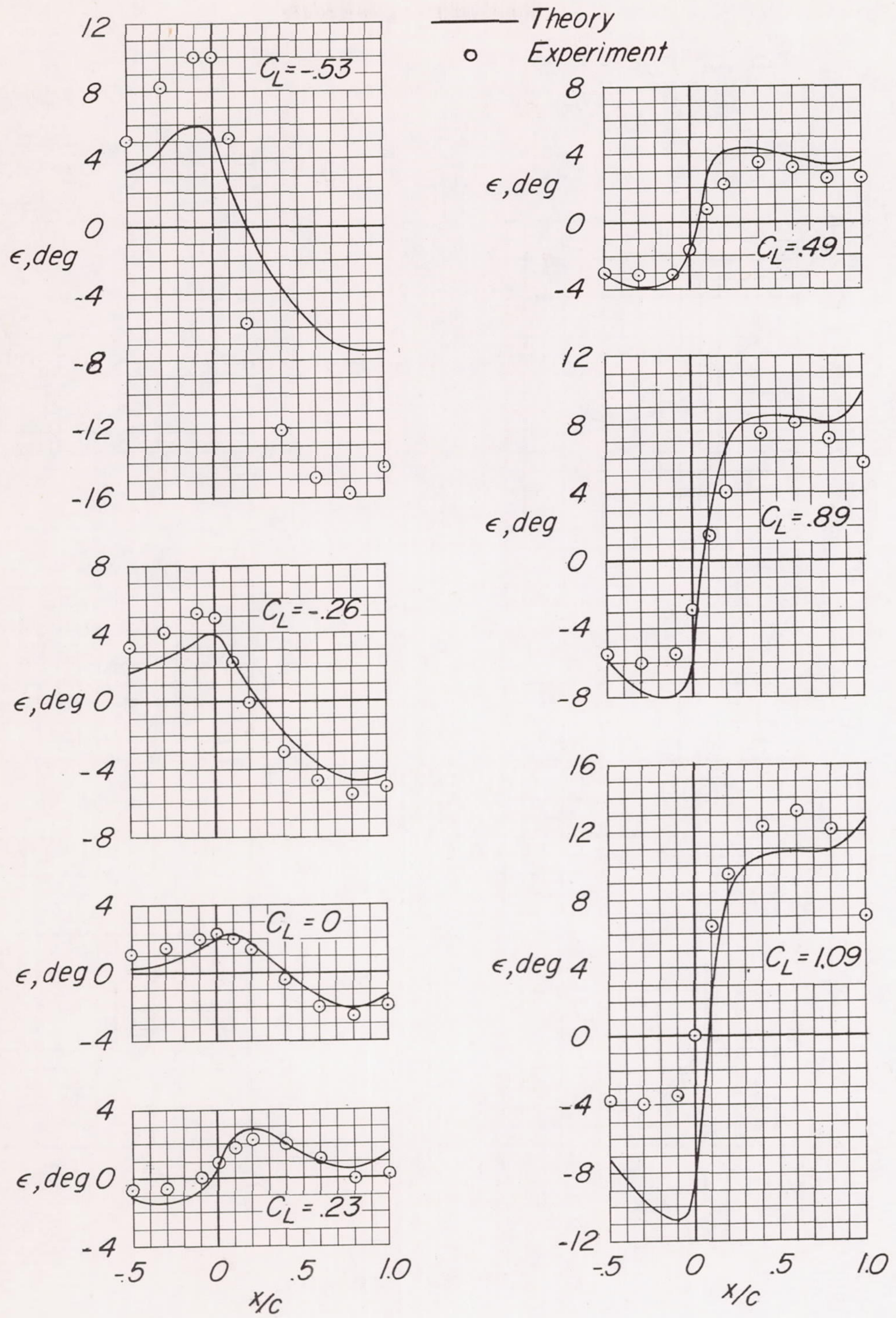

(a) Downwash angles.

Figure 8.- Flow characteristics at the midsemispan location of the swept wing for various lift coefficients. z/c = -0.15.

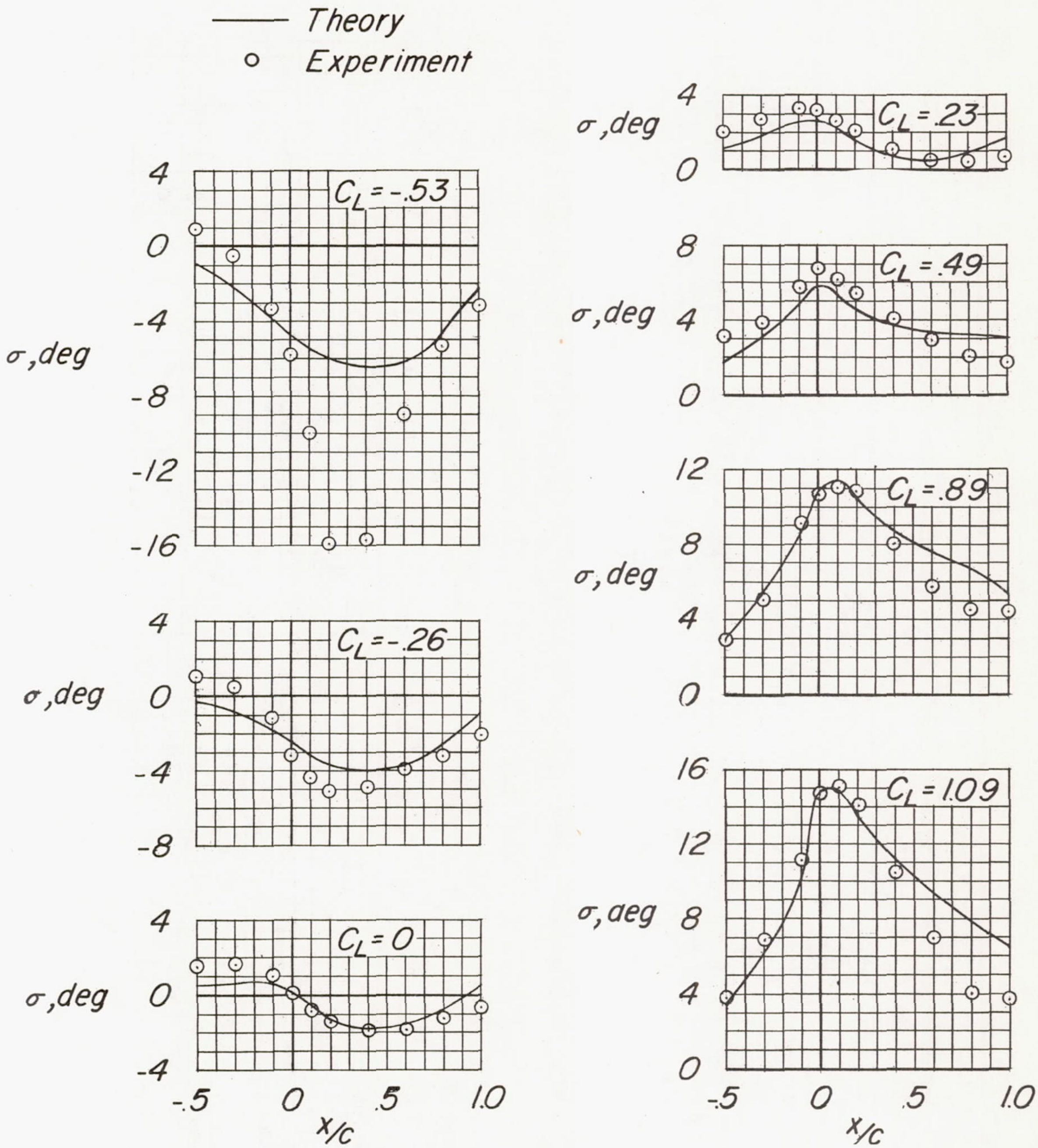

(b) Sidewash angles.

Figure 8.- Continued.

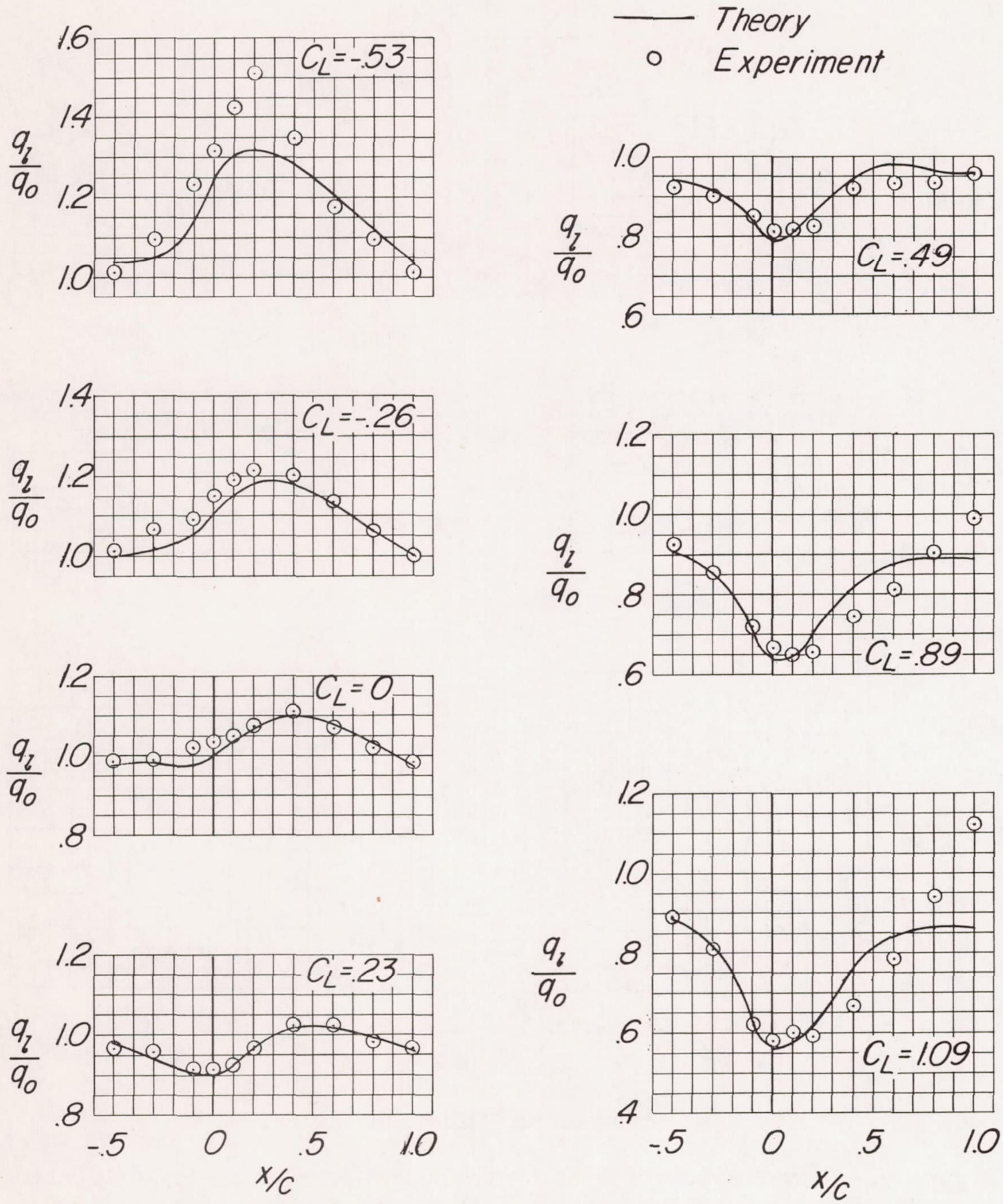

(c) Dynamic-pressure ratios.

Figure 8.- Concluded.

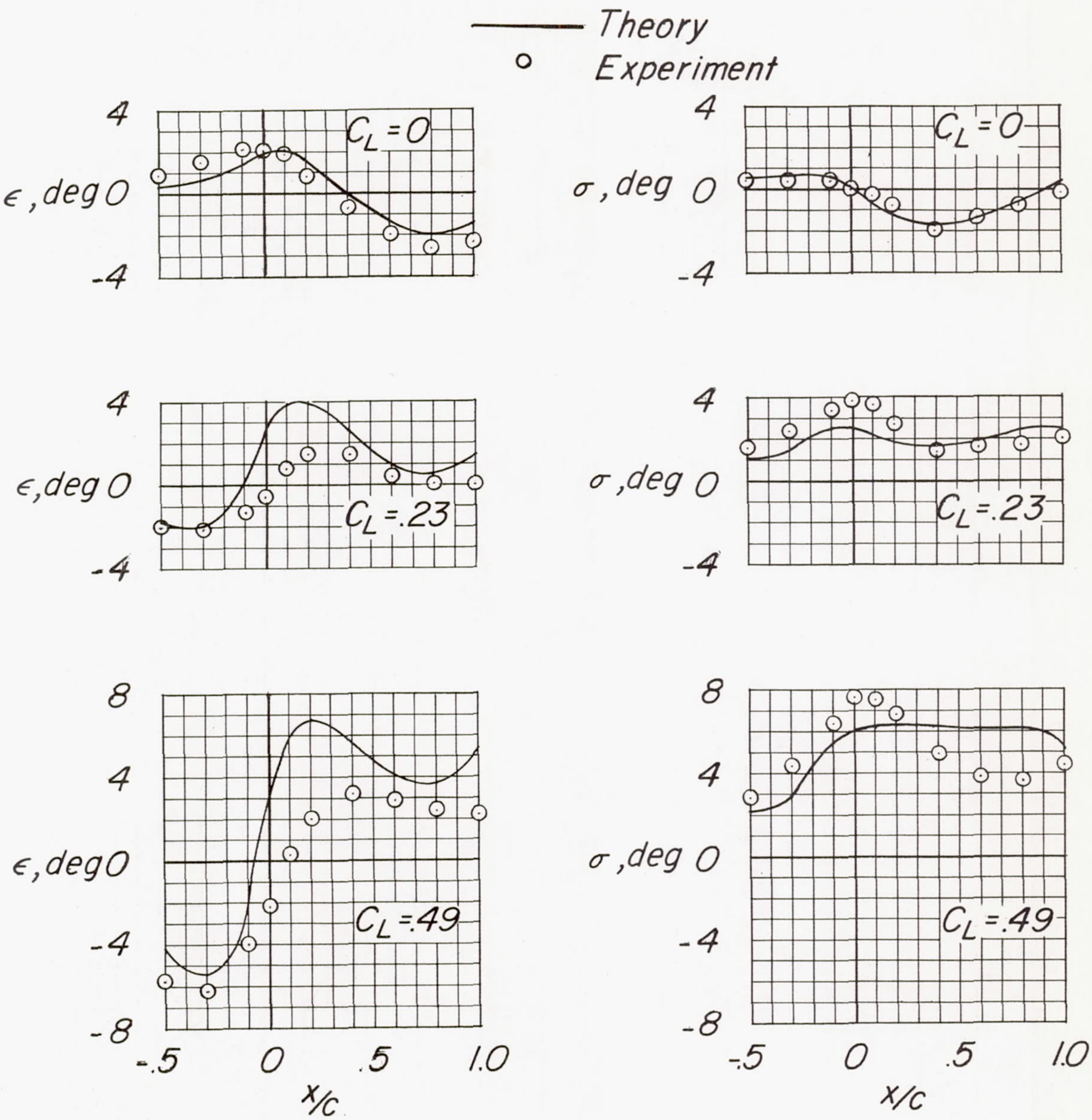

(a) Downwash and sidewash angles.

Figure 9.- Flow characteristics at the three-quarter semispan location of the swept wing for various lift coefficients. z/c = -0.15.

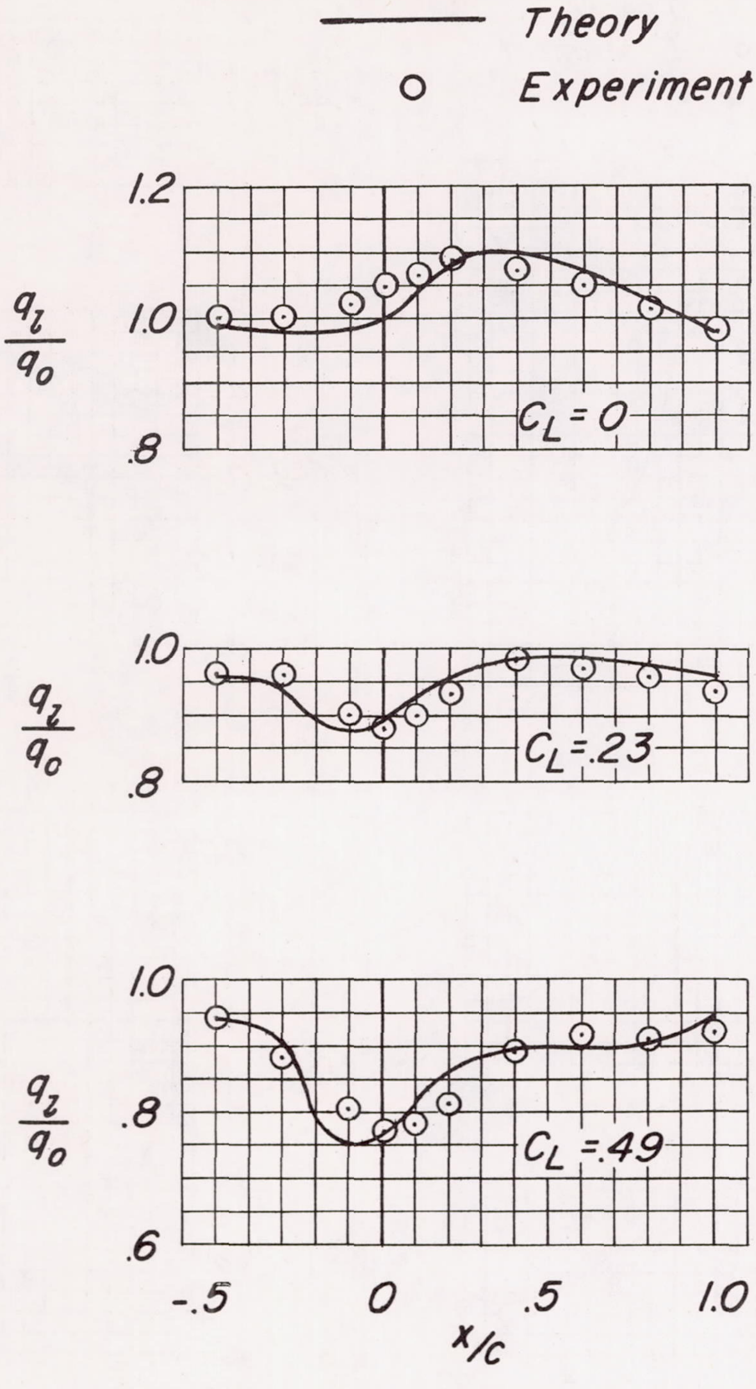

(b) Dynamic-pressure ratios.

Figure 9.- Concluded.

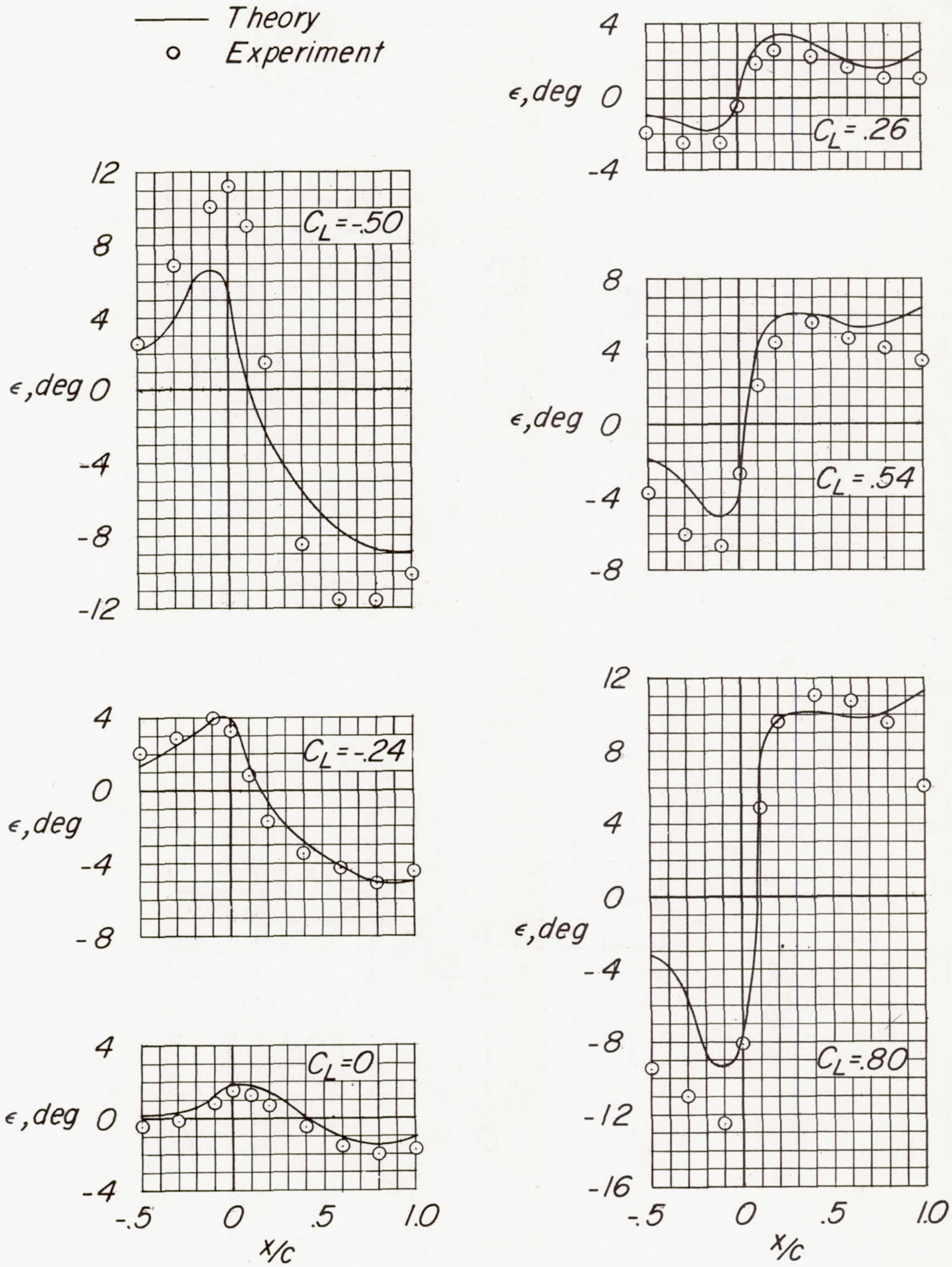

(a) Downwash angles.

Figure 10.- Flow characteristics at the midsemispan location of the unswept wing for various lift coefficients. z/c = -0.15.

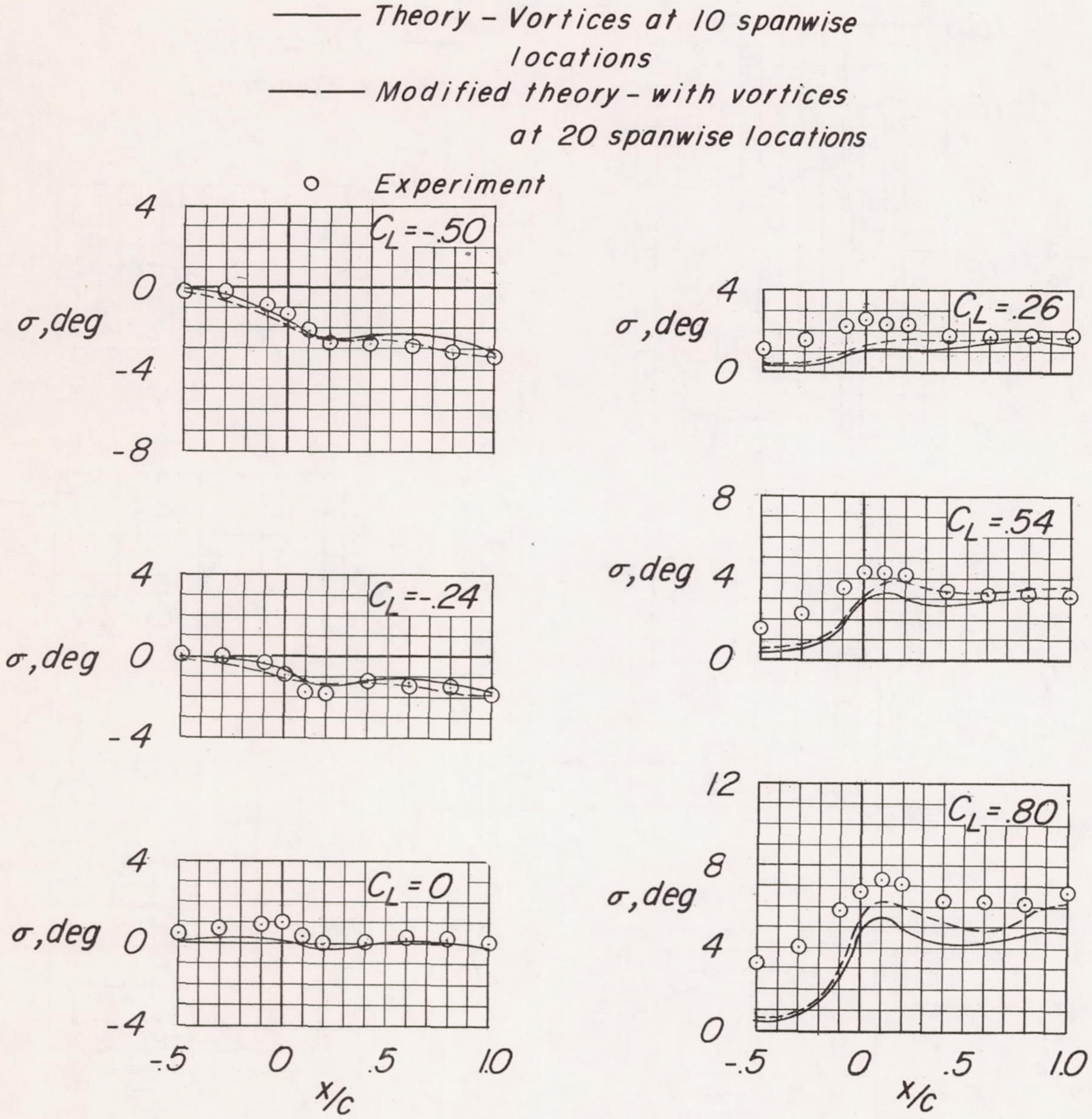

(b) Sidewash angles.

Figure 10.- Continued.

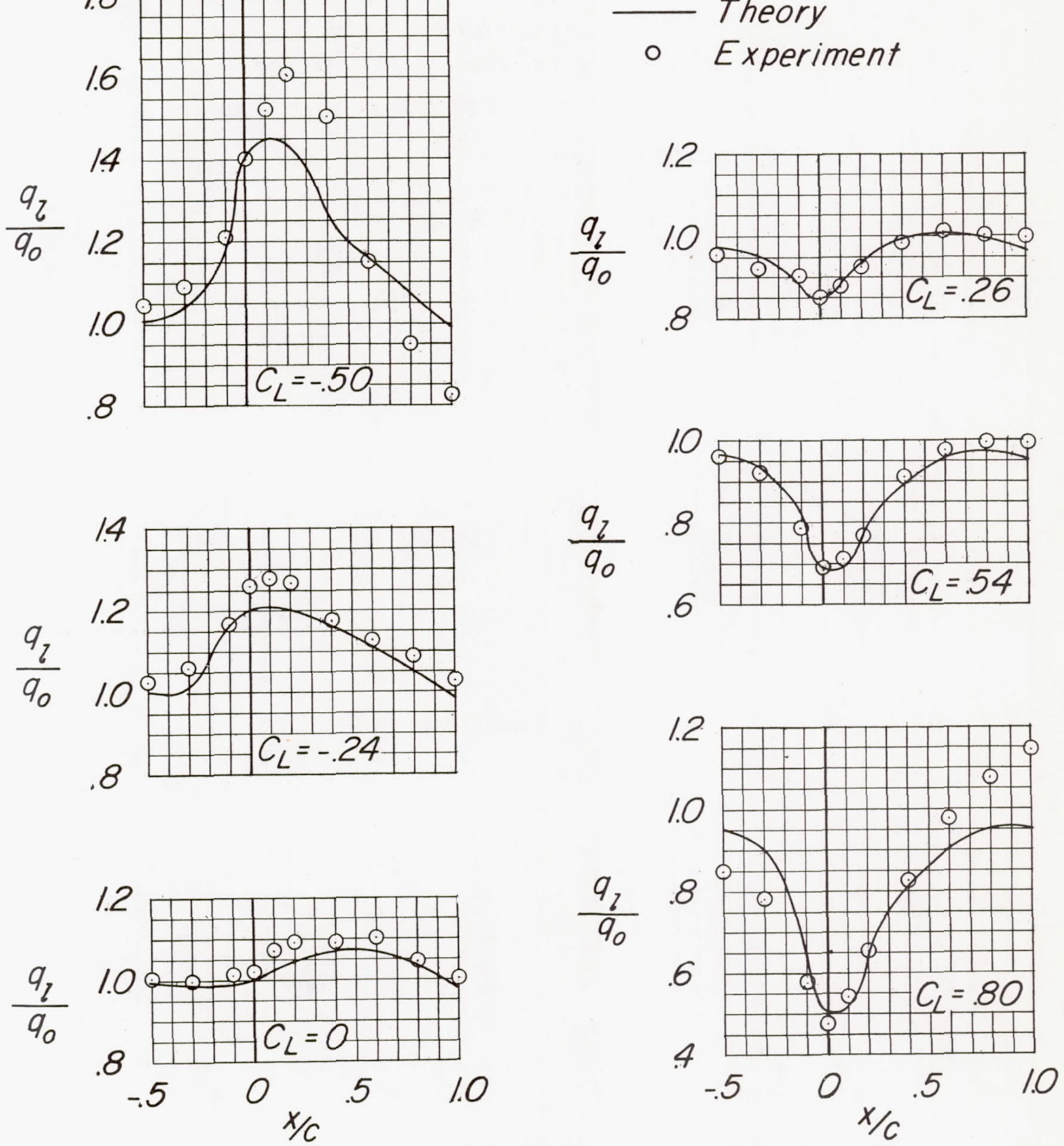

(c) Dynamic-pressure ratios.

Figure 10.- Concluded.

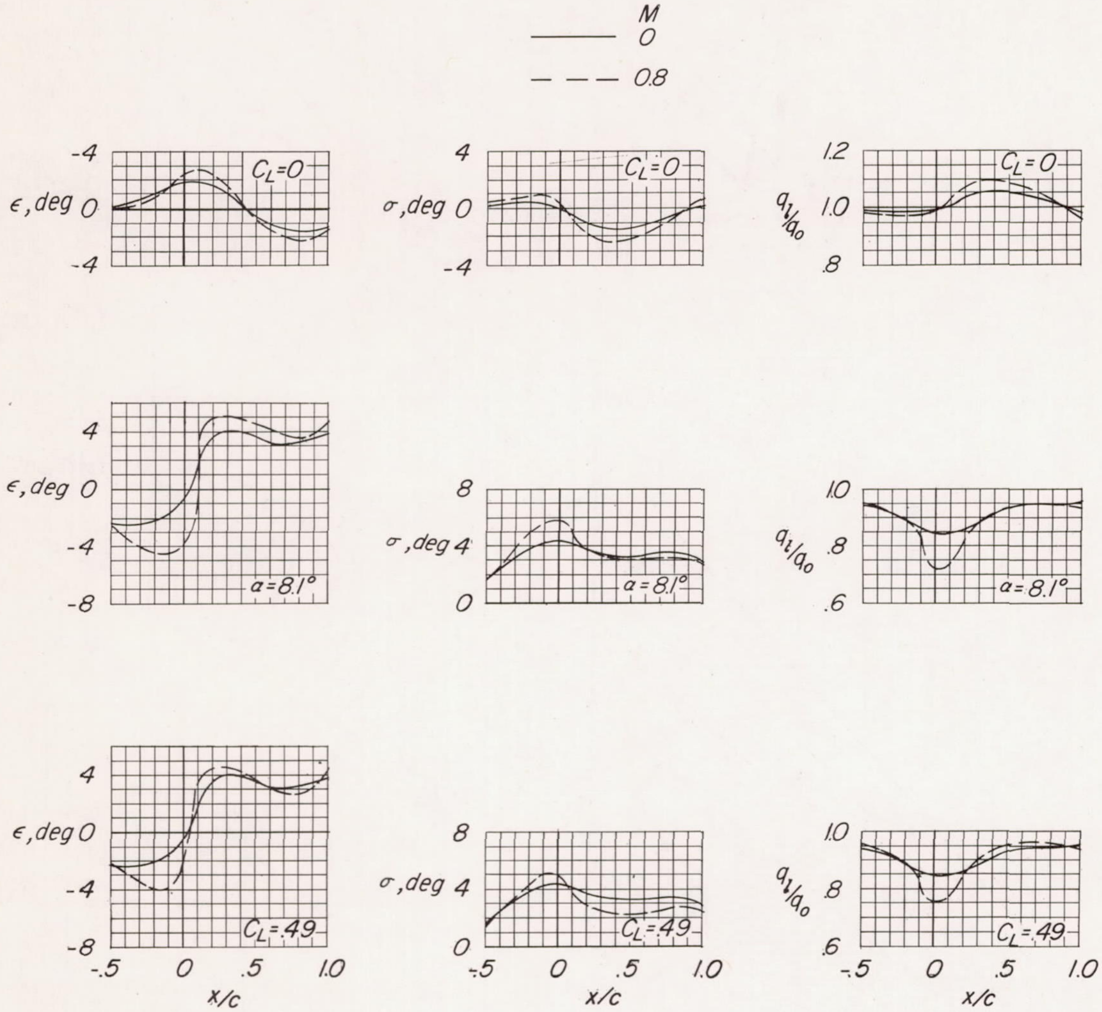

Figure 11.- Calculated effects of Mach number on flow characteristics beneath the midsemispan location of the swept wing. $z/c = -0.25$.

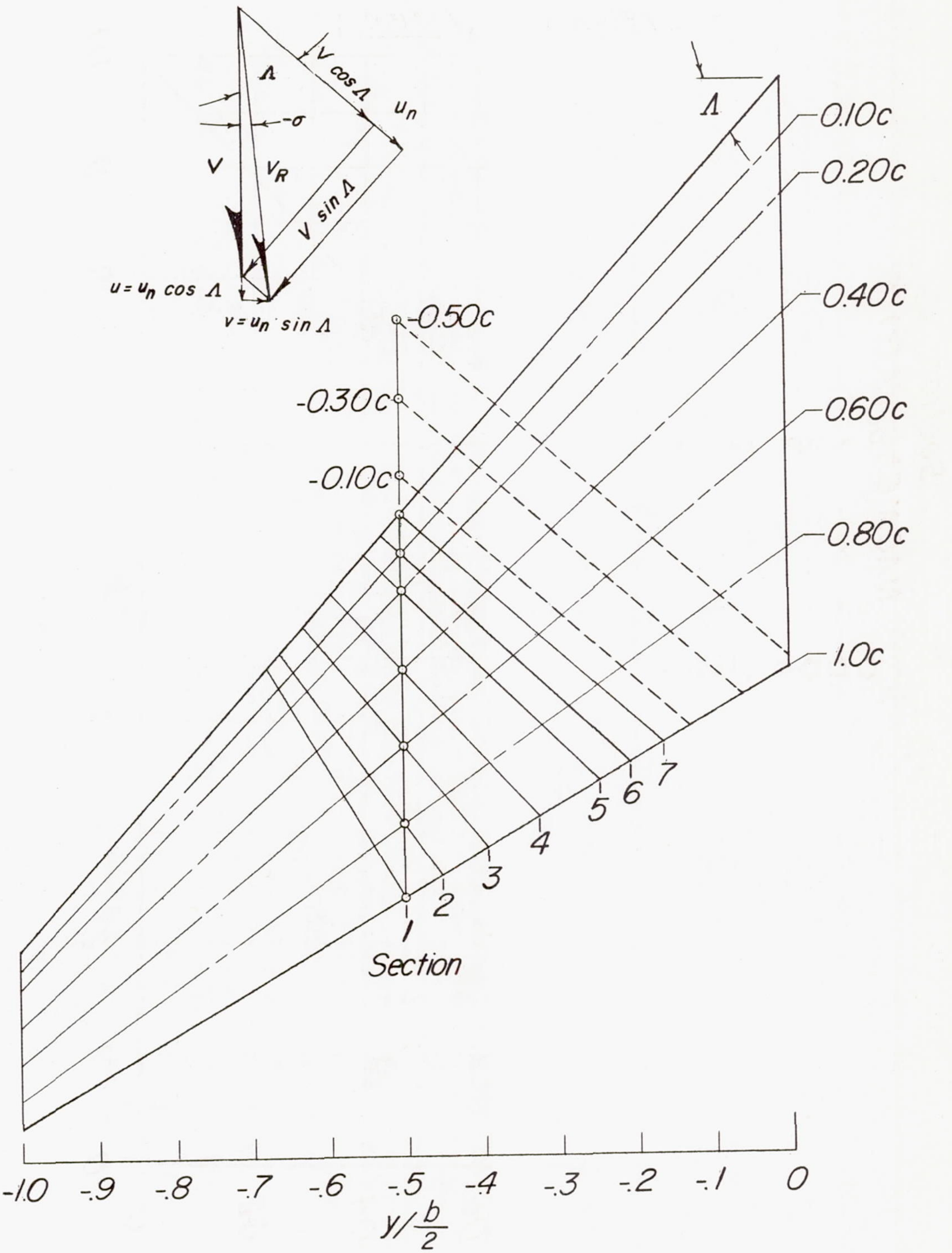

Figure 12.- Geometric characteristics of wing used in simple sweep theory.

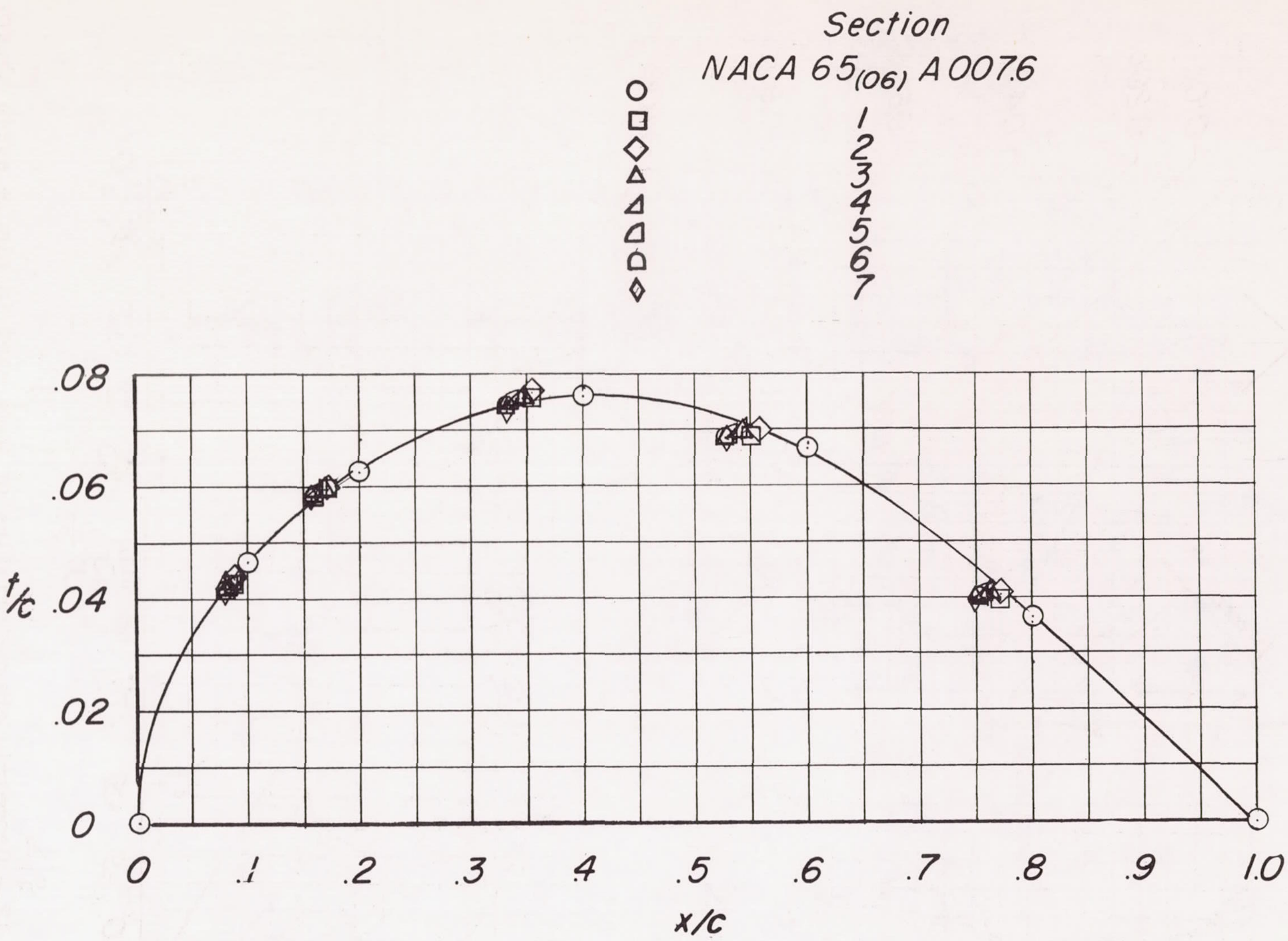

Figure 13.- Thickness distributions of airfoil sections normal to local sweep lines of sweptback wing.

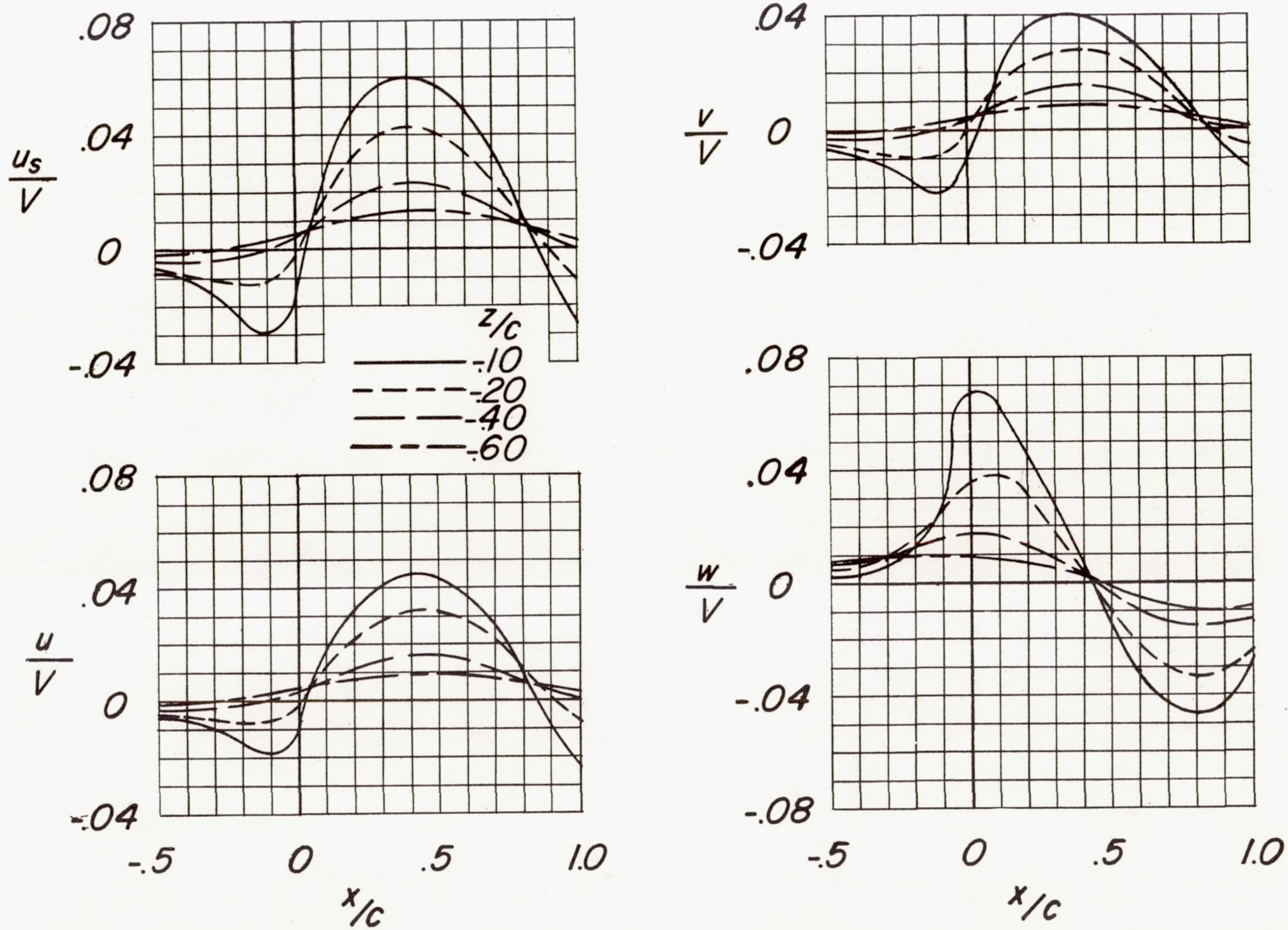

Figure 14.- Calculated velocities induced at midsemispan location of the swept wing at zero lift for several heights.

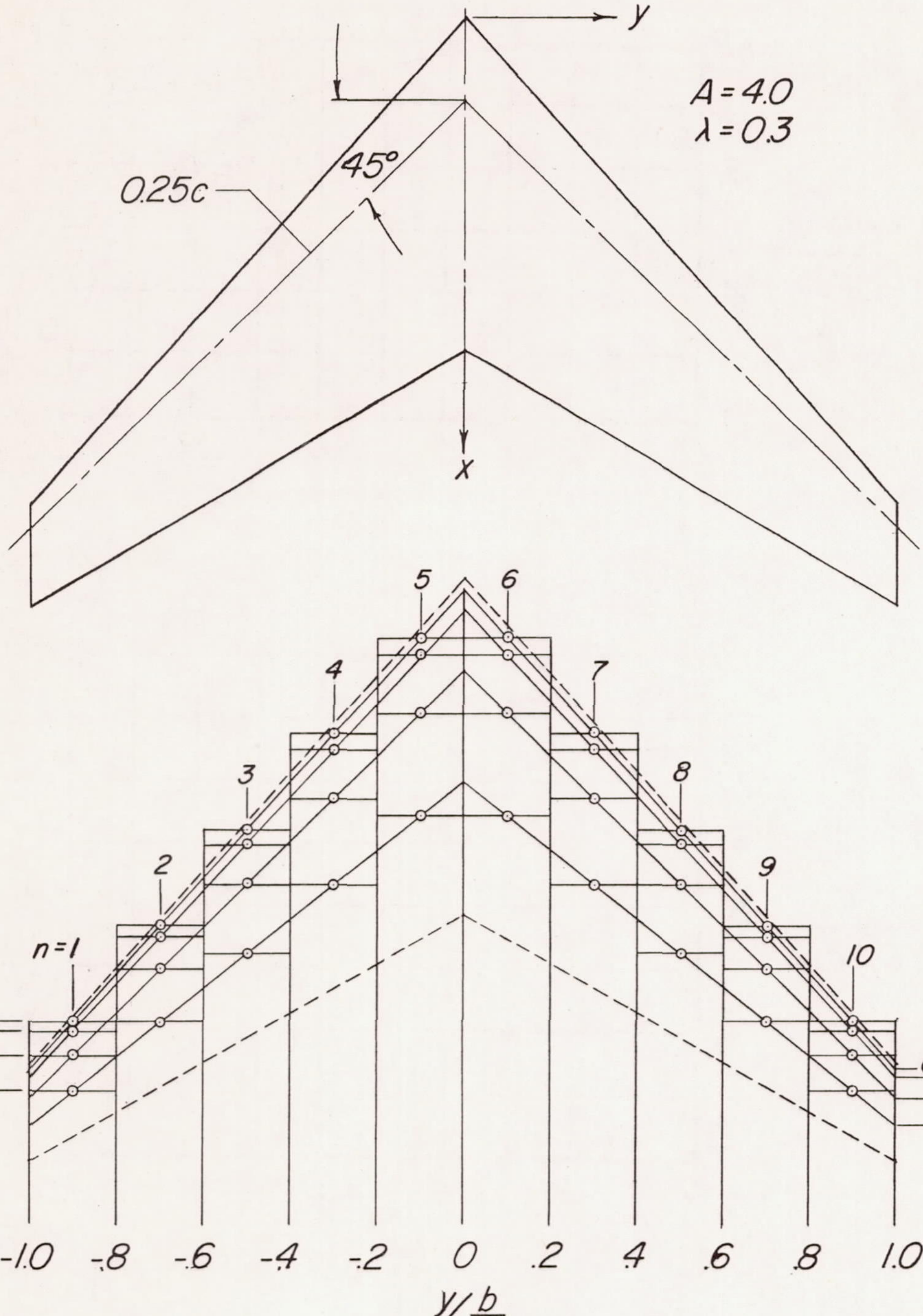

Figure 15.- Vortex arrangement assumed to approximate swept-wing lift characteristics.

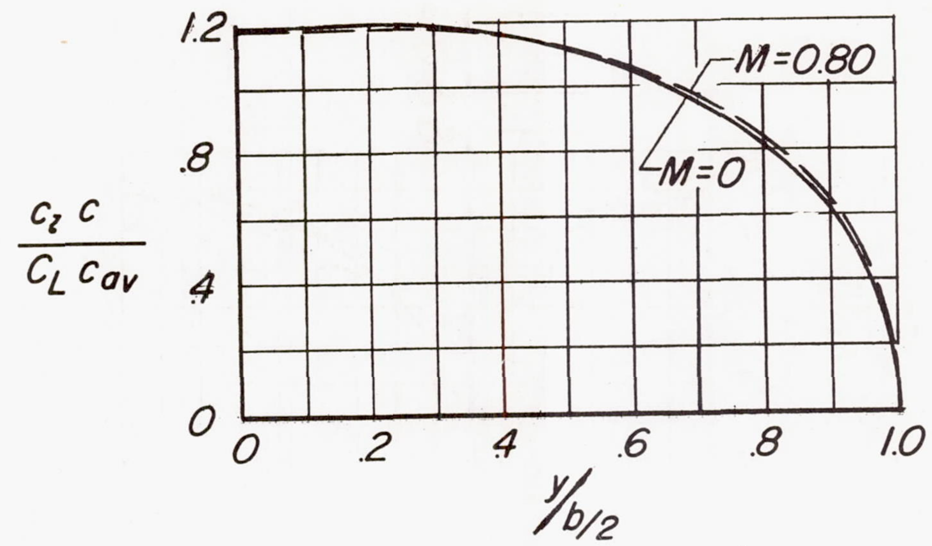

(a) Swept wing.

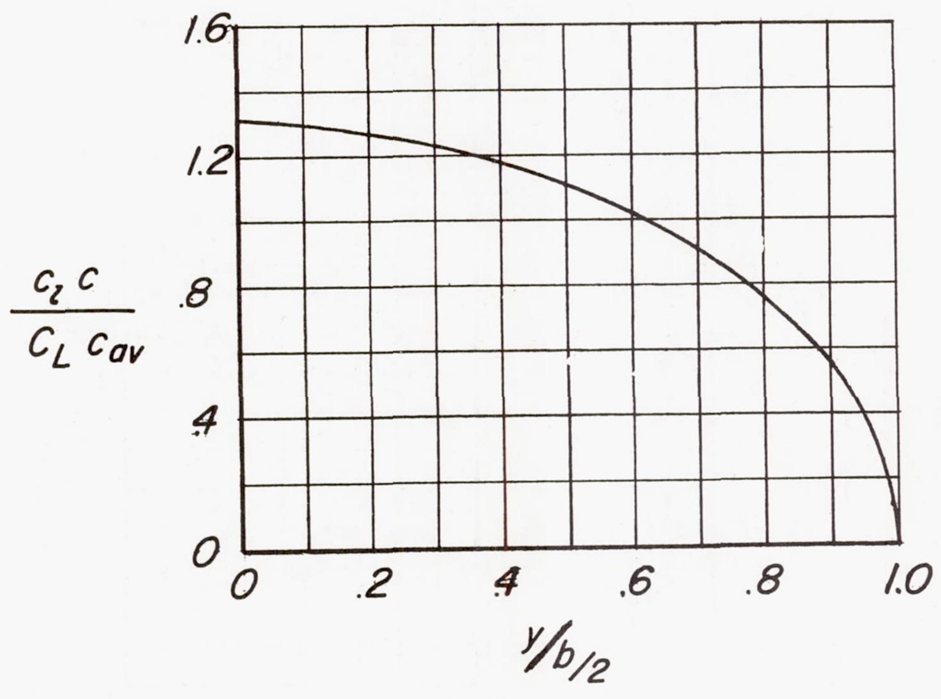

(b) Unswept wing.

Figure 16.- Theoretical span-load distributions.

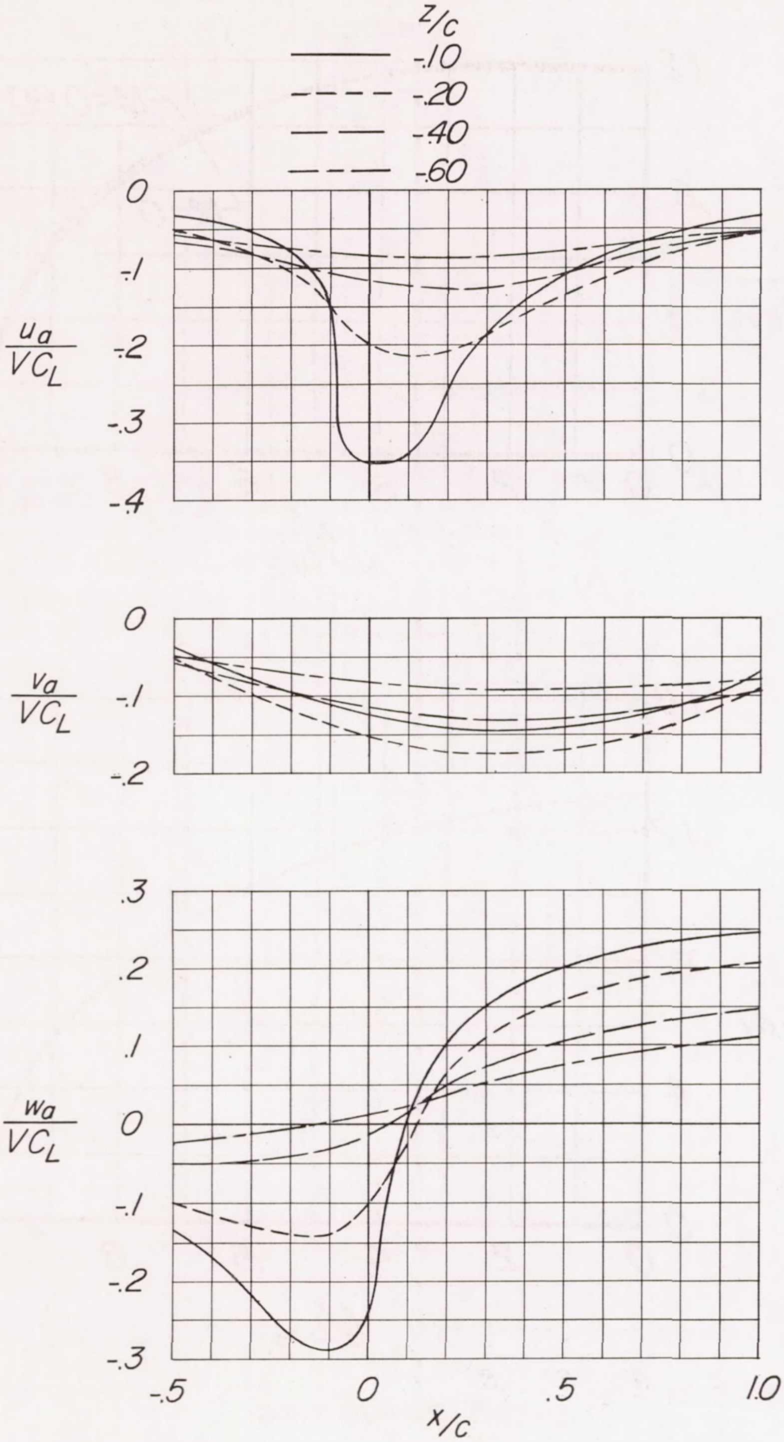

Figure 17.- Calculated additional velocities at the midsemispan location of the swept wing for unit lift coefficient.

$$\frac{V_a}{VC_L} = \frac{\partial\left(\frac{\phi(x,y)}{VC_L\ b/2}\right)}{\partial(y/b/2)} \approx \frac{\Delta\left(\frac{\phi(x,y)}{VC_L\ b/2}\right)}{\Delta(y/b/2)}$$

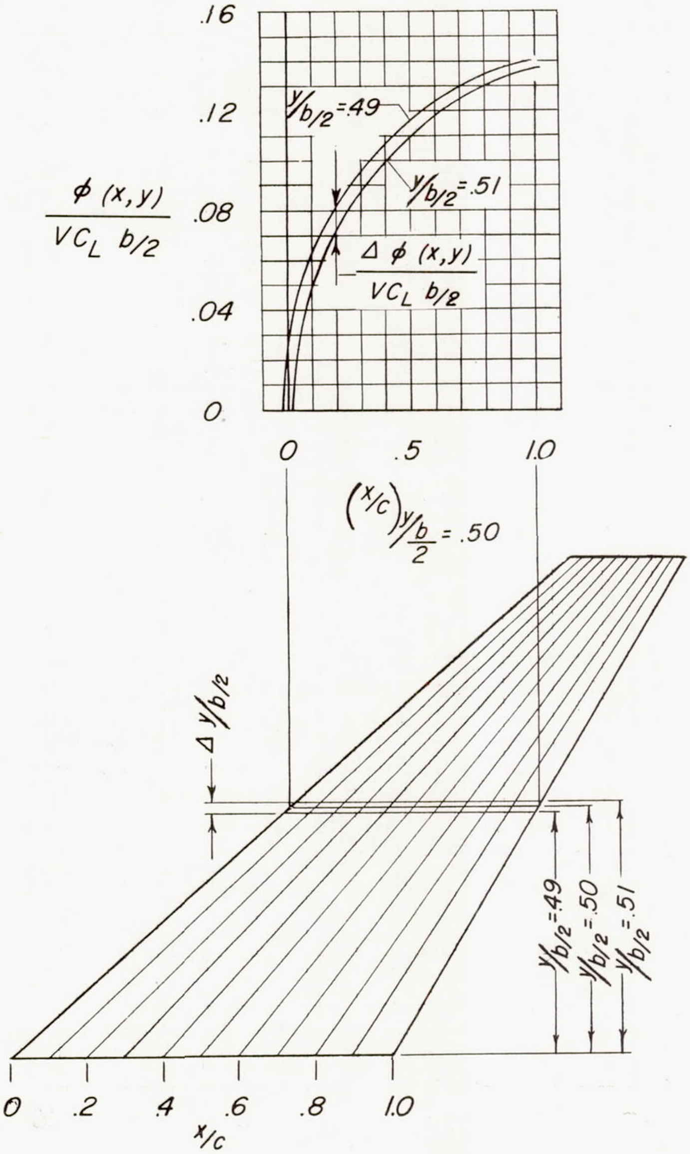

Figure 18.- Schematic illustration of graphical differentiation to determine sidewash velocity on chord plane of swept wing.

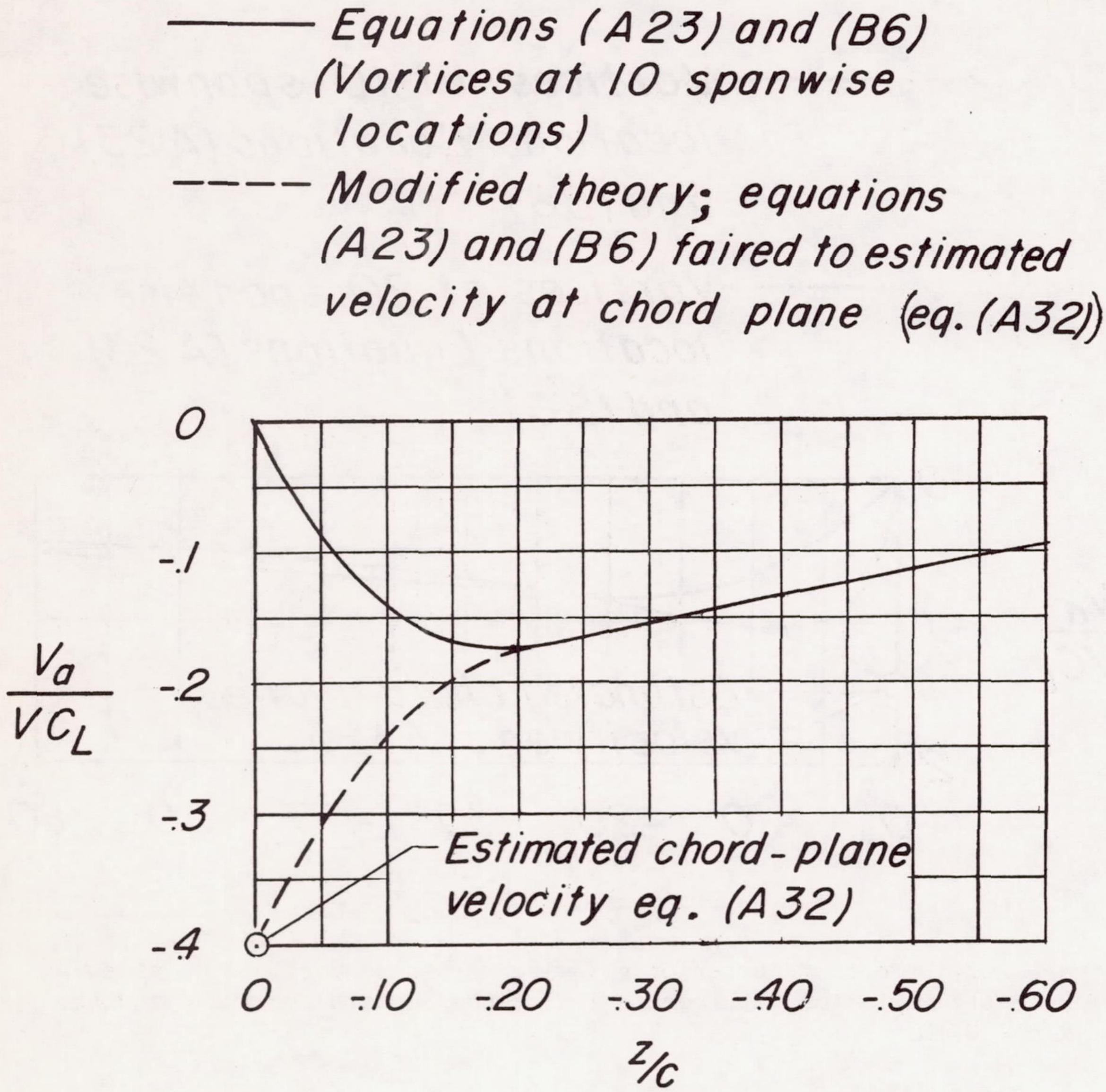

Figure 19.- Variation of sidewash velocity with vertical distance below swept wing. $x/c = 0.20$.

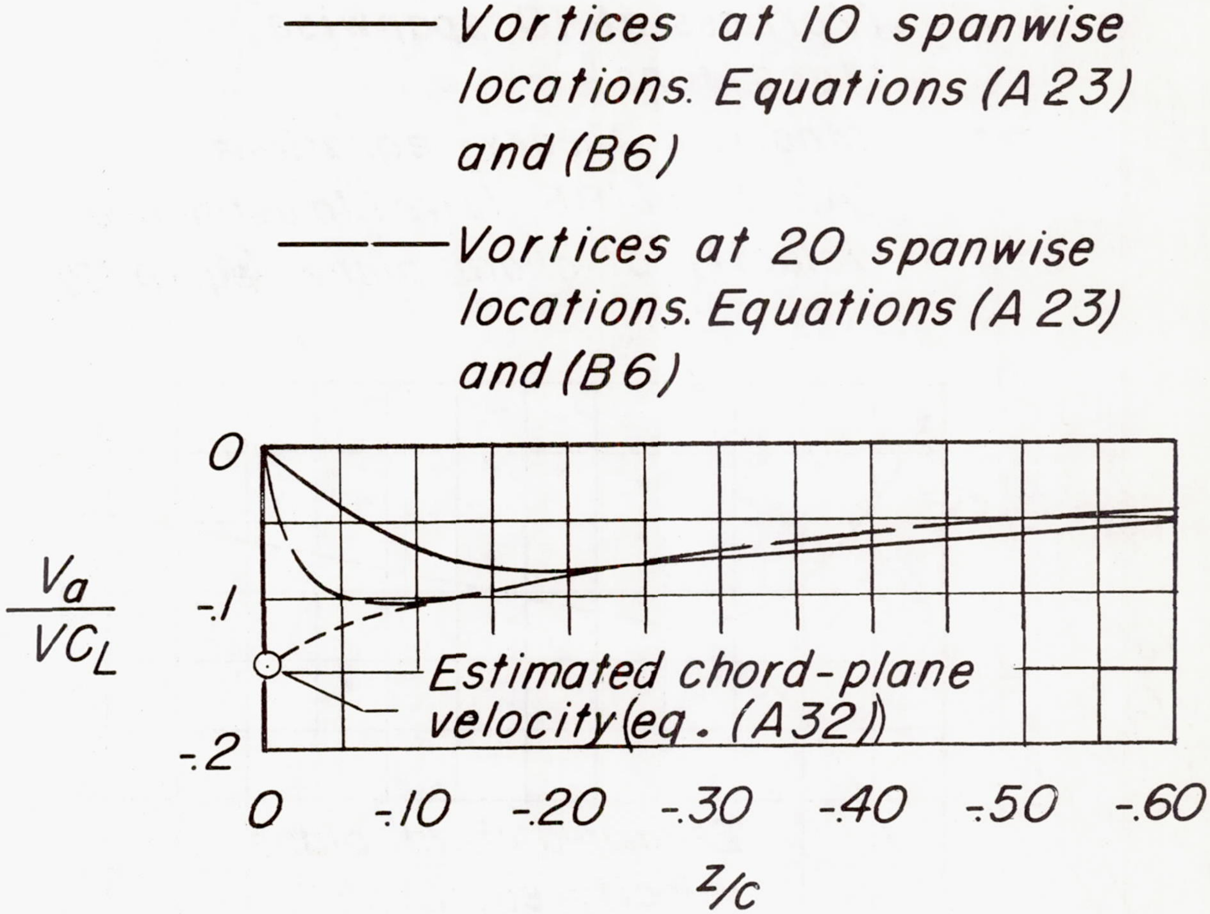

Figure 20.- Effect of number of spanwise horseshoe vortices on sidewash velocity variation with vertical distance beneath the unswept wing. $x/c = 0.10$.

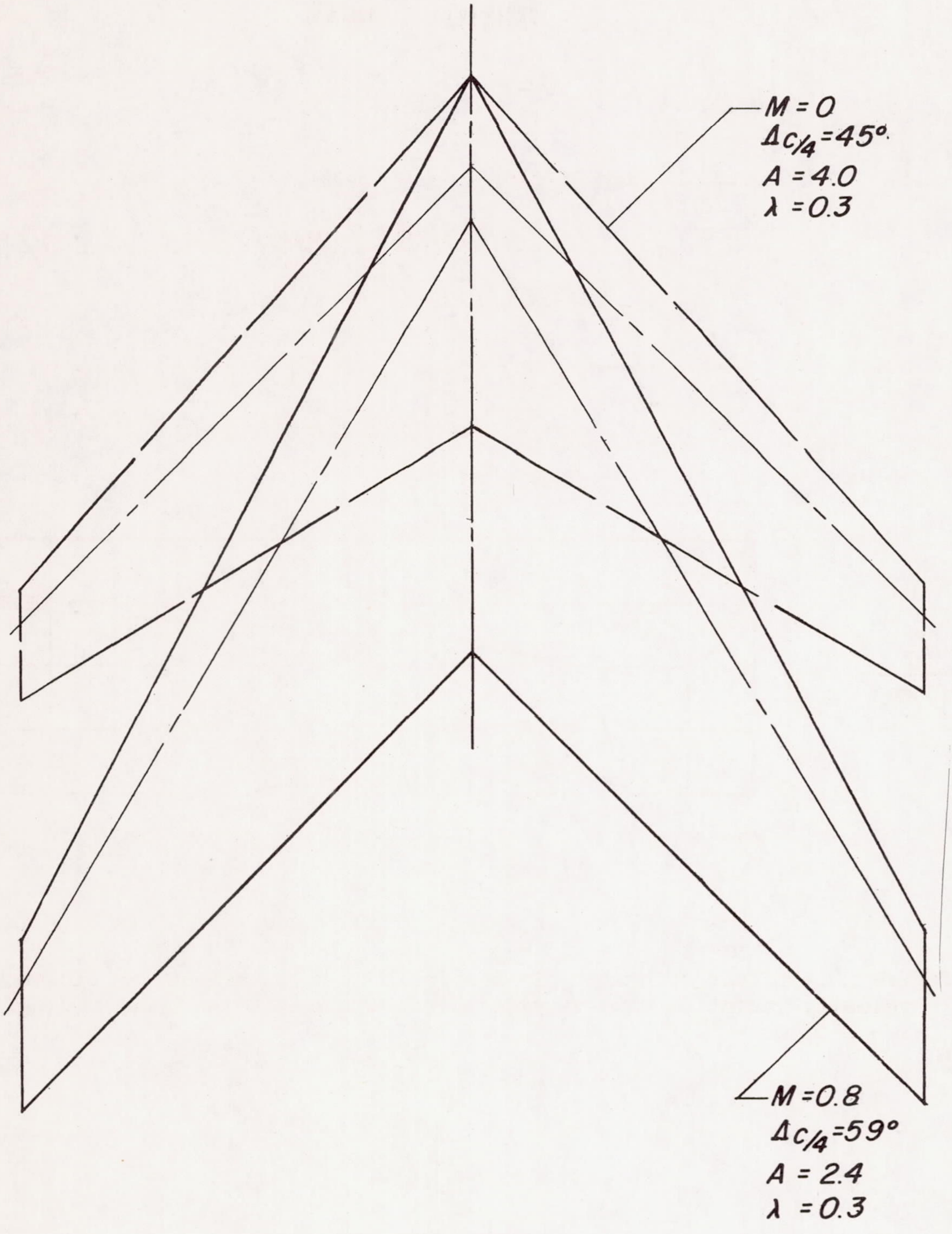

Figure 21.- Equivalent swept-wing plan form for M = 0.80.